General Disclaimer

One or more of the Following Statements may affect this Document

- This document has been reproduced from the best copy furnished by the organizational source. It is being released in the interest of making available as much information as possible.

- This document may contain data, which exceeds the sheet parameters. It was furnished in this condition by the organizational source and is the best copy available.

- This document may contain tone-on-tone or color graphs, charts and/or pictures, which have been reproduced in black and white.

- This document is paginated as submitted by the original source.

- Portions of this document are not fully legible due to the historical nature of some of the material. However, it is the best reproduction available from the original submission.

FINAL REPORT

MULTIPATH STUDY
FOR A
LOW ALTITUDE SATELLITE UTILIZING A DATA RELAY SATELLITE SYSTEM

OCTOBER 1970

Contract No. NAS 5-11602

Goddard Space Flight Center
Contracting Officer / Grafton Young
Technical Monitor / Paul Heffernan

Prepared By:
Project Manager / Dennis Egger
Hughes Aircraft Company
Space Systems Division

For
Goddard Space Flight Center
Greenbelt, Maryland

HUGHES
HUGHES AIRCRAFT COMPANY
SPACE SYSTEMS DIVISION

07

FINAL REPORT

MULTIPATH STUDY
FOR A
LOW ALTITUDE SATELLITE UTILIZING
A DATA RELAY SATELLITE SYSTEM

OCTOBER 1970

Contract No. NAS 5-11602

Goddard Space Flight Center
Contracting Officer / Grafton Young
Technical Monitor / Paul Heffernan

Prepared By:
Project Manager / Dennis Eggert
Hughes Aircraft Company
Space Systems Division

For
Goddard Space Flight Center
Greenbelt, Maryland

HUGHES
HUGHES AIRCRAFT COMPANY
SPACE SYSTEMS DIVISION

PREFACE

This study was performed as part of Contract Number NAS 5-11602 entitled "Study of a Low-Altitude Satellite Utilizing a Data Relay Satellite System" for the National Aeronautics and Space Administration, Goddard Space Flight Center. The purpose of this study is to investigate the technical considerations associated with a low-altitude satellite (LAS) operating in conjunction with a data relay satellite system (DRSS). One of the major problems is interference in the communication link between the two satellites by transmitted radiation reflected and distorted by the earth's surface. This problem, termed "multipath," is the subject of this report.

PRECEDING PAGE BLANK NOT FILMED

CONTENTS

PRECEDING PAGE BLANK NOT FILMED

ILLUSTRATIONS

TABLES

1. INTRODUCTION

The descriptive term "multipath" refers to a communication link in which there exists more than one signal propagation path between the signal source and the receiver. The phenomenon of interest in this study occurs in the transmission of electromagnetic energy between a low-altitude satellite (LAS) and a data relay satellite (DRS) at geostationary altitude. For this study, low altitudes are in the 100 to 1000 mile range.

There are basically two paths between the satellites (Figure 1-1): a direct path, and a path by reflection from the earth's surface. The total reflecting surface may be thought of as being composed of many smaller reflecting surfaces, and hence, the total reflection path is a collection of many reflection paths. The signal received via the reflection path is delayed and distorted with respect to the received direct signal, resulting in an undesirable interference. Further, under frequently occurring conditions, the magnitude of the received reflected signal may be larger with respect to the direct signal power. Later in this report it is shown that, for a range of geometrical conditions and a transmission frequency of 140 MHz over the sea, the average reflected power incident on the receiving antenna will be only 2 dB less than the direct signal power. Interference of this magnitude has rather profound consequences on a communication system operating in this environment.

The principal objective of this study is to quantitatively characterize the multipath phenomenon. Of major interest is the power received via both the direct and earth reflection paths. And, since free space propagation can easily be computed, the reflection process becomes the main subject of study.

The goal, therefore, is twofold:

1) To develop a means for estimating the magnitude and nature of the reflected power

2) To present numerical estimates of the reflected signal characteristics in graphical and tabular form for reasonable ranges of the important parameters

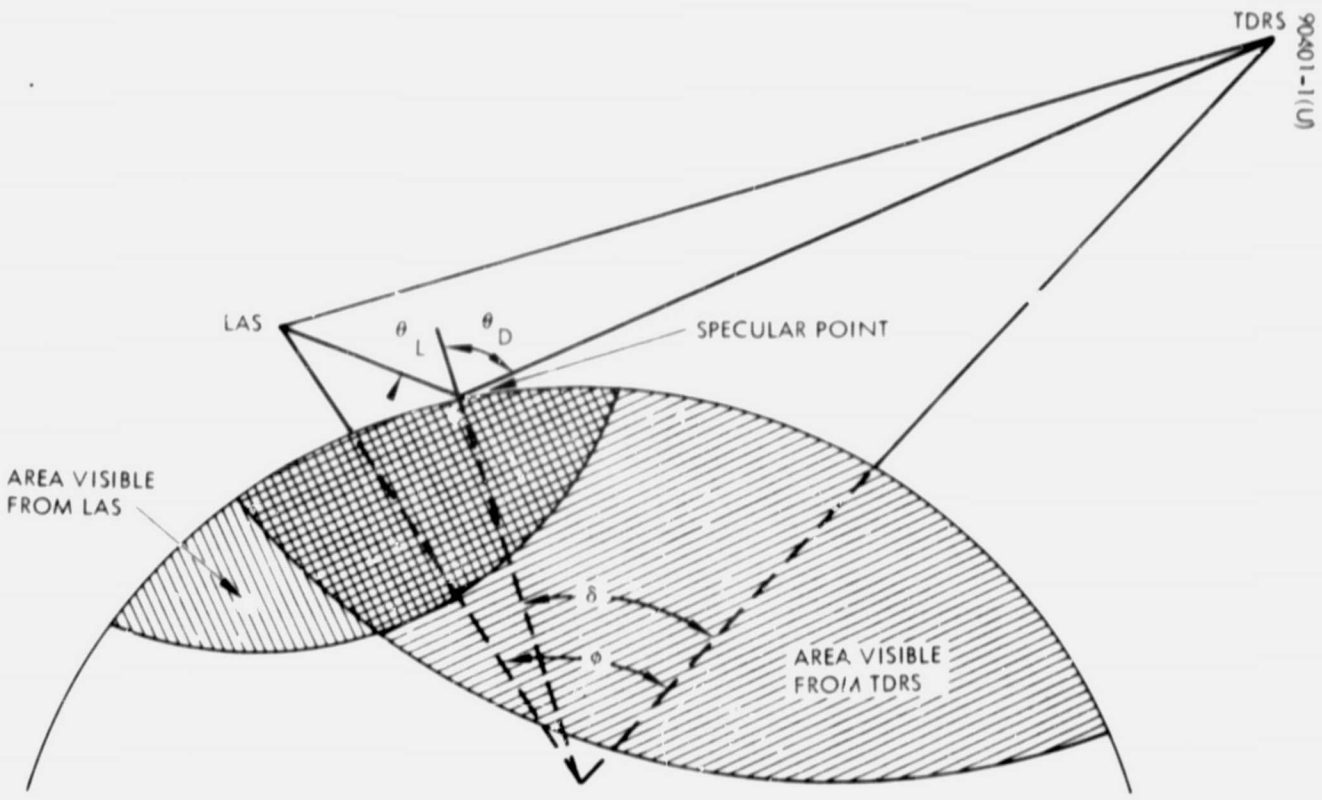

Figure 1-1. LAS-DRS Geometry

In addition, the fading characteristics of the combined signal are discussed, and a section is devoted to methods of communication improvement in the multipath environment. The major parameters include:

1) Geocentric LAS-DRS separation angle, φ

2) LAS altitude, h

3) Transmission frequency, f

4) Surface electrical properties (sea or land)

5) RMS surface slope (roughness factor), η

6) RMS surface variation, σ

7) Antenna polarizations

The reflection process is time varying and statistically nonstationary because of the changing geometry due to orbital motion. However, the short-term statistics may be considered stationary, thus allowing tractable statistical analysis of the reflection process. For a rough earth, the surface may be considered composed of many small patches, each with its own geometry, resulting in a reflected power which is time delayed and frequency shifted. Thus, the multipath phenornenon may be characterized by the following aspects of the total reflected power:

1) Magnitude

2) Time response of a transmitted impulse

3) Frequency spectrum of a transmitted CW signal

Quantitative estimates of these effects are presented in Section 3.

1.1 BACKGROUND

At the heart of earth reflection analysis is the analysis of reflection from a flat rough surface, which did not begin until about 1950. The analysis can be divided according to the type of surface model used. One type considers surfaces composed of randomly distributed deterministic shapes. An example of such a model may be found in Reference 1 where Twersky analyzed a surface of hemispherical bosses distributed on a plane. A second model treats the surface height as a random variable. This approach seems more reasonable and has dominated rough surface analysis in recent years. A model based on a statistical description of the surface roughness is used in this study and is discussed in Subsection 2.4.

Statistically, rough surfaces can be divided into three classes: slightly rough, intermediate, and very rough. These classes can

be quantitatively distinguished by means of a smoothness factor which includes the ratio of the rms surface variation and electromagnetic wavelength (see Subsection 2.2). But only the slightly rough and very rough surfaces can be treated mathematically with useful results; however, extrapolation between these two classes can yield useful estimates of surfaces with intermediate roughness. Suppose that a perfectly smooth surface becomes slightly rough. The specularly reflected energy decreases as the roughness grows, but still contains the major portion of the energy. But, in addition, there is a smaller amount of energy scattered away from the specular direction due to the roughness. The signal reflected specularly is phase-coherent, while the scattered signal is incoherent (random phase) at any distant reception point. As roughness increases, the coherent power decreases and incoherent power increases until, even in the specular reflection direction, all received power is incoherent. The coherent component is computed using the expression for reflection from a smooth plane, with additional factors included for the effect of roughness and the sphericity of the earth. The derivation of the expression is given in Reference 2, and the results are discussed in Subsection 2.3.

Two approaches to the slightly rough earth are well documented. A perturbation technique is used by Peake (Reference 3) and Barrick and Peake (Reference 4) and later extended by Valenzuela (Reference 5). The results of these authors' approaches require the assumption that the rms surface variation be much smaller than a wavelength and that the surface slopes be small. Another derivation technique employing the tangent plane approximation, or Kirchoff approximation, as it is sometimes called, is given by Davies (Reference 6) and Beckmann (Reference 2). These derivations require, in addition to the above assumptions, that the surface radii of curvature be everywhere much greater than a wavelength. The results of these analyses are useful for estimating the power reflected in directions other than the specular direction, but it can be shown that this incoherent power is significantly less than the coherent power reflected in the specular direction.

Reflection from very rough surfaces has been analyzed using several techniques, all of which lead to equivalent results. Basic assumptions common to these analyses are:

1) The rms surface variation is larger than a wavelength

2) The surface radii of curvature are much larger than a wavelength

Assumption 2 is not always satisfied, particularly for land, but for the sea, which is a better reflector, it is satisfied quite frequently. Isakovich (Reference 7) provides the first comprehensive vector treatment of rough surface reflection from a physical optics point of view, and Davies essentially duplicated this work in a scalar formulation. This work was extended by Beckmann (Reference 2), Semenov (Reference 8), Stogryn (Reference 9), and others. Muhleman (Reference 10) considered the surface to be composed of

small, connected, perfectly conducting facets, and used the probability distribution of the facet normals in his analysis. Hagfors (Reference 11) extended these results, showing that they are equivalent to those of the other authors mentioned above. A third, but related, approach by Kodis (Reference 12) related the reflected power in a given direction to the number of specular points, i.e., the number of points satisfying specular geometry with respect to transmitter and receiver. Barrick (Reference 13) extended this work by developing expressions for the number of specular points and average radii of curvature, obtaining results identical to the other analysis approaches. The form of these results is discussed in Subsection 2.4.

The LAS/DRS multipath problem has been considered by several investigators. Durrani and Staras (Reference 14) began their analysis where the rough surface analysis discussed above ended. They took the general result for rough earth reflection, which pertains to a surface patch, and formulated the integral for total average received power. The method of steepest descent was used, along with a number of approximations, to arrive at a formula for the ratio of average received reflected power and received direct power which is defined as the "relative power" in Subsection 2.4. Some of the approximations made by Durrani and Staras are not accurate for all values of the geometric parameters. Further, because of the integral approximation approach, an accurate assessment of the effects of antenna gain and polarization cannot be made. Massey (Reference 15) and Birch (Reference 16) are concerned principally with modulation, coding, and signal design to reduce multipath effects, and they add no additional information concerning the magnitude and nature of the reflected power beyond that given in Reference 14.

In this study, the general rough surface solution of References 2, 8, 9, 11, and 13 is used to compute the received incoherent power, and the slightly rough, coherent power is determined from the results of Beckmann and Spizzichino (Reference 2). The rough earth results are achieved by numerical integration of the surface integral via machine computation. This method numerically sums the power contributions due to many surface patches and, in the process, allows determination of the impulse response and frequency response of the reflection process. Thus, the multipath phenomenon may be characterized as mentioned previously. Further, the significant parameters may be readily varied and, in particular, the effect of antenna gain and polarization may be evaluated.

1.2 PRINCIPAL RESULTS

Estimates of the reflected power and the effects of the parameters listed previously are illustrated graphically and discussed in Section 3. Section 4 presents techniques for improving communication in the multipath environment. A few of the more significant results and conclusions are presented here.

1.2.1 Interference Magnitude

In the absence of techniques for discriminating against the reflected signal, the interference by this signal can seriously degrade the performance of an LAS/DRSS communication link. If the electromagnetic radiation is polarized horizontally with respect to the reflecting area, i.e., normal to the plane containing the LAS, DRS, and earth's center, then at 140 MHz the average magnitude of the reflected signal will be only 2 dB less than that of the directly received signal (R_p = -2 dB). This can be seen from Figure 3-1. Further, from Figure 3-6 for this case, the reflected signal power will exceed that of the direct signal approximately 20 percent of the time, and from Figure 3-7, the total received power will fade below the direct signal by 5 dB 10 percent of the time.

1.2.2 Improvement Techniques

A directional antenna on the LAS will provide a significant improvement by discriminating geometrically against the reflected power. However, many missions require an omnidirectional radiation pattern. For this case, circularly polarized antennas on both the LAS and DRS will provide discrimination against the reflected signal. If an LAS antenna system can be designed to transmit/receive the same sense of circular polarization in all directions, then the average reflected power will be less than 9 dB below the directly received power. This conclusion derives from Figures 4-3 through 4-6. Then, from Figure 3-7, the reflected power will be less than the direct power 99.96 percent of the time and more than 3 dB below the direct signal 98.2 percent of the time.

Signal processing techniques with improvement potential are discussed briefly in Section 4, and include pseudo-noise (PN) coding, diversity techniques, frequency hopping, burst transmission, and data rate limiting. The most attractive and widely applicable of these techniques is PN coding. With this technique, the data signal is modulated by a signal corresponding to a PN sequence prior to transmission. This combined signal is demodulated at the receiver in a correlation process which discriminates against the reflected signal. It appears that effective use of PN coding requires a minimum RF bandwidth of approximately 20 kHz. Larger bandwidths will allow longer total communication time, better multipath rejection, and shorter signal acquisition times.

2. ANALYSIS AND MATHEMATICAL MODELING

The multipath phenomenon requires mainly geometric analysis in arriving at a mathematical model useful for quantitative estimates of the reflected power. The analytical treatment may be broken into three fundamental areas: 1) large-scale geometry involving the orbital positions of the two vehicles and the earth's mean surface, 2) smaller scale, surface roughness considerations, and 3) antenna radiation characteristics. These topics are treated in the above order in the following six subsections.

2.1 LARGE-SCALE GEOMETRY

In the following analysis, the LAS is considered as the transmitter and the DRS as the receiver. This allows consistency and provides convenience in the ensuing discussions since the communication link, including the multipath reflection effects, is bilateral.

2.1.1 Separation Angle and Transmission Plane

The two line segments from the center of the earth to the two satellites may be used as a geometrical basis for analysis of the multipath phenomenon. The primary geometrical parameters are the length of these two lines and the angle between them, defined here as the separation angle, φ. In general, these three quantities vary with time unless the orbits are circular, in which case only the separation angle is varying. At any instant in time, the two lines define a plane which intersects the earth's surface. This basic geometry is illustrated in Figure 2-1.

The direct transmission path lies in this plane, and the reflection from the earth's surface is nominally symmetric about it. This plane is subsequently referred to as the transmission plane, and it is a useful basis for the geometric analysis required in studying the reflection process. The separation angle may be related to the orbital parameters of the two satellites by considering the lines from the earth's center to the satellites as vectors in an inertial coordinate system, as shown in Figure 2-2. Referring to this figure,

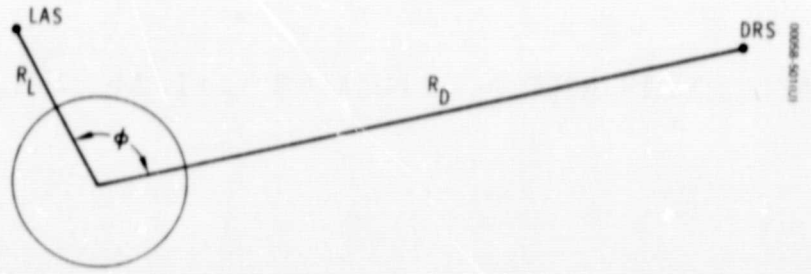

Figure 2-1. Basic Geometric Quantities in LAS/DRSS Multipath Analysis

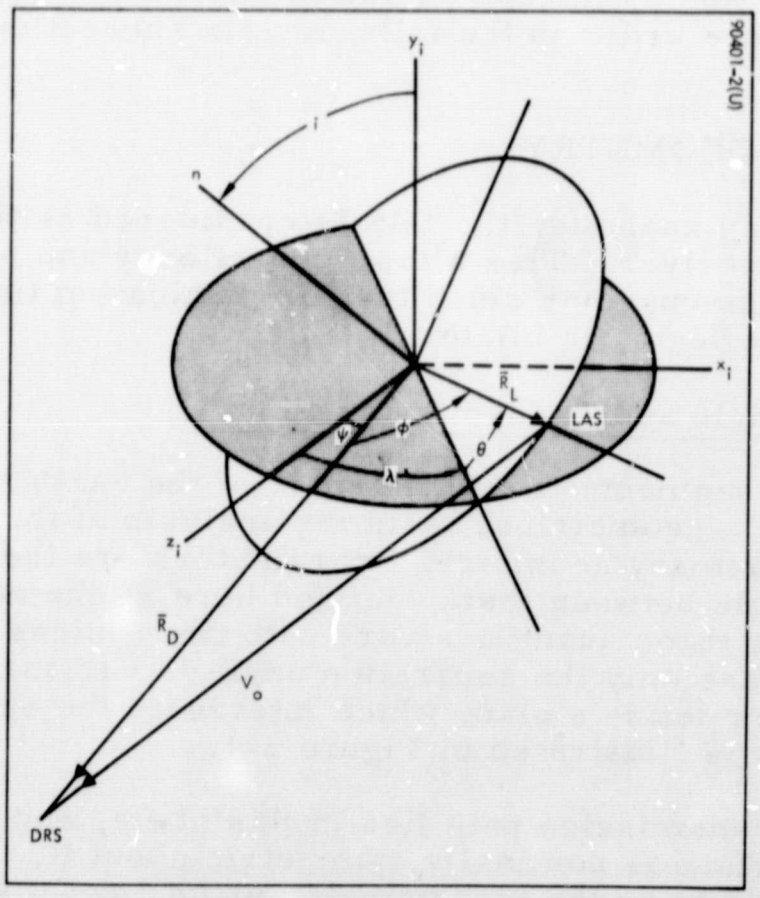

Figure 2-2. Orbital Parameters

$$\bar{R}_L = R_L \begin{pmatrix} \cos\theta \sin\lambda + \cos i \sin\theta \cos\lambda \\ \sin\theta \sin i \\ \cos(\cos\lambda - \cos i \sin\theta \sin\lambda \end{pmatrix} \quad (1)$$

$$\bar{R}_D = R_D \begin{pmatrix} \sin\psi \\ 0 \\ \cos\psi \end{pmatrix} \quad (2)$$

Then

$$\cos\varphi = \frac{\bar{R}_L \cdot \bar{R}_D}{R_L R_D}$$

$$\cos\varphi = \cos\theta \cos(\psi-\lambda) + \cos i \sin\theta \sin(\psi-\lambda) \quad (3)$$

Once the time variation of θ, ψ, and λ is known, the time variation of φ may be determined from Equation 3.

2.1.2 Coordinate Systems

Using the transmission plane as a geometric basis, several useful coordinate systems may be defined. Referring to Figure 2-3, the coordinate system E_1 E_2 E_3 is defined as follows: E_1 coincides with R_D, the line segment to the DRS; E_2 is orthogonal to E_1 and lies in the transmission plane; and E_3 completes the system, lying perpendicular to the transmission plane. All vectors in the analysis of the reflection and direct transmission paths will be expressed in terms of this coordinate system.

Two other coordinate systems required for describing the radiation patterns of the antennas are shown in Figure 2-3. The D_1 D_2 D_3 system is parallel to the E_1 E_2 E_3 system, but is centered at the DRS antenna. The L_1 L_2 L_3 coordinate system is centered at the LAS antenna. The L_1 coordinate is parallel to the R_L line and points away from the earth, L_2 is orthogonal to L_1 and is in the E_1 E_2 plane, and L_3 is parallel to E_3 and D_3.

2.1.3 Specular Point

The specular point is that point on the earth's surface, in the transmission plane, where the angle of incidence is equal to the angle of reflection

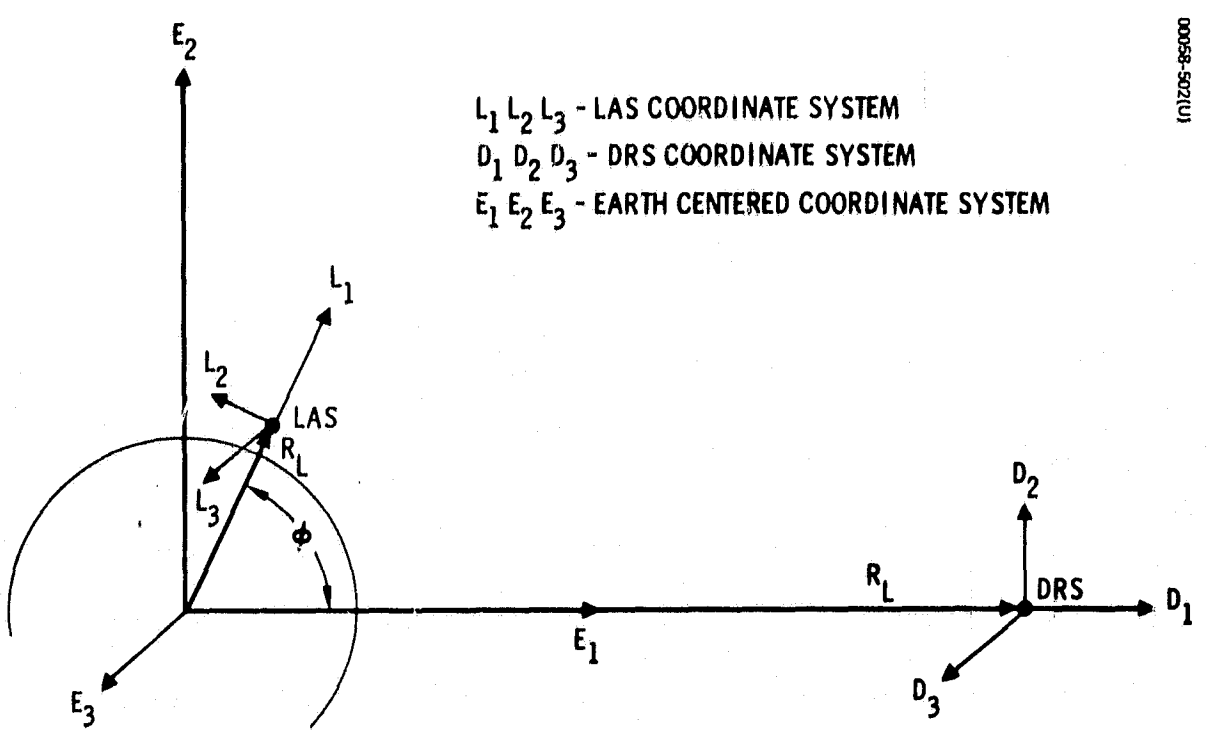

Figure 2-3. Coordinate Systems

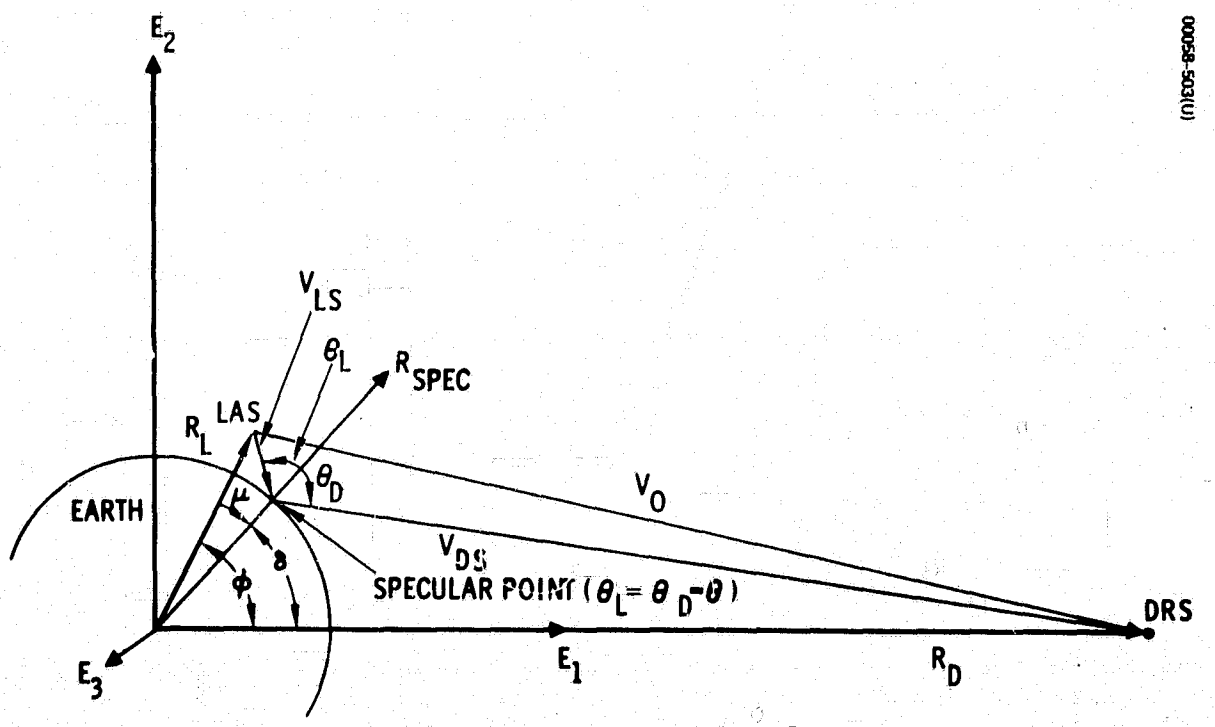

Figure 2-4. Specular Point Quantities

measured from the local vertical. The geometry associated with this point is shown in Figure 2-4. It can be shown that

$$\theta_L = \frac{1}{2}(\varphi-\delta) + \tan^{-1}\left[\frac{R_L + R_E}{R_L - R_E}\tan\frac{1}{2}(\varphi-\delta)\right] \quad (4)$$

$$\theta_D = \frac{1}{2}\delta + \tan^{-1}\left[\frac{R_D + R_E}{R_D - R_E}\tan\frac{1}{2}\delta\right] \quad (5)$$

The specular point is the point where $\theta_L = \theta_D$, and is specified by the angle δ, which can be found as a function of φ by equating the two expressions of Equations 4 and 5. Figure 2-5 shows δ as a function of φ for three different values of the LAS altitude. Figure 2-6 illustrates the relationship between the incidence angle, θ, and the separation angle, φ.

The specular point is at or near the center of the region on the earth's surface from which the reflection toward the DRS occurs. Consequently, in summing the effects of reflection from many small surface "patches," this point will provide an origin for variation of the surface patch location.

2.1.4 Scattering Patch Geometry and Reflection Plane

Consider a small patch, dS, of the earth's surface near the specular point. The location of the center of such a point can be specified by the two angles α and β, as shown in Figure 2-7. The angle α is measured in the transmission plane, and β is measured in the plane defined by R_α and E_3. Thus, the area, dS, of the small patch is given by

$$dS = R_E^{\,2} \cos\beta \, d\alpha \, d\beta \quad (6)$$

The vector V_L is directed from the LAS to the patch, and V_D is directed from the patch to the DRS. These two vectors are given by

$$\bar{V}_L = \bar{R}_S - \bar{R}_L \quad (7)$$

$$\bar{V}_D = \bar{R}_D - \bar{R}_S$$

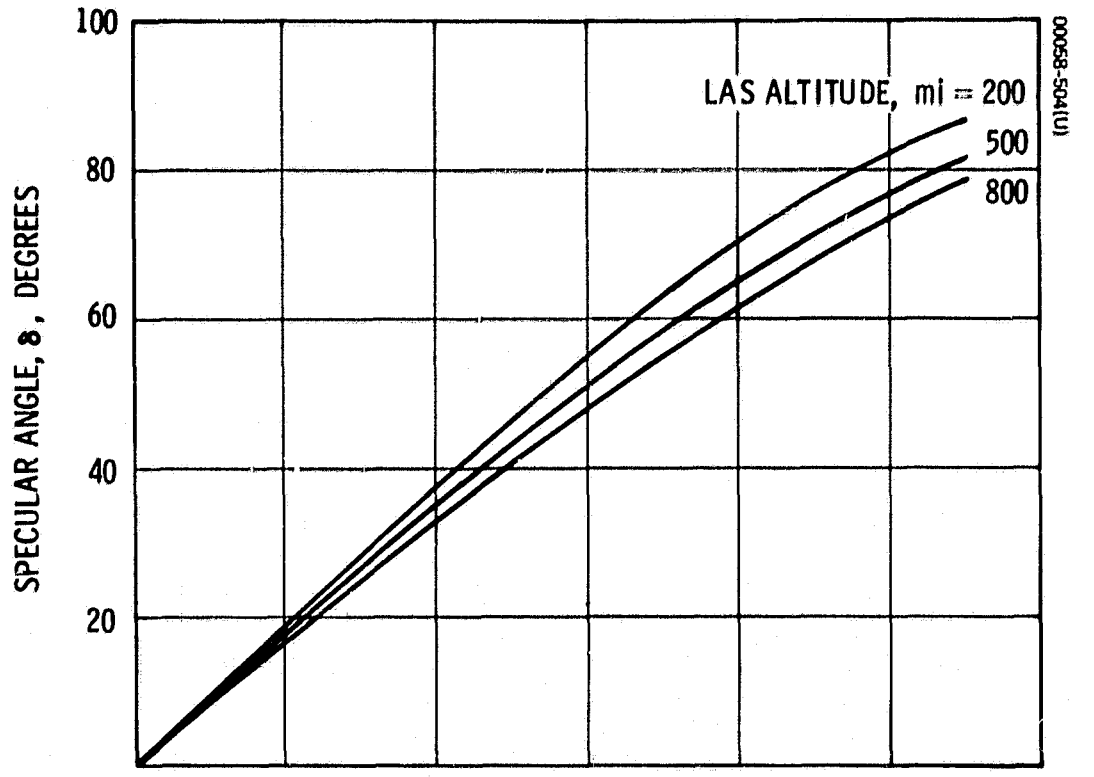

Figure 2-5. Specular Angles Versus Separation Angle

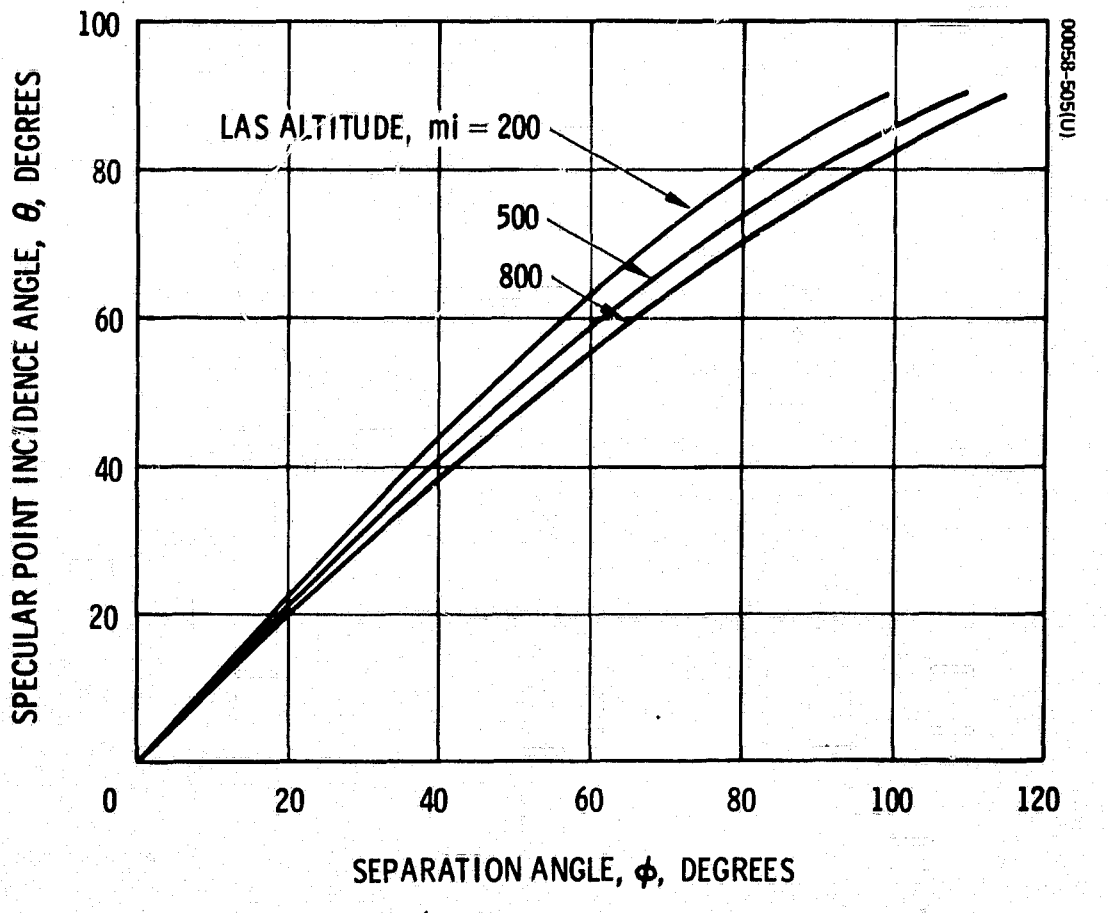

Figure 2-6. Specular Point Incidence Angle Versus Separation Angle

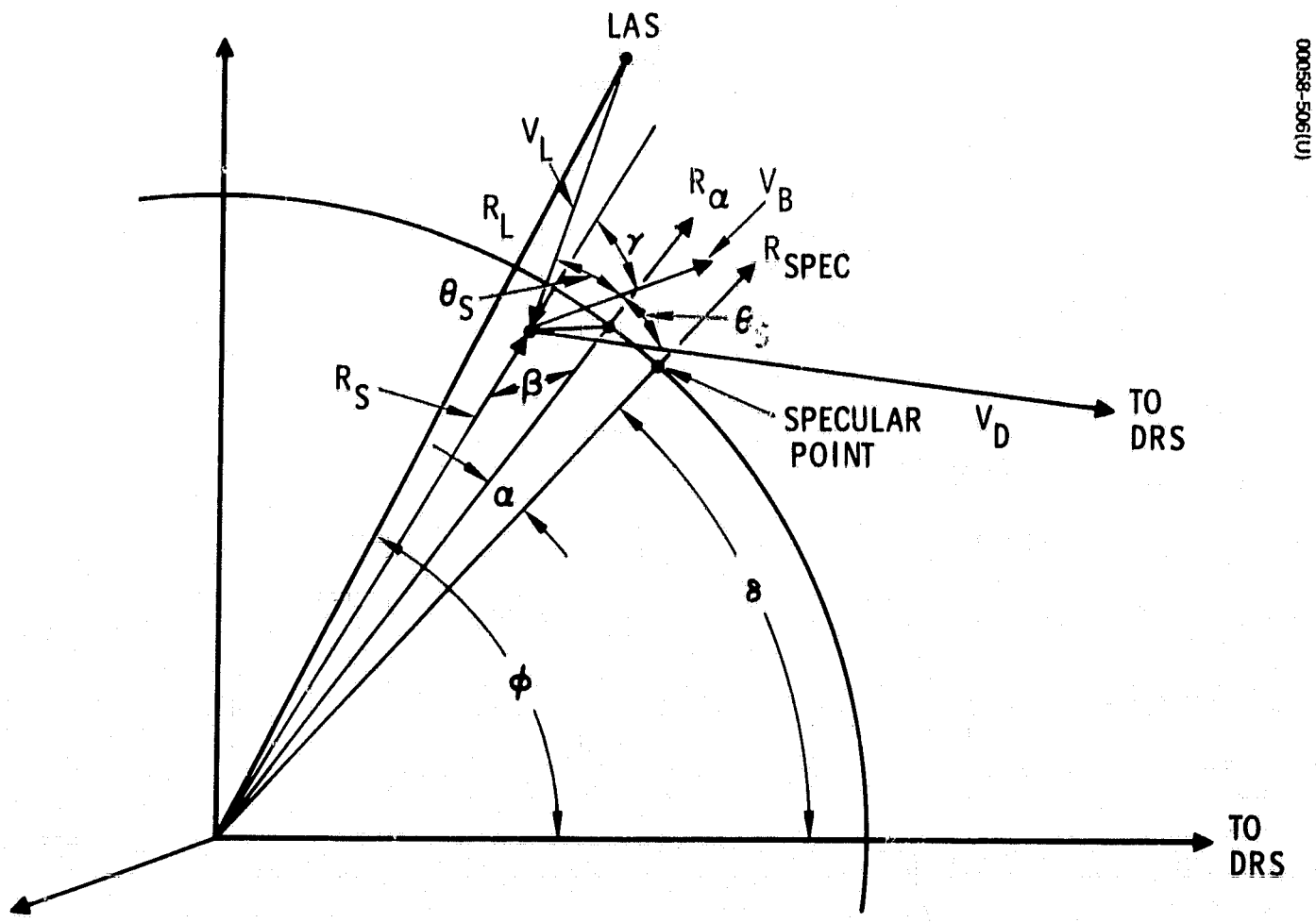

(U)9058-8500

Figure 2-7. Scattering Patch Geometry

where

$$\bar{R}_D = R_D \begin{pmatrix} 1 \\ 0 \\ 0 \end{pmatrix} \tag{8}$$

$$\bar{R}_L = R_L \begin{pmatrix} \cos \varphi \\ \sin \varphi \\ 0 \end{pmatrix} \tag{9}$$

$$\bar{R}_S = R_E \begin{pmatrix} \cos (\delta + \alpha) \\ \sin (\delta + \alpha) \\ \sin \beta \end{pmatrix} \tag{10}$$

Also of interest is the vector, $\bar{V}_B$, which bisects the angle between $\bar{V}_L$ and $\bar{V}_D$.

$$\bar{V}_B = \frac{\bar{V}_D}{V_D} - \frac{\bar{V}_L}{V_L} \tag{11}$$

The angle, γ, between $\bar{V}_B$ and $\bar{R}_S$ is given by

$$\cos \gamma = \frac{\bar{V}_B \cdot \bar{R}_S}{V_B R_S} \tag{12}$$

The reflection plane is the plane containing both $\bar{V}_L$ and $\bar{V}_D$. Energy reflected from dS to the DRS propagates in this plane.

2.1.5 Distribution of the Separation Angle, φ

Since the separation angle, φ, is the primary geometric parameter and several of the multipath characteristics will be determined as a function

of this angle, it is of interest to know the frequency of occurrence of a given value of φ. In other words, to aid in interpreting the data which is a function of φ it is helpful to know with what frequency a given value of φ will occur. Equation 3 relates φ to the three basic orbital parameters i, θ, and $\psi - \lambda$ (see Figure 2-2). To determine the statistical distribution of φ, some assumptions concerning the distribution of these orbital parameters must be made.

For the purpose of numerical evaluation, the following assumptions are made:

1) The orbits of the LAS and DRS are circular; thus, over an extended time period, the angle θ will be uniformly distributed between 0 and 360 degrees.

2) Over a complete mission, all values of the angle $\psi - \lambda$ between 0 and 360 degrees will occur with equal frequency.

3) The inclination, i, remains constant.

4) The altitude of the LAS is 500 statute miles.

The last assumption determines the maximum value of φ, which can be shown to be 108.7 degrees. Any value of φ, determined from Equation 3 which is greater than this value, is meaningless since the earth blocks transmission between the two spacecraft for larger separation angles. And when transmission is blocked, no direct or multipath signal is received; thus, communication terminates or is reestablished via another DRS for which the separation angle allows transmission.

Based on these assumptions, a computation was made of both the relative frequency and the cumulative frequency of the separation angle, φ, for LAS inclinations of 0, 30, 60, and 90 degrees. The results are shown in Figures 2-8 and 2-9. From Figure 2-8, it can be seen that the density functions peak at the inclination angle. Figure 2-9 can be used to estimate the percentage of time for which the separation angle lies in a given range. For example, for an inclination of 60 degrees, the separation angle, φ, lies between 40 and 80 degrees 66.4 - 15.8 = 50.6 percent of the time. Figure 2-10 indicates the effect of LAS altitude.

2.2 EARTH REFLECTION AND SCATTERING

Mathematical modeling of electromagnetic energy reflection from the earth's surface requires assumptions concerning the roughness in order to arrive at analytical expressions useful for obtaining numerical results. Based upon the results corresponding to two or more roughness conditions, reflection characteristics for intermediate roughness conditions may be estimated. In this study, both smooth and rough models are employed to estimate reflection for these conditions and intermediate conditions. The assumptions associated with these two models will be discussed in the next two subsections. But, before proceeding with the analysis associated with

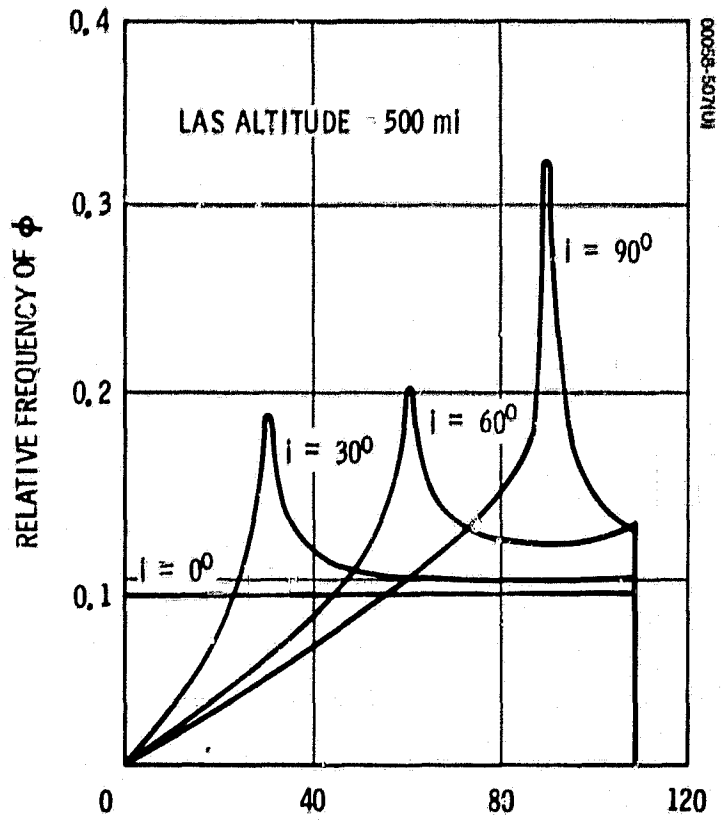

Figure 2-8. Relative Frequency of Separation Angle

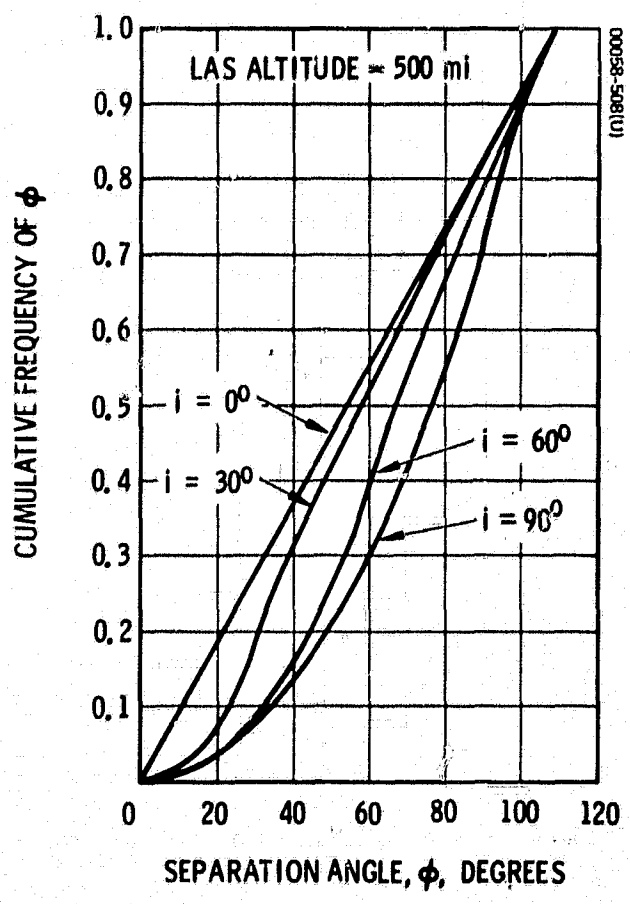

Figure 2-9. Cumulative Frequency of Separation Angle

these two extreme surface conditions, a discussion of what constitutes a rough or smooth earth is warranted.

A surface is defined as smooth when the fields reflected by the surface from an incident plane wave propagate only in a single direction. This implies that the fields reflected by one portion of the surface are highly correlated or in a fixed relationship to fields scattered by other portions of the surface so that the reflected energy propagates as a wave in a single direction. Similarly, a surface is qualitatively defined as rough when the fields scattered by the surface from an incidence plane wave are diffuse or propagate in various directions.

To provide a quantitative criterion for surface roughness, consider two points on a flat surface separated by a height difference, h, as shown in Figure 2-11. The waves reflected from these two surface points will differ in phase by an amount given by

$$\Delta\psi = \frac{4\pi h \cos\theta}{\lambda} \tag{13}$$

where θ is the angle of incidence as shown in Figure 2-11 and λ is the EM wavelength. For a surface with randomly distributed surface variations, a surface smoothness factor, q, may be defined by

$$q = \frac{4\pi\sigma \cos\theta}{\lambda} \tag{14}$$

where σ is the standard deviation of the surface variation. Although there is no sharp change from a smooth to rough surface, a criterion often used as a dividing line is the Rayleigh criterion which states that a smooth earth satisfies the following inequality

$$q < \frac{\pi}{2} \tag{15}$$

If the surface variations are normally distributed, then it can be shown (see Reference 2, pages 80-89) that for a flat, perfectly reflecting surface, the fraction of the incident power which is reflected as coherent radiation is given by a coherency factor, ρ, defined by

$$\rho = e^{-q^2} \tag{16}$$

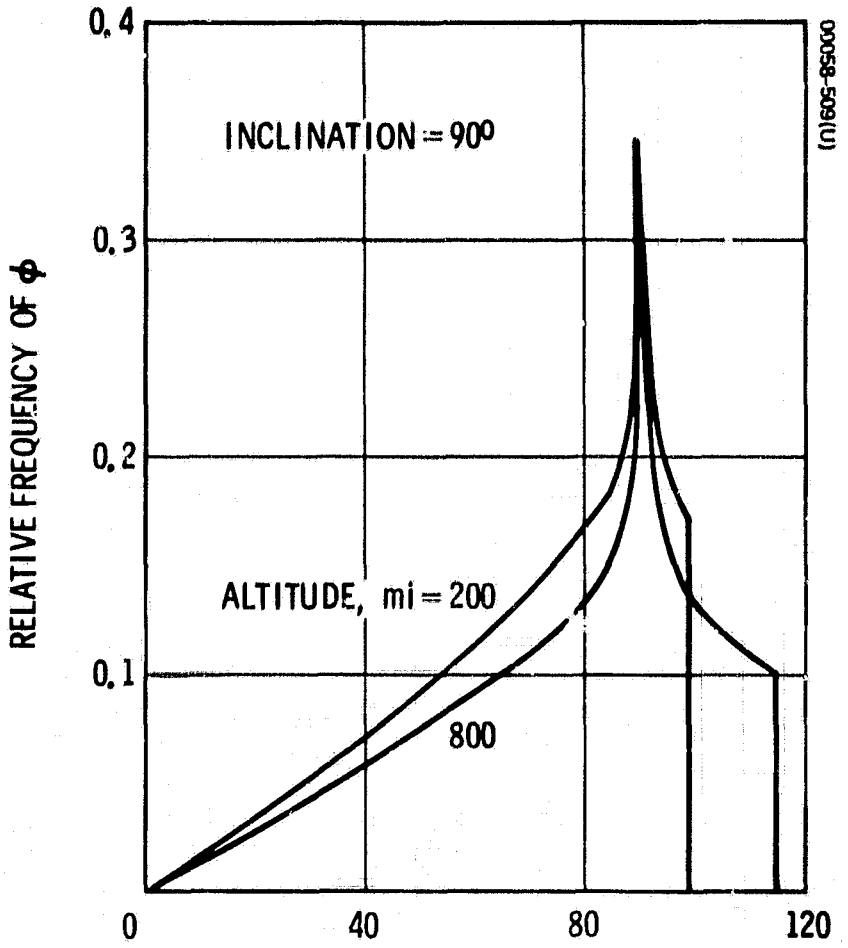

Figure 2-10. Relative Frequency of ϕ for Inclination of 90 Degrees

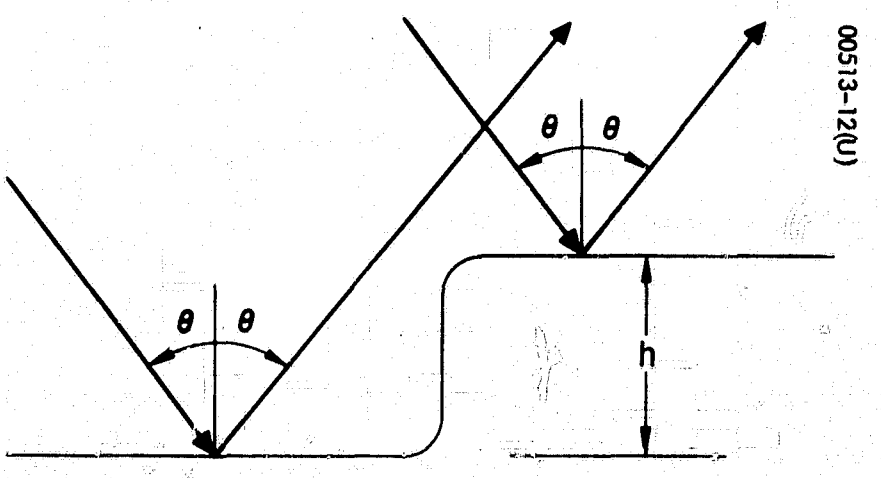

Figure 2-11. Basic Surface Variation Geometry

Thus, a surface satisfying the Rayleigh criterion for smoothness may reflect only 8.5 percent of the incident radiation coherently.

A more restrictive smoothness criterion might require that the portion of the incident power coherently reflected by a smooth surface be at least 90 percent. This leads to a criterion for smoothness of:

$$q < 0.324 \tag{17}$$

Similarly, a restrictive criterion for a rough surface might require that the portion of the incident power coherently reflected by a rough surface be no more than 10 percent. This leads to a criterion for roughness of:

$$q > 1.52 \tag{18}$$

The region $0.324 < q < 1.52$ can be considered a transition region, both specular and diffuse scattering being present.

The Beaufort sea state scale is presented in Table 2-1 where wind speed and the rms surface variation, σ, are related. Figure 2-12 shows the surface smoothness factor, q, as a function of σ and incidence angle for the VHF frequency of 140 MHz. The values of rms surface variation used for this figure correspond to those of Table 2-1. It can be seen that, for most sea states, the surface is not smooth except at very large incidence angles, and for most of the higher sea states, the surface is rough for a wide range of incidence angle. But, for values of σ between 0.03 and 0.5 meters, the surface roughness lies in the transition region, causing the reflected radiation to have both coherent and incoherent components. For higher frequencies, the earth appears rougher and the reflected power will be principally incoherent for all sea states and all angles except near grazing.

Modeling of rough surfaces based upon assumed surface statistical properties has been successfully attempted for three roughness conditions:

1) $q = 0$

2) $0 < q < 1$

3) $q > 2.14$

Barrick and Peake (Reference 4) develop expressions for reflected power corresponding to $0 < q < 1$ without using the Kirchoff approximation required by Beckmann (Reference 2) and others. However, as is noted in Reference 4, these expressions are most applicable to backscattering, whereas LAS/DRS geometry leads principally to forward scattering, except at small separation angles. And, for the frequencies of interest in this study, i.e., $f \geq 136$ MHz, the earth's surface will appear to be very rough ($q > 2$) most of the time for

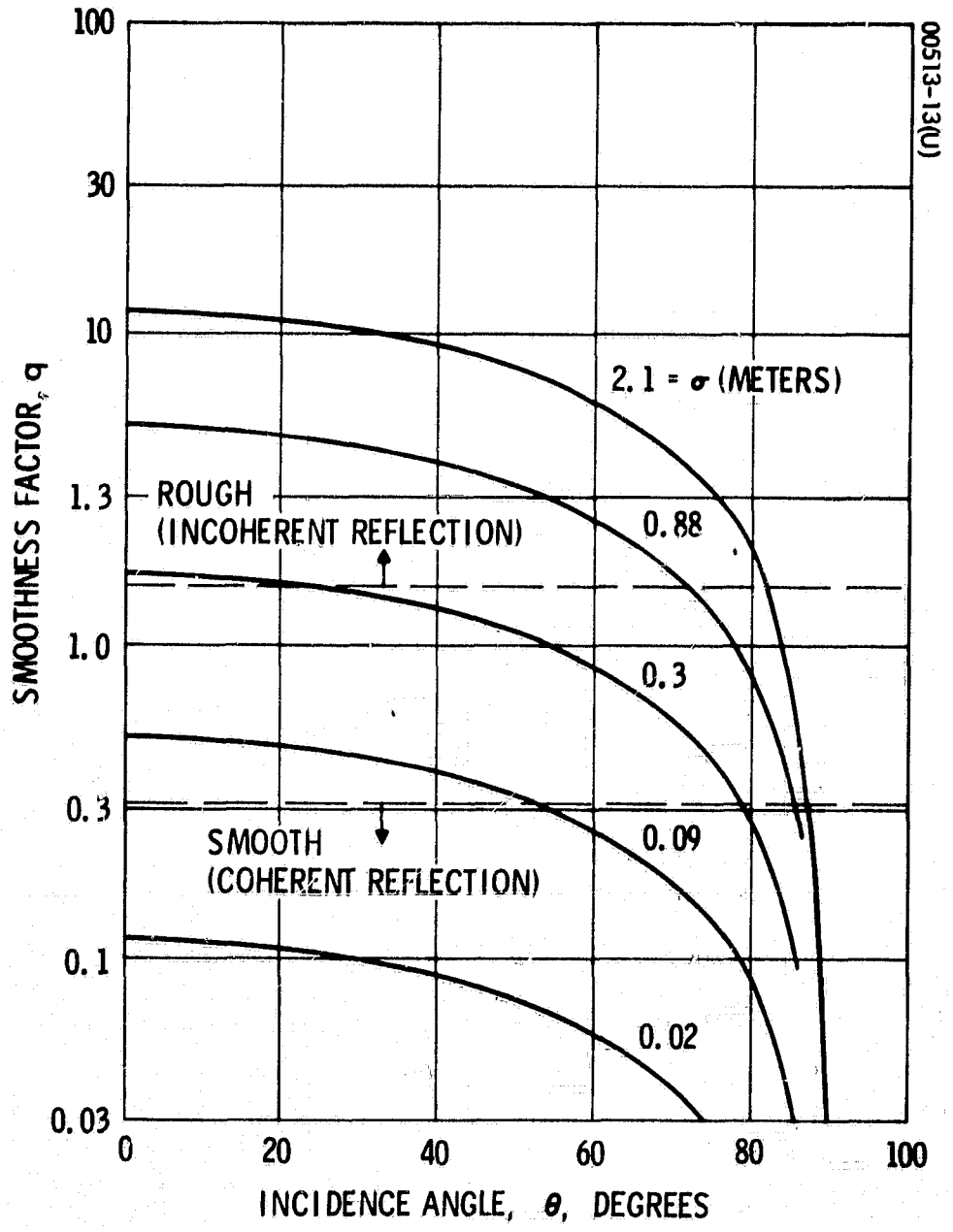

Figure 2-12. Smoothness Factor, q, for f = 140 MHz

TABLE 2-1. RELATIONSHIP AMONG BEAUFORT SEA STATE SCALE, WIND SPEED, AND RMS SURFACE VARIATION

Beaufort Sea State Scale	Wind Speed, knots	RMS Surface Variation, σ, meters
1	1-3	0.02
2	4-6	0.09
3	7-10	0.30
4	11-16	0.88
5	17-21	2.1
6	22-27	4.0
7	28-33	7.0
8	34-40	11.3
9	41-47	17.4
10	48-55	25.2
11	56-63	35.0

small separation angles. Thus, only two models are used in this study: the slightly rough model of Reference 2, which includes perfectly smooth conditions, and a very rough model developed and discussed in References 2, 8, 9, and 13. It is felt that intermediate conditions can be estimated from the results of these two models. Each model consists of a single mathematical expression for the ratio of received reflected power and received direct power. For convenient reference, the models will be called smooth and rough earth models, respectively.

2.3 SMOOTH EARTH

First consider reflection from a smooth plane surface. There is no simple rule for computing the exact fields reflected by such a surface, but an approximate field may be obtained as follows. When the source of the waves is far from the reflecting plane, the incident waves are substantially plane waves over any limited area. Because the angle at which a plane wave is reflected by the surface is equal to the angle of incidence, the reflected wave appears to come from an image source (Reference 2). Referring to

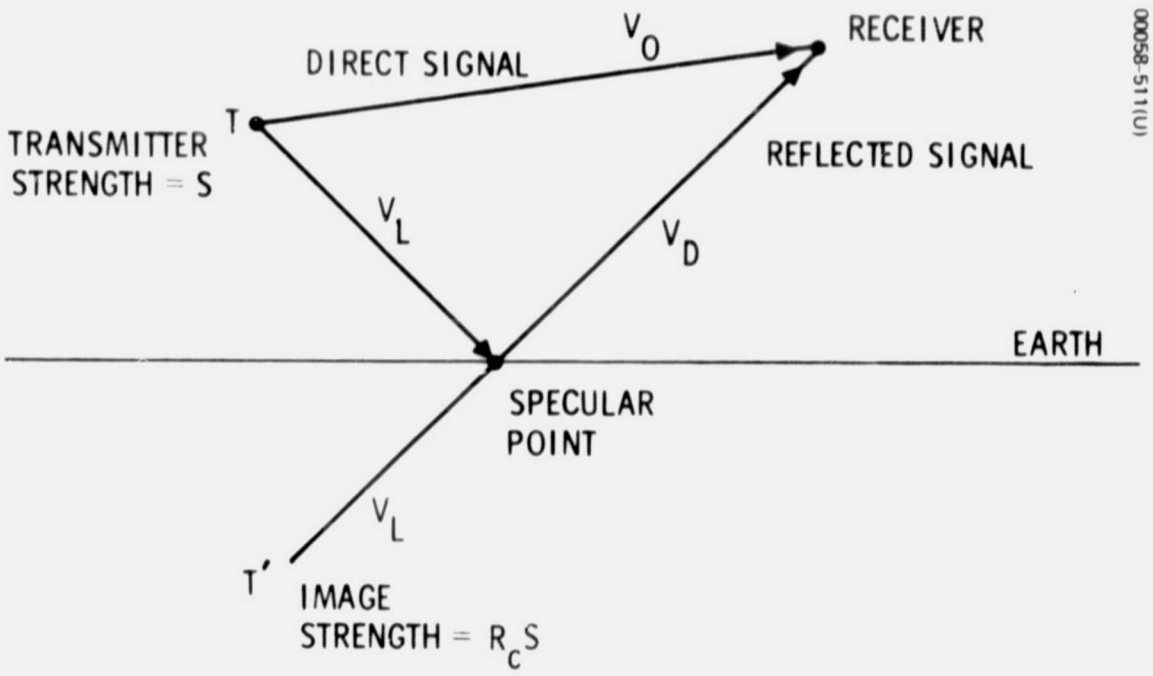

Figure 2-13. Reflection From a Smooth Flat Earth

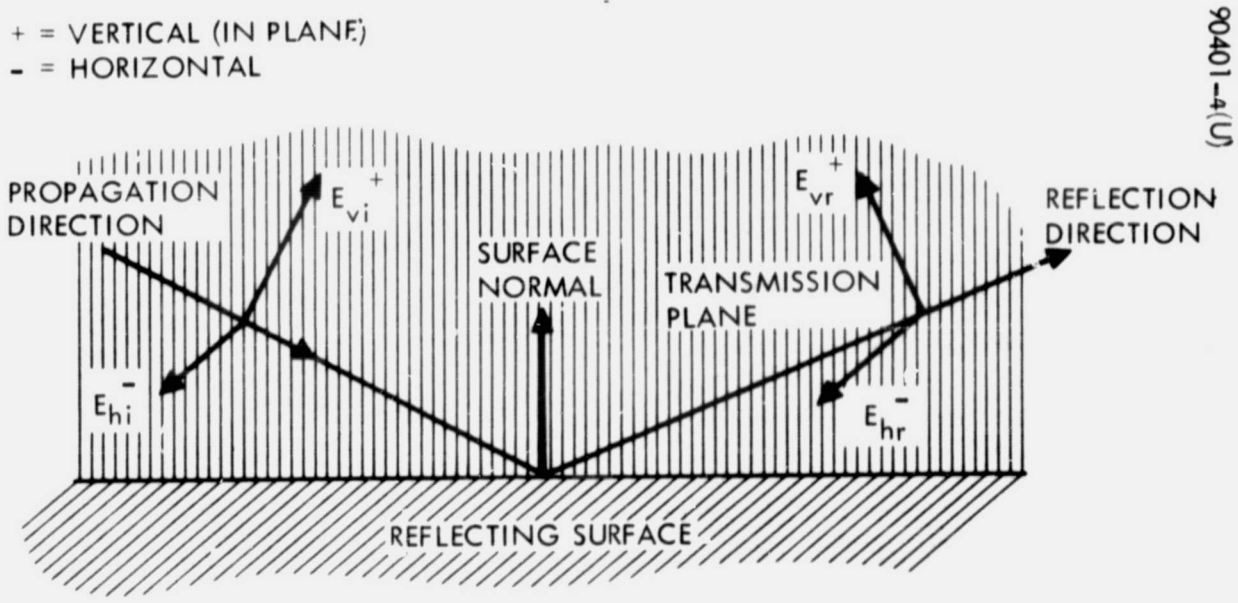

Figure 2-14. Polarization Vector Components Defined With Respect to Transmission Plane

Figure 2-13, the source or transmitter is located at T, radiating a field of strength S. The image is located at T' and of strength R_c times S, where R_C is the surface reflection coefficient which depends on the angle of incidence and polarization of the wave. This is the same result obtained by ray theory or geometrical optics which are based on the assumption that the electromagnetic fields behave locally as plane waves.

Assuming for the moment that the electromagnetic field is a scalar quantity, the equations for the received direct and reflected signals are given, respectively, by

$$P_d = \frac{G_1 G_2 \lambda^2}{(4\pi)^2 V_o^2} P \tag{19}$$

$$P_r = \frac{G_3 G_4 \lambda^2}{(4\pi)^2 (V_L + V_D)^2} P \left|R_c\right|^2 \tag{20}$$

where G_1 is the gain of the transmitting antenna in the direction of the direct path; G_2 is the gain of the receiving antenna in the direction of the direct path; P is the transmitted power; λ is the wavelength; G_3 is the gain of the transmitting antenna in the direction of the reflection path; G_4 is the gain of the receiving antenna in the direction of the reflection path; R_c is the Fresnel reflection coefficient; and V_L, V_D, and V_o are defined in Figure 2-13.

Electromagnetic fields can be represented as vectors, and the reflection of electromagnetic plane waves is dependent on the polarization of the EM wave where polarization refers to the orientation of the vector representing the electric field, E. When considering reflection from a smooth surface, this direction is most conveniently referenced to the transmission plane, i.e., the plane containing the incoming propagation direction, the surface normal, and reflection propagation direction.

Referring to Figure 2-14, the polarization of an EM wave with respect to the reflecting surface and transmission plane is defined. The horizontally polarized plane wave's electric field is perpendicular to the transmission plane, while the vertically polarized component lies in this plane. Note, Figure 2-13 shows that, by convention, the component of E_{vi} (the incident vertical field), which is parallel to the reflecting surface, changes direction upon reflection. All other field components remain in their original direction. Using these conventions with Equations 16 or 17, only the Fresnel reflection coefficients are needed to compute the received power.

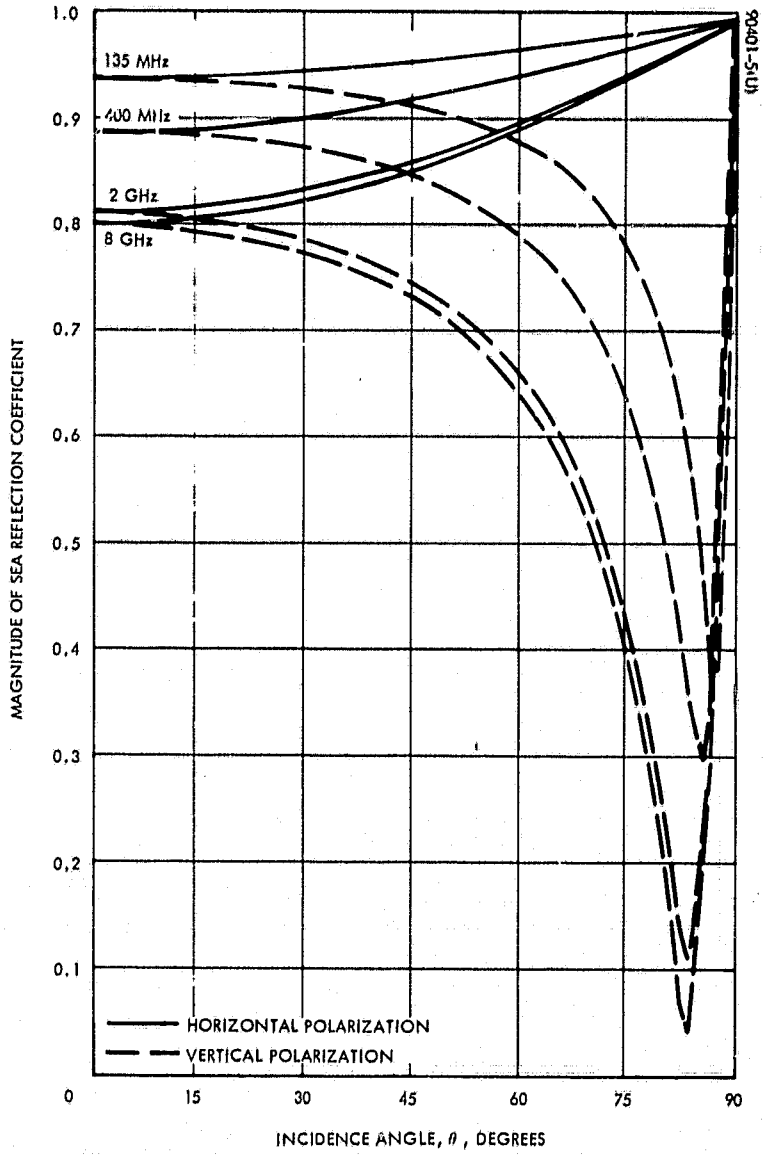

Figure 2-15. Magnitude of Sea Reflection Coefficients

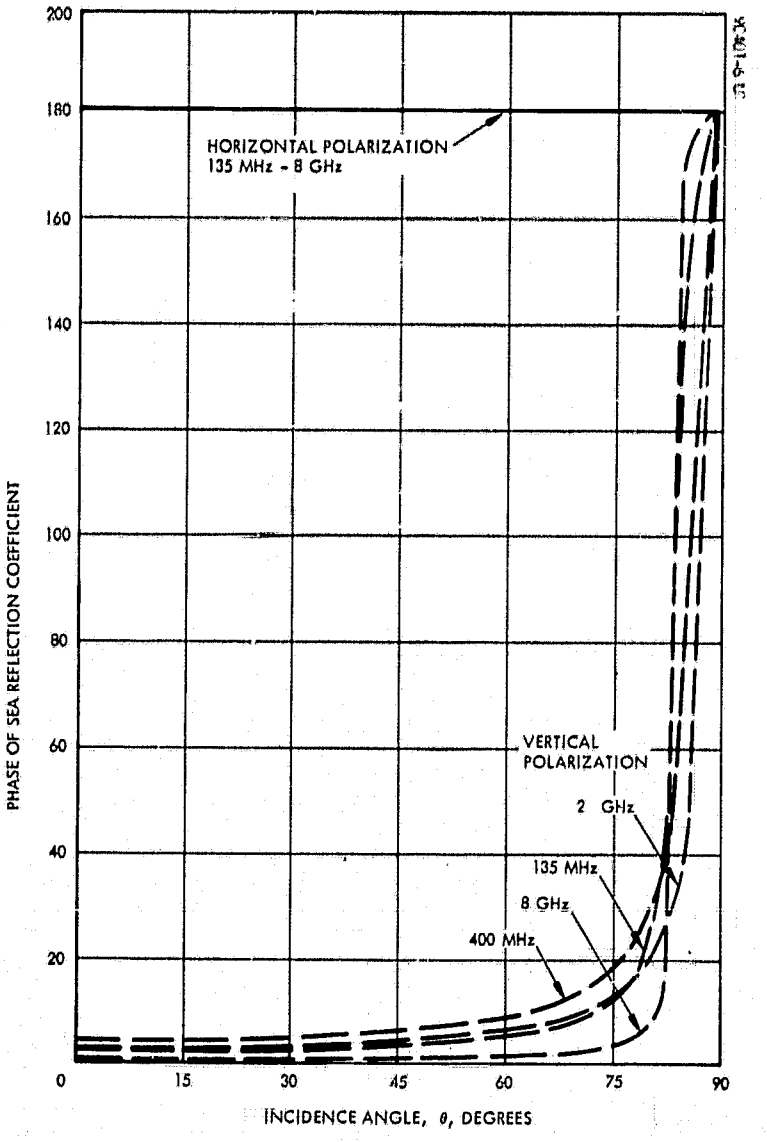

Figure 2-16. Phase of Sea Reflection Coefficients

2.3.1 Reflection Coefficients

A theoretical expression for the reflection coefficient of a plane earth may be obtained directly from Maxwell's equations. The earth is characterized by its relative complex dielectric constant, ϵ'.

$$\epsilon' = \frac{\epsilon}{\epsilon_o} - 60\, j\lambda c \tag{21}$$

where ϵ is the earth's dielectric constant, c is the earth's conductivity, ϵ_o is the free space dielectric constant, and λ is the free space wavelength. The reflection coefficients of a smooth plane earth surface are then given by:

Vertical polarization:

$$R_v = \frac{\epsilon' \cos\theta - \sqrt{\epsilon' - \sin^2\theta}}{\epsilon' \cos\theta + \sqrt{\epsilon' + \sin^2\theta}} \tag{22a}$$

Horizontal polarization:

$$R_h = \frac{\cos\theta - \sqrt{\epsilon' - \sin^2\theta}}{\cos\theta + \sqrt{\epsilon' + \sin^2\theta}} \tag{22b}$$

where θ is the angle of incidence.

Figures 2-15 through 2-18 show the magnitude and phase of R_h and R_v as a function of the incidence angle. For vertical polarization, the incidence angle where the reflection coefficient has minimum magnitude is called the Brewster angle.

From these curves, the following points are of interest:

1) The reflection coefficients for land are relatively independent of radio wave frequency (for the frequency range of interest in this study).

2) The pseudo-Brewster angle is 72 degrees for earth and between 82 to 85 degrees for sea in the frequency range of interest.

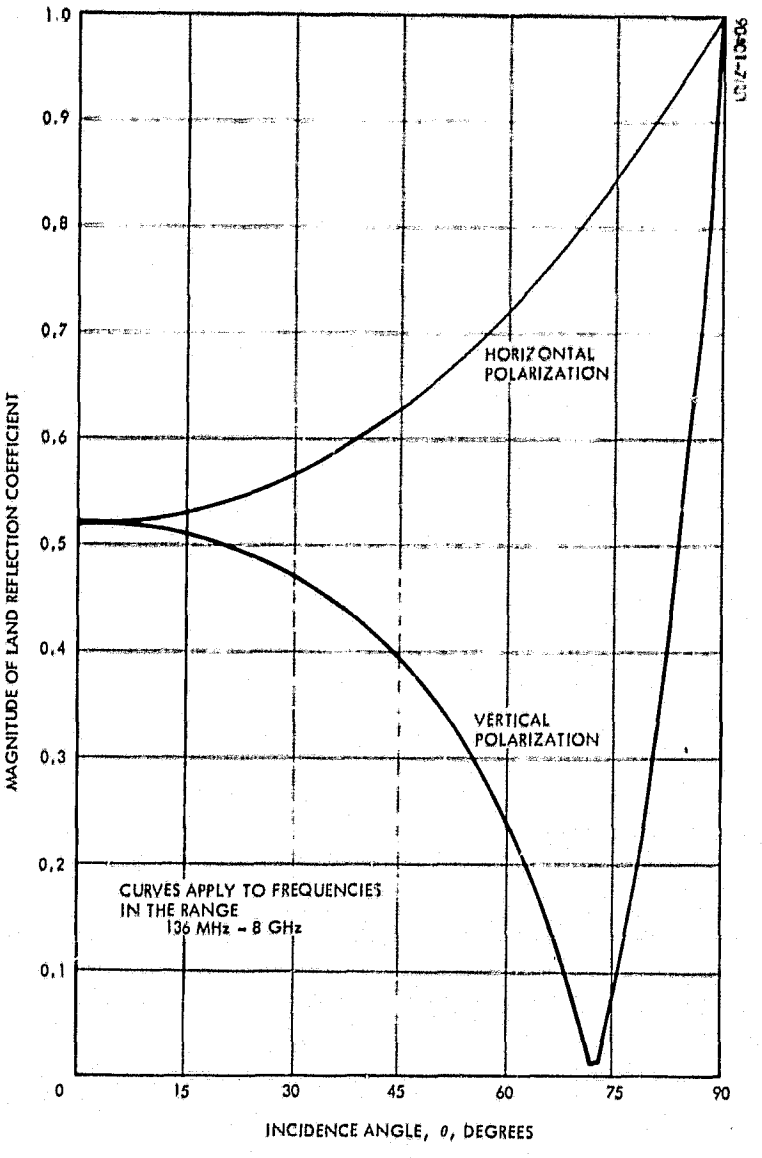

Figure 2-17. Magnitude of Land Reflection Coefficients

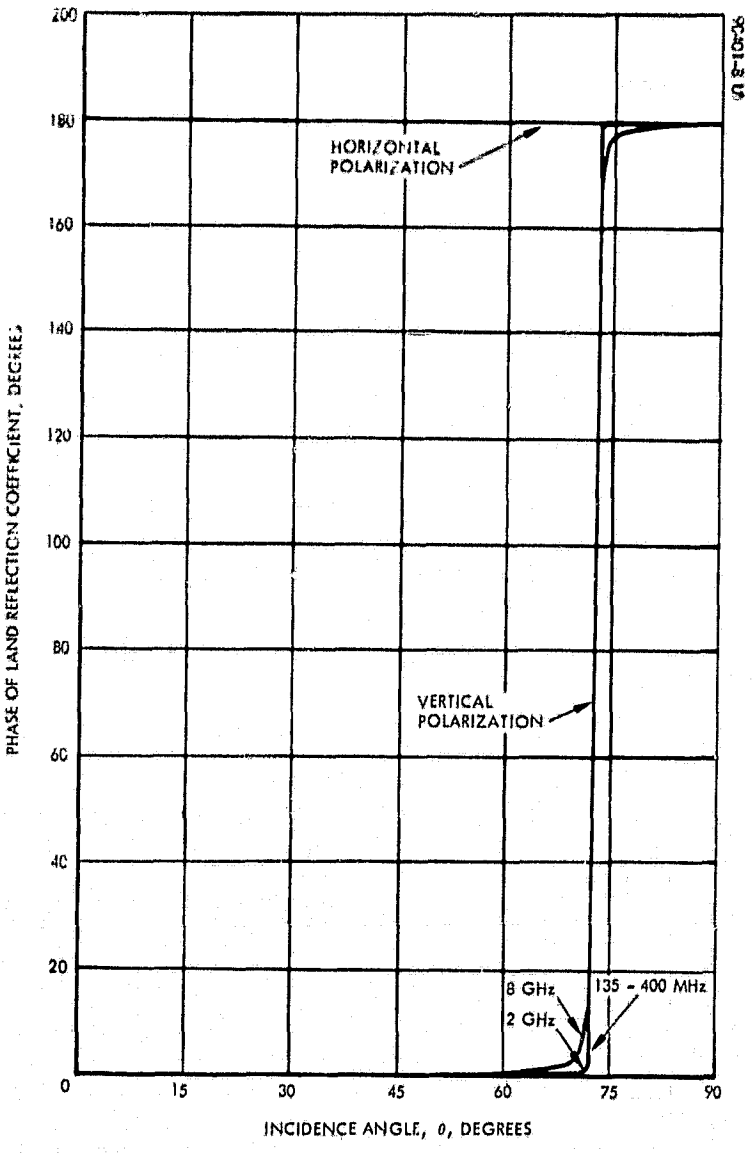

Figure 2-18. Phase of Land Reflection Coefficients

3) For angles of incidence less than the pseudo-Brewster angle, the angle of the horizontal reflection coefficient is near 180 degrees and the angle of the vertical reflection coefficient is near 0 degrees. Thus, for angles of incidence less than the pseudo-Brewster angle, the horizontal and vertical reflection coefficients differ by approximately 180 degrees, which means a predominantly right circularly polarized wave will be reflected as a predominantly left circularly polarized wave.

4) For angles of incidence less than the pseudo-Brewster angle, the reflection coefficients of the sea are greater than the reflection coefficients of the land.

2.3.2 Divergence Factor

To this point, the model used in analyzing the reflection of EM waves by the smooth earth assumed the earth was an infinite smooth plane. A divergence factor, D, may be defined to account for the earth's curvature. It is defined as the ratio of the power reflected by the spherical earth to the power reflected by an infinite plane.

Referring to Figure 2-4, simple geometric calculations lead to a divergence factor given by (see Reference 2):

$$D = \frac{1}{(1+\xi)(1+\xi/\cos\theta)} \tag{23}$$

where

$$\xi = \frac{2V_{LS}\,V_{DS}}{R_E\,(V_{LS}+V_{DS})} \tag{24}$$

R_E is the radius of the earth.

A more precise analysis by Bremmer (Reference 17) gives the divergence factor D as

$$D = \frac{1}{1+\xi\,(1+\cos^2\theta)/\cos\theta+\xi^2} \tag{25}$$

In later numerical computation, the more accurate Equation 25 is used. Figure 2-19 shows the divergence factor as a function of separation angle and LAS altitude.

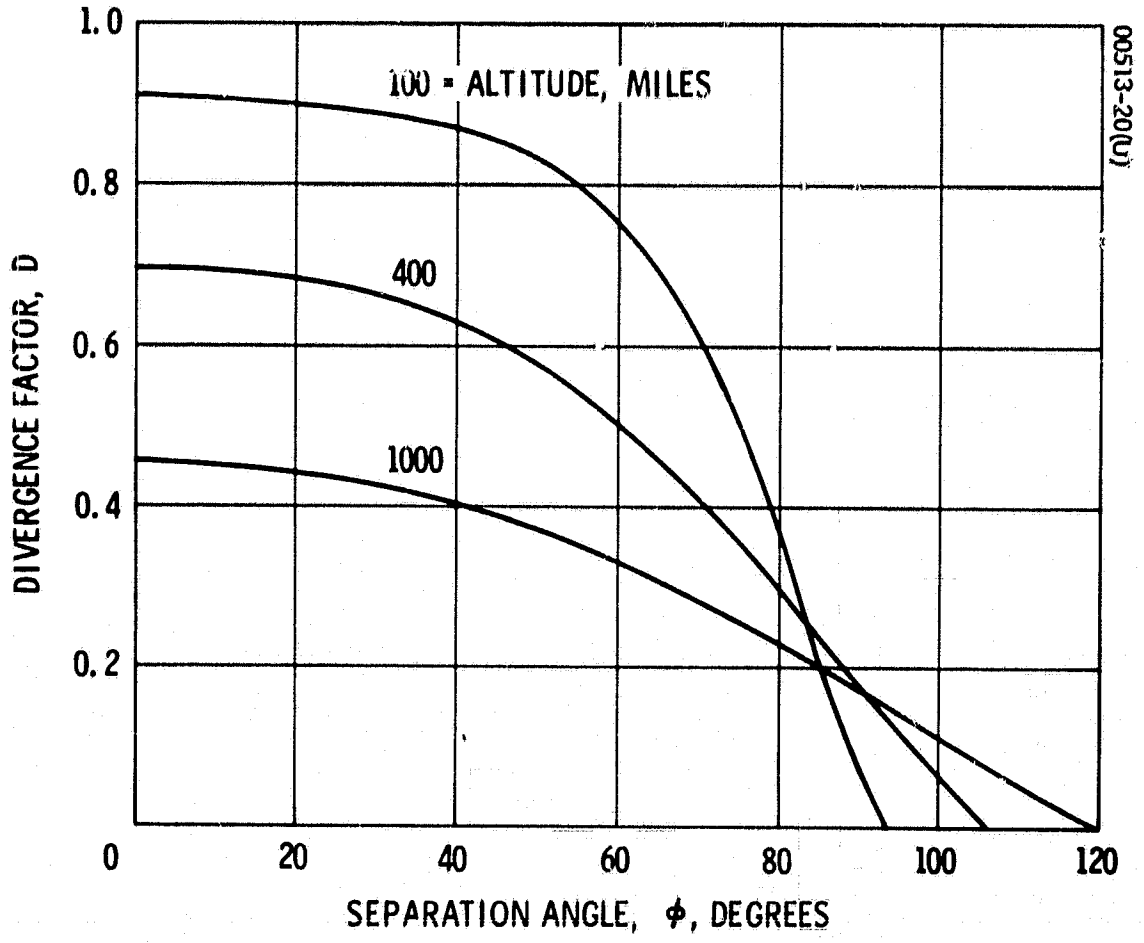

Figure 2-19. Divergence Factor as Determined by Bremmer

2.3.3 Slightly Rough Surface

It is shown in Reference 2 that, for a slightly rough surface where $q \ll 1$, a major portion of the incident power is reflected coherently in the specular direction. The major additional assumption is that the radii of curvature of the surface be much larger than a wavelength, i.e., that the surface consists of large-scale undulations. This condition is common for the sea, which presents the most serious multipath problems due to its highly reflective properties. If, in addition, the surface variation has a gaussian probability distribution, the power reflected by a slightly rough surface may be estimated by multiplying the smooth surface reflected power by a roughness coefficient which is identical to the coherency factor, ρ, defined by Equation 16.

2.3.4 Relative Power

For evaluating the effect of earth reflection on the LAS/DRS communication link, the relative magnitudes of the direct and reflected power are of principal interest. The reflected power may be normalized to the direct power by defining the relative power, R_p, as the ratio of the two. Including the divergence factor and roughness coefficient, the relative power is given by

$$R_p = \frac{P_r}{P_d} = \left(\frac{G_3\, G_4}{G_1\, G_2}\right) \left[\frac{V_o^{\,2}}{(V_L + V_D)^2}\right] \rho D \left|R_c\right|^2 \qquad (26)$$

Numerical results using Equations 16, 21, 22, 25, and 26 are presented in Section 3.

Equation 26 represents the smooth earth model where slight roughness is included, i.e., smooth here means not rough ($q < 1$).

2.4 ROUGH EARTH

The scattering of electromagnetic waves by a rough surface ($q \gg 1$) is treated extensively in References 2, 4, 8, 9, 12, and 13. The specific problem of interest in this study was also the subject of Reference 14. But, in the process of arriving at a formula for the relative power for the rough earth case, the authors made many approximations, some of which are not accurate for all values of the geometric parameters. The approach in this study is to use the reflected power expression derived in Reference 2, but, whereas the authors of Reference 14 began their approximation of the required integration starting with this formula, the intent here is to perform this integration numerically via machine computation without approximation.

In addition to assuming that the smoothness factor, q, is large, a second important assumption in the derivation of the reflected power formula is that the radii of curvature of the surface are large with respect to a wavelength. Although this condition is not always satisfied, especially for land, it is a common condition for the sea and for much land area. And since, as was mentioned in the previous subsection, the sea is the best earth surface reflector, this condition is not severely restrictive.

To develop an expression for the expected value of the total received reflected power, P_r, consider the power density, Φ, incident on a small scattering patch, dS. Φ is given by

$$\Phi = \frac{G_3 P}{4\pi V_L^2} \tag{27}$$

where G_3 is the transmitter antenna gain in the direction of the scattering patch, P is the radiated power, and V_L is the distance from the LAS to the scattering patch, as shown in Figure 2-7.

The expected value of the power reflected toward the DRS is defined in terms of a scattering cross section by

$$\langle dP_s \rangle = \Phi \, dC \tag{28}$$

where dC is the scattering cross section for the scattering patch dS and is defined below. Using Equations 27 and 28, the expected value of the received power, P_r, reflected from dS is given by

$$\langle dP_r \rangle = \frac{G_3 G_4 \lambda^2 P}{(4\pi)^3 V_L^2 V_D^2} dC \tag{29}$$

where G_4 is the receiver antenna gain in the direction of dS, and V_D is the distance from this patch to the DRS. As in the previous subsection, the quantity of major interest is the relative power, defined for a rough surface as the expected value (average) of the ratio of received reflected power to received direct power. Combining Equations 19 and 29

$$R_P = \left\langle \frac{P_r}{P_d} \right\rangle = \frac{\langle P_r \rangle}{P_d} = \frac{V_o^2}{4\pi G_1 G_2} \int_S \frac{G_3 G_4}{V_L^2 V_D^2} dC \tag{30}$$

where S represents the total surface area common to the view of both vehicles.

2.4.1 Scattering Cross-Section

If the surface variation is considered to have random characteristics, which appears to be a good assumption for a large area, then determination of the scattering cross section requires statistical analysis. The details of the required analysis are presented in Reference 2 and will not be repeated here. It is shown in Reference 2 that a statistical distribution of the surface variation about a mean value is sufficient for determining radiation fields. But this distribution does not describe the surface completely because it does not account for the separation of the peaks and valleys. A second function, the autocorrelation function, may be used to describe this aspect of the surface and is necessary for determining the average reflected power. In this study, the following two assumptions are made about the nature of these two functions:

1) The surface height variation about a zero mean value is distributed according to the gaussian density function

$$p(z) = \frac{1}{\sigma\sqrt{2\pi}} e^{-z^2/2\sigma^2}$$

where σ is the standard deviation or rms variation value defined in Subsection 2.2. For this study, this distribution is assumed to apply over the entire surface of each elemental scattering patch.

2) The surface autocorrelation function is given by

$$A(x) = e^{-x^2/T^2}$$

where x represents the distance between two surface points, and T is a constant called the correlation distance.

An important point concerning the autocorrelation function is that it applies to any two points regardless of the angular orientation of the line segment between them; thus, the roughness is considered isotropic. The gaussian autocorrelation function is employed by Beckmann (Reference 2), Stogryn (Reference 9), Hagfors (Reference 11), Barrick (Reference 13), and others; but Fung and Moore (Reference 18) suggest a more complex function which they claim is better behaved. Although this function may be made to account for smaller scale roughness in addition to the large undulating roughness by introducing an additional parameter, it still behaves like a gaussian function for very large roughness $q \gg 1$. No experimental evidence has yet been

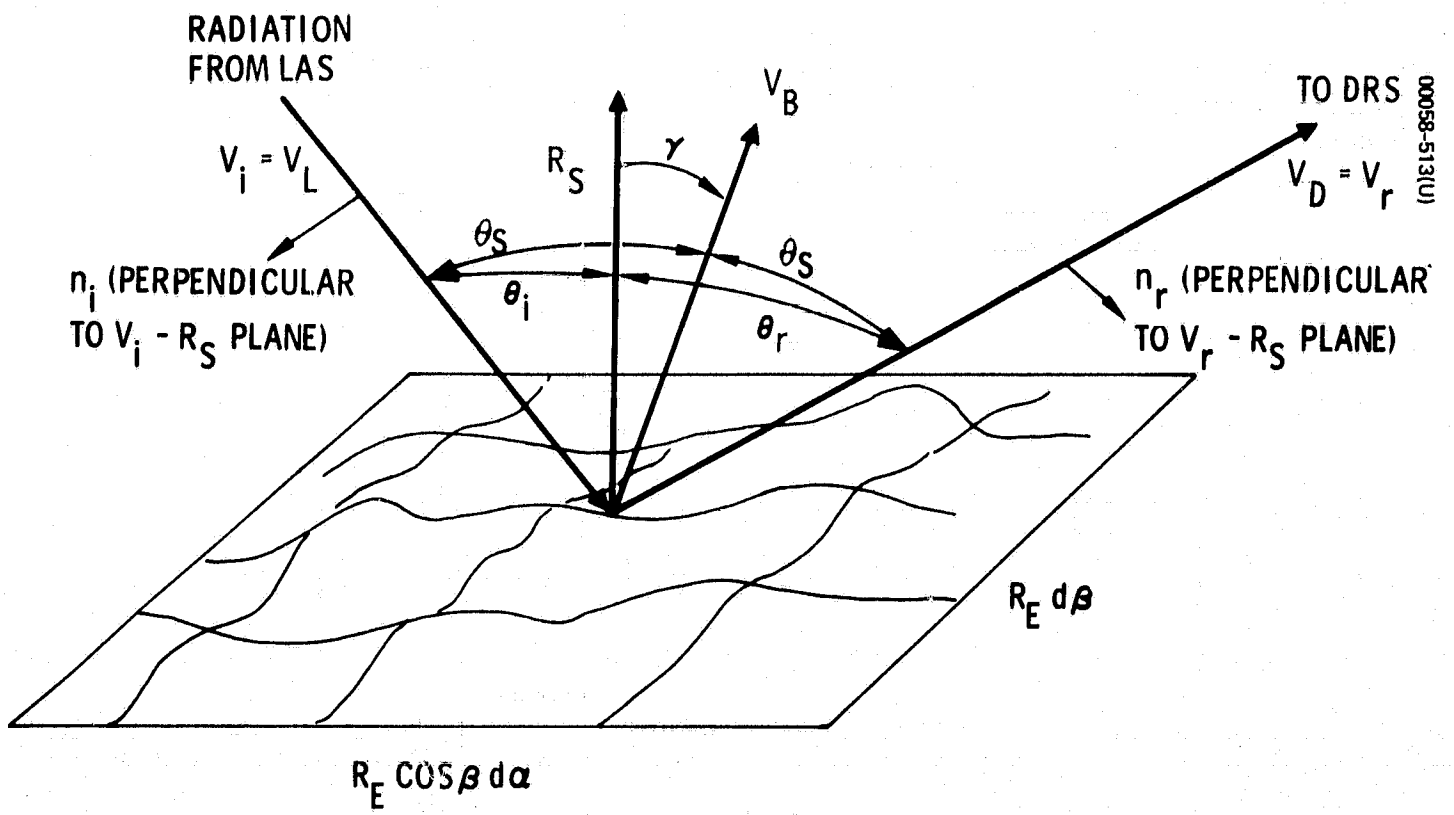

Figure 2-20. Scattering Patch of Area
$dS = R_E^2 \cos\beta d\alpha d\beta$

presented to verify the autocorrelation function of Fung and Moore, and, in addition, no single mathematical expression for the scattering cross-section is possible. Thus, the more tractable solution resulting from the above two statistical assumptions is used here.

Based upon this statistical description of the surface, a lengthy derivation, the details of which are given in Reference 2, yields the following expression for the scattering cross section, dC:

$$dC = \frac{|R_c|^2}{\eta^2 \cos^4 \gamma} \exp\left(-\frac{\tan^2 \gamma}{\eta^2}\right) dS \qquad (31)$$

where R_c is the reflection coefficient corresponding to θ_s in Figures 2-7 and 2-20; γ is the angle between V_B; and the local vertical, R_s, as shown in Figure 2-20; dS is the area of the surface patch; and η is defined as the roughness factor given by

$$\eta = \frac{2\sigma}{T}$$

The roughness factor can be shown to be the rms value of the surface slope with respect to local horizontal.

The scattering cross section dC corresponding to the surface patch dS can be interpreted as the portion of the patch dS which is oriented in such a way as to provide specular reflection from the LAS to the DRS. From Figures 2-7 and 2-20, it can be seen that as the distance on the earth between dS and the specular point increases, the angle, γ, also increases and, hence, the scattering cross section decreases.

2.4.2 Shadowing

The derivation of Equation 31 assumes that every region of the surface patch, dS, contributes to the scattered fields. This assumption neglects the shadowing of a surface by itself, an effect that is very important at large angles of incidence which correspond to large satellite separation angles. Indeed, the shadowing effect reduces the scattered fields to zero at an angle of incidence of 90 degrees.

Several authors have treated the subject of shadowing. Beckmann (Reference 19) derives a shadowing function which yields the portion of a surface area not shaded, i.e., that portion which is illuminated by the incident radiation. This shadowing function involves the incidence angle, θ, and

roughness parameter, η, and it may be interpreted as the probability of a given point on the surface being illuminated. Beckmann claimed that this shadowing function should be included as a multiplicative factor in the expression for average reflected power given by Equation 29.

However, Brockelman and Hagfors (Reference 20) claim that the shadowing function should be the conditional probability that a point is illuminated given that the surface at that point is properly oriented for reflection. Probability fundamentals favor this latter approach. The probability that the surface at a point is properly oriented is given by $dC/dS|R_c|^2$ (see Equation 31). Thus, if

A = occurrence of properly oriented surface

B = occurrence of illumination (no shadowing)

then the probability that the surface at a point will be both properly oriented and unshaded is given by

$$P(A, B) = P(A)\, P(B/A)$$

where

$$P(A) = dC/dS|R_c|^2$$

$P(B/A)$ = shadowing function, S

If the two occurrences were independent, then $P(B/A) = P(B)$ and Beckmann's approach would be valid.

Brockelman and Hagfors were unable to develop a shadowing function appropriate to their approach, but both Smith (Reference 21) and Wagner (Reference 22) were successful. However, Smith considered only illumination of the surface by the transmitter, whereas Wagner included visibility by the receiver. If,

C = occurrence of visibility by receiver

Wagner's results yield the conditional probability $P(B, C/A)$. Thus, for the LAS/DRS reflection signal, Wagner's results are more applicable. Wagner's analysis treats reflection in two dimensions, but the results appear to be applicable to the three-dimensional reflection process of LAS/DRS communication.

Several new quantities must be defined. The angles θ_i and θ_r are shown in Figure 2-20 and may be calculated from

$$\cos \theta_i = \frac{-V_i \cdot R_s}{|V_i| \, |R_s|} \tag{32}$$

$$\cos \theta_r = \frac{V_r \cdot R_s}{|V_r| \, |R_s|} \tag{33}$$

Now define

$$\left.\begin{aligned} g_i &= \frac{\cot \theta_i}{\eta} \\ g_r &= \frac{\cot \theta_r}{\eta} \\ B_i &= \frac{1}{2}\left[\frac{1}{g_i\sqrt{\pi}} \exp\left(-g_i^2\right) - \operatorname{erfc}(g_i)\right] \\ B_r &= \frac{1}{2}\left[\frac{1}{g_r\sqrt{\pi}} \exp\left(-g_r^2\right) - \operatorname{erfc}(g_r)\right] \end{aligned}\right\} \tag{34}$$

Two cases must now be considered in calculating the probability of visibility by both the transmitter and receiver. This probability may be expressed as

$$P(B, C/A) = P(C/B, A)\, P(B/A)$$

Case I: Forward Scatter

Referring to Figure 2-20, if the angle between n_i and n_r is less than 90 degrees, then the reflection is called "forward scatter." For this case, Wagner assumes that visibility by the receiver is independent of visibility by the transmitter. This assumption is consistent with that made by others in their

analyses. The expression for the shadowing function, S, is then calculated by Wagner to be given by

$$S = \frac{u(\cot\theta_i' - \tan\gamma')\, u(\cot\theta_r' - \tan\gamma') \left(1 - e^{-(B_i+B_r)}\right)}{(B_i + B_r)}$$

where u( ) is the unit step function and θ_i', θ_r', and γ' are the angles between V_L, V_D, V_B and the projection of R_S onto the reflection plane. However, because of the geometric relationship which exists between V_L, V_D, R_S and V_B, $\tan\theta_i' > \tan\gamma'$ and $\tan\theta_r' > \tan\gamma'$ and, hence,

$$S = \frac{1 - e^{-(B_i+B_r)}}{(B_i + B_r)} \qquad (35)$$

Case II: Backscatter

Referring to Figure 2-20 if the angle between n_i and n_r is greater than 90 degrees, then the reflection is termed "backscatter" and

$$P(C/B, A) = 1$$

That is, if the point is visible from the LAS, then it is visible from the DRS. This is not strictly true for three-dimensional reflection, but, for LAS/DRS geometry, this case arises principally when the incidence angles are small. So both P(C/B,A) and P(B/A) will be nearly equal to unity. The shadowing function then becomes

$$S = P(B/A) = \frac{u(\cot\theta_i' - \tan\gamma') \left(1 - e^{-B_i}\right)}{B_i}$$

where, as before, $u(\cot\theta_i' - \tan\gamma') = 1$. Thus,

$$S = \frac{1 - e^{-B_i}}{B_i} \qquad (36)$$

The criterion for distinguishing between the above two cases is simple:

$$n_i \cdot n_r \geq 0 \rightarrow \text{Case I}$$

$$n_i \cdot n_r < 0 \rightarrow \text{Case II}$$

The shadowing function given by Equation 35 is plotted in Figure 2-21 for the specular point where $\theta_i = \theta_r$. Figure 2-22 shows the various probabilities defined above according to different authors as a function of $\theta = \theta_i = \theta_r$ for $\eta = 0.4$.

2.4.3 Divergence Factor

It should be noted here that this rough surface analysis does not include a divergence factor, and rightfully so. The divergence factor is proper for the smooth earth case, but for the rough earth, the earth's curvature is automatically accounted for by the geometrical computations implicit in the determination of γ, V_L, and V_D in Equation 31.

2.4.4 Relative Power

Combining Equations 30 and 31 and including the shadowing function, the relative power for a rough surface is given by

$$R_p = \frac{V_o^2}{4\pi G_1 G_2} \int_S \frac{G_3 G_4}{V_L^2 V_D^2} \frac{|R_c|^2 S(\theta)}{\eta^2 \cos^4 \gamma} \exp\left(-\frac{\tan^2 \gamma}{\eta^2}\right) dS \qquad (37)$$

This equation represents the rough earth model, but the effects of antenna polarization have not yet been considered. In the next two subsections, the effects of reflection on an arbitrarily polarized wave and the description of antenna characteristics are treated to provide more complete interpretation of R_c and the antenna gains.

2.5 DEPOLARIZATION

Equation 37 may be used to estimate the relative power for radiation which is polarized either vertically or horizontally with respect to the surface, i.e., for which the electric field vector is oriented parallel to or

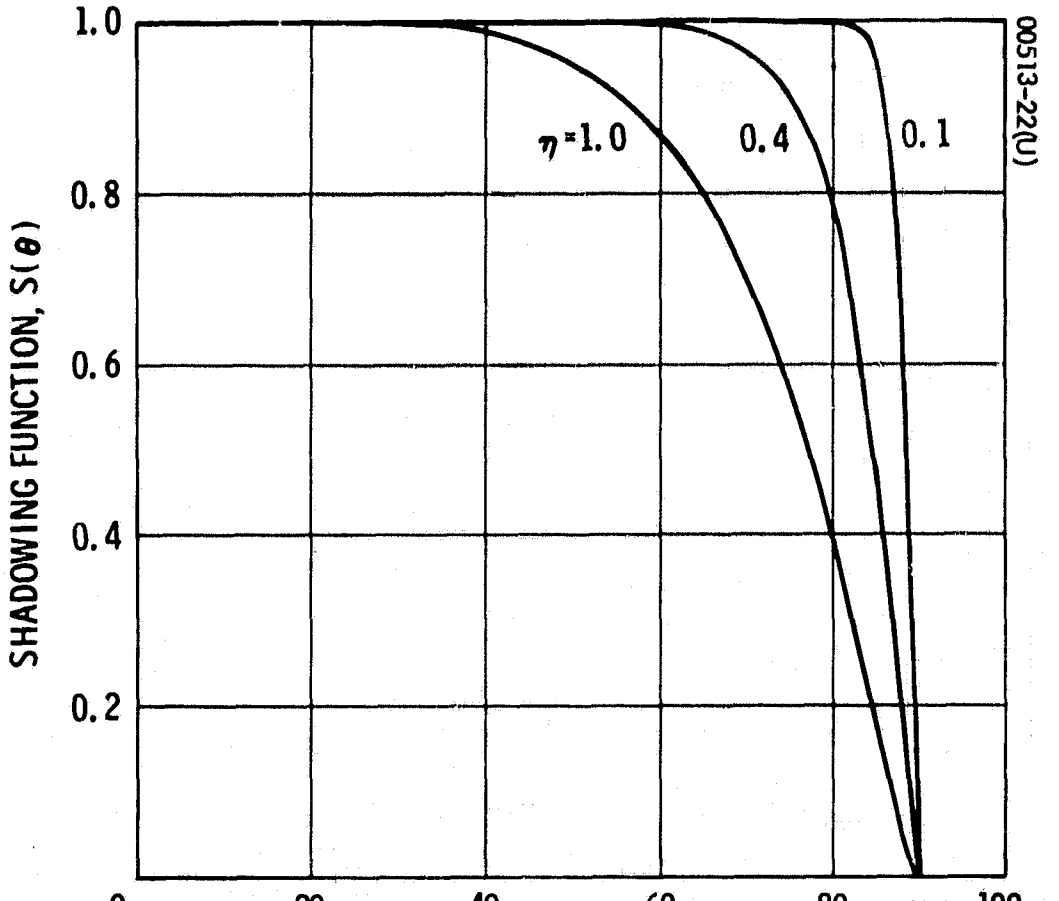

Figure 2-21. Shadowing Function
$S(\theta) = P(B, C/A)$

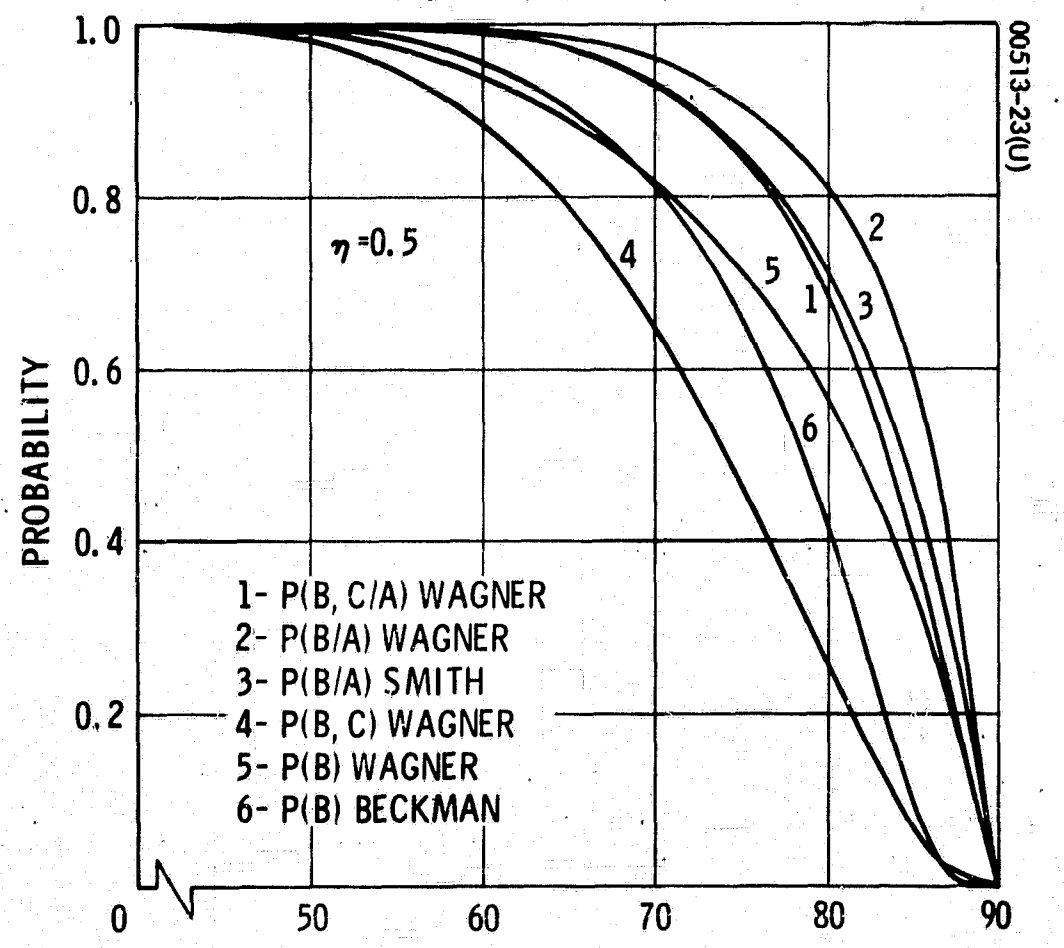

Figure 2-22. Probabilities of No Shadowing According to Several Authors

perpendicular to the reflection plane. For instance, for vertical polarization, the reflection coefficient, R_v, must be substituted for R_c, and the gains G_1, G_2, G_3, and G_4 must correspond to the respective antenna gains for this polarization. But, when the electric field vector is oriented arbitrarily with respect to the reflection plane, both reflection coefficients must be used in calculating the reflected wave, and the polarization of the reflected wave may be radically altered. This phenomenon is treated briefly in Reference 2, but the development and results are difficult to apply to the scattering problem of interest in this study.

To derive the depolarization equations, the three coordinate systems shown in Figure 2-23 will be used. The unit vectors are defined as follows: k_i lies along the incident propagation direction; e_{hi} is perpendicular to the plane containing k_i and the radius, R_S, from the earth's center to the reflecting point S; e_{vi} is orthogonal to k_i and e_{hi} as shown; s_3 coincides with the bisector of the angle between V_i and V_r; s_1 is perpendicular to the reflecting plane defined by V_i and V_r; s_2 lies in this plane orthogonal to s_1 and s_3; k_r lies along the reflection propagation direction to the receiver; e_{hr} is perpendicular to the plane containing k_r and R_S; and e_{vr} lies in this plane perpendicular to k_r. These definitions may be translated mathematically as follows:

$$k_i = \frac{V_i}{|V_i|} \qquad k_r = \frac{V_r}{|V_r|}$$

$$e_{hi} = \frac{k_i \times R_S}{|k_i \times R_S|} \qquad e_{hr} = \frac{k_r \times R_S}{|k_r \times R_S|} \qquad (38)$$

$$e_{vi} = e_{hi} \times k_i \qquad e_{vr} = e_{hr} \times k_r$$

$$s_3 = \frac{k_r - k_i}{|k_r - k_i|}$$

$$s_1 = \frac{V_i \times V_r}{|V_i \times V_r|} = \frac{k_i \times k_r}{|k_i \times k_r|} \qquad (39)$$

$$s_2 = \frac{k_r + k_i}{|k_r + k_i|}$$

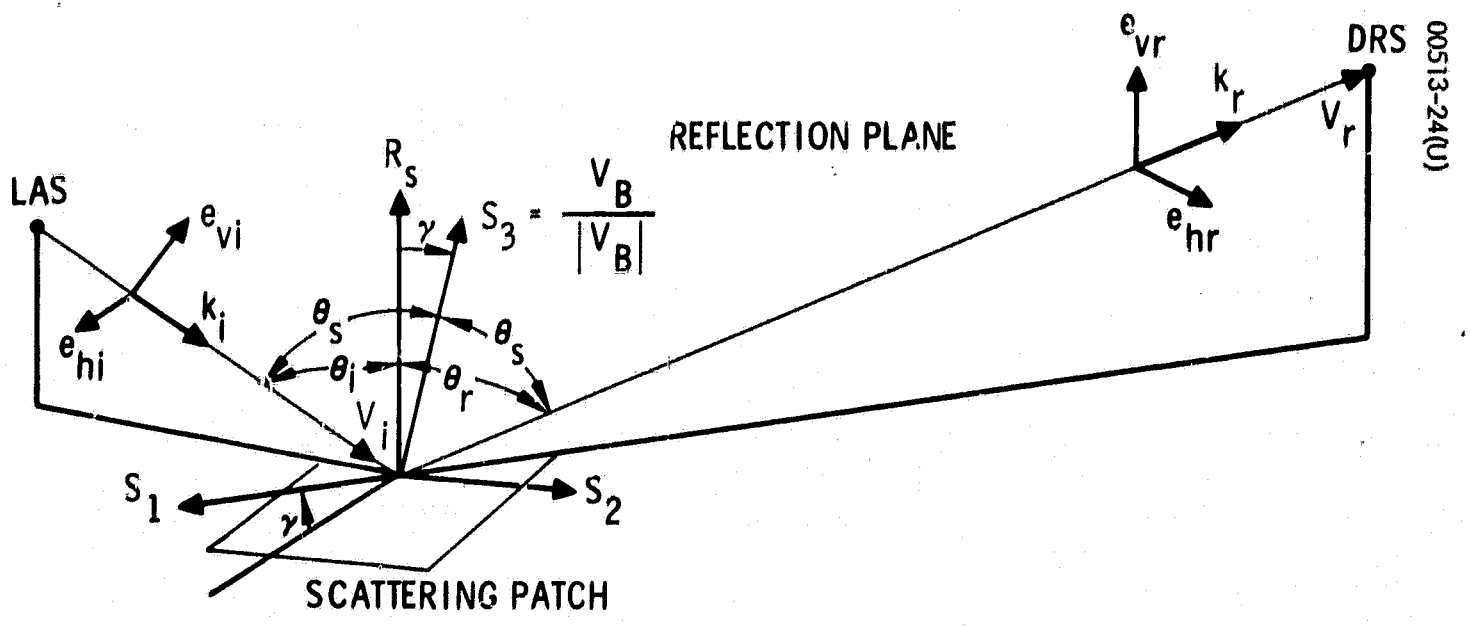

Figure 2-23. Depolarization Geometry

The electric field vector may be expressed in terms of the transmission unit vectors

$$\bar{E}_i = E_{hi}\, e_{hi} + E_{vi}\, e_{vi} \tag{40}$$

The quantities E_{hi} and E_{vi} are complex numbers defined by

$$E_{hi} = Q_{hi}\, e^{j(\omega t + \varphi_h)}$$

$$E_{vi} = Q_{vi}\, e^{j(\omega t + \varphi_v)}$$

For this analysis, the time varying base, $e^{j\omega t}$, can be omitted since only the relative phases between the two components are important. Thus,

$$E_{hi} = Q_{hi}\, e^{j\varphi_h} \qquad E_{vi} = Q_{vi}\, e^{j\varphi_v} \tag{41}$$

The first step in the development is to decompose E_i into components parallel to and perpendicular to s_3. It is useful also to maintain the identity of the original polarization directions in these components. Thus, the following definitions are made for the components of E.

E_{hhs} : perpendicular to s_3, originated from E_{hi}

E_{hvs} : parallel to s_3, originated from E_{hi}

E_{vhs} : perpendicular to s_3, originated from E_{vi}

E_{vvs} : parallel to s_3, originated from E_{vi}

It can be seen from the vector definitions of Figure 2-23 that

$$
\left.
\begin{aligned}
E_{hhs} &= E_{hi}\left[(e_{hi}\cdot s_1)\,s_1 + (e_{hi}\cdot s_2)\,s_2\right] \\
E_{hvs} &= E_{hi}\,(e_{hi}\cdot s_3)\,s_3 \\
E_{vhs} &= E_{vi}\left[(e_{vi}\cdot s_1)\,s_1 + (e_{vi}\cdot s_2)\,s_2\right] \\
E_{vvs} &= E_{vi}\,(e_{vi}\cdot s_3)\,s_3
\end{aligned}
\right\} \quad (42)
$$

In the reflection process, $\bar{E}_{hhs}$ and $\bar{E}_{vhs}$ require the reflection coefficient for horizontal polarization, R_h, while $\bar{E}_{hvs}$ and $\bar{E}_{vvs}$ require the vertical reflection coefficient, R_v. The next step is to apply the reflection coefficient to the vector field components of Equations 42 and then to express the field with respect to e_{hr} and e_{vr} coordinates. The following definitions will simplify the resulting expressions.

$$
\left.
\begin{aligned}
A_{hh} &= (e_{hi}\cdot s_1)\,(e_{hr}\cdot s_1) + (e_{hi}\cdot s_2)\,(e_{hr}\cdot s_2) \\
B_{hh} &= (e_{hi}\cdot s_3)\,(e_{hr}\cdot s_3) \\
A_{hv} &= (e_{hi}\cdot s_1)\,(e_{vr}\cdot s_1) + (e_{hi}\cdot s_2)\,(e_{vr}\cdot s_2) \\
B_{hv} &= (e_{hi}\cdot s_3)\,(e_{vr}\cdot s_3) \\
A_{vh} &= (e_{vi}\cdot s_1)\,(e_{hr}\cdot s_1) + (e_{vi}\cdot s_2)\,(e_{hr}\cdot s_2) \\
B_{vh} &= (e_{vi}\cdot s_3)\,(e_{hr}\cdot s_3) \\
A_{vv} &= (e_{vi}\cdot s_1)\,(e_{vr}\cdot s_1) + (e_{vi}\cdot s_2)\,(e_{vr}\cdot s_2) \\
B_{vv} &= (e_{vi}\cdot s_3)\,(e_{vr}\cdot s_3)
\end{aligned}
\right\} \quad (43)
$$

Then

$$\left.\begin{aligned} E_{hhr} &= E_{hi}\,(R_h\,A_{hh} + R_v\,B_{hh}) = E_{hi}\,K_{hh} \\ E_{hvr} &= E_{hi}\,(R_h\,A_{hv} + R_v\,B_{hv}) = E_{hi}\,K_{hv} \\ E_{vhr} &= E_{vi}\,(R_h\,A_{vh} + R_v\,B_{vh}) = E_{vi}\,K_{vh} \\ E_{vvv} &= E_{vi}\,(E_h\,A_{vv} + R_v\,B_{vv}) = E_{vi}\,K_{vv} \end{aligned}\right\} \quad (44)$$

where E_{hi}, E_{vi}, R_h, and R_v are complex numbers. The received electric field vector is given by

$$\begin{aligned} \bar{E}_r &= (E_{hhr} + E_{vhr})\,e_{hr} + (E_{vvr} + E_{hvr})\,e_{vr} \\ &= E_{hr}\,e_{hr} + E_{vr}\,e_{vr} \end{aligned} \quad (45)$$

Equations 44 preserve the depolarization process in that E_{hvr} is the component of the reflected electric field in the e_{vr} direction , which originated from the e_{hi} component of the transmitted field.

2.5.1 Polarization Factor

A convenient method for describing the field is via a polarization factor, P, defined by

$$P = \frac{E_v}{E_h} \quad (46)$$

since E_v and E_h are components in some coordinate system, P is also referenced to that coordinate system. For instance, from Equation 41

$$P_i = \frac{E_{vi}}{E_{hi}} = \frac{G_{vi}}{G_{hi}}\,e^{j(\varphi_v - \varphi_h)} \quad (47)$$

represents the polarization of the transmitted field with respect to the k_i, e_{hi}, e_{vi} coordinates. And

$$\bar{E}_i = E_{hi}(P_i\, e_{vi} + e_{hi}) \tag{48}$$

From Equation 45, it can be seen that

$$P_r = \frac{E_{vr}}{E_{hr}} = \frac{E_{vvr} + E_{hvr}}{E_{hhr} + E_{vhr}} \tag{49}$$

Using Equations 44 and 46, P_r can be expressed as a function of P_i.

$$P_r = \frac{P_i(R_h A_{vv} + R_v B_{vv}) + R_h A_{hv} + R_v B_{hv}}{P_i(R_h A_{vh} + R_v B_{vh}) + R_h A_{hh} + R_v B_{hh}} = \frac{P_i K_{vv} + K_{hv}}{P_i K_{vh} + K_{hh}} \tag{50}$$

Since most of the reflected power is reflected from the earth's surface near the transmission plane defined in Subsection 2.1, a special case of interest occurs for smooth earth geometry when V_i, V_r, and R_S of Figure 2-23 are all coplanar, i.e., when the incident and reflected power both lie in the transmission plane. For this case e_{hi}, s_1, and e_{hr} are parallel and e_{vi}, e_{vr}, s_3, and s_2 lie in the transmission plane. It can be shown that

$$A_{hh} = 1$$

$$B_{hh} = A_{hv} = B_{hv} = A_{vh} = B_{vh} = 0$$

$$A_{vv} = -\cos^2\theta$$

$$B_{vv} = \sin^2\theta$$

and so Equation 50 reduces to

$$P_r = P_i \left(\frac{R_v}{R_h} \sin^2 \theta - \cos^2 \theta \right) \tag{51}$$

When $\theta \approx 90$ degrees, it can be seen from Figures 2-15 and 2-16 that $R_v \approx R_h$; thus, $P_r \approx P_i$, and the two coordinate systems coincide. Consequently, the polarization is unchanged. When $\theta \approx 0$ degrees, $P_r = -P_i$, thus the reflected polarization is 180 degrees different in phase with respect to the receiver coordinates than that which was transmitted. Then, for instance, if the LAS is transmitting a right circularly polarized wave omnidirectionally away from the spacecraft (a hypothetical case for illustration only), and the DRS is "overhead" ($\varphi = 0$, $\theta \approx 0$), then the wave reflected toward the DRS will be left circularly polarized. This phenomenon allows the possibility of discrimination between the direct and reflected signals and is discussed further in Section 4.

2.5.2 Power Reflection Coefficient

For a general polarization, a power reflection coefficient, Γ_r, can be defined. This reflection coefficient replaces the quantity $|R_c|^2$ in Equations 26 and 37 and is defined by

$$\Gamma_r = |R_c|^2 = \frac{\text{specularly reflected power}}{\text{incident power}}$$

$$= \frac{|E_{hr}|^2 + |E_{vi}|^2}{|E_{hi}|^2 + |E_{vi}|^2}$$

From the definitions of the polarization factors given by Equations 47 and 49

$$\Gamma_r = \frac{|E_{hr}|^2}{|E_{hi}|^2} \frac{(1 + |P_r|^2)}{(1 + |P_i|^2)} \tag{52}$$

2.6 ANTENNA CHARACTERISTICS AND RECEIVED POWER

The characteristics of interest here are the radiation pattern and polarization which must be related to the scattering process. The polarization factor described in the previous subsection will be useful in representing the gain and polarization of the antennas. There are five polarization factors of interest which are referenced to coordinates shown in Figure 2-23.

P_i = incident factor referenced to e_{hi}, e_{vi}, k_i

P_r = reflected factor referenced to e_{hr}, e_{vr}, k_r

P_d = transmit direct factor referenced to e_{hd}, e_{vd}, k_d

P_{rd} = receiving antenna direct factor reference to e_{hd}, e_{vd}, $-k_d$

P_{rr} = receiving antenna reflection factor referenced to e_{hr}, e_{vr}, $-k_r$

From the orbital geometry, it can be seen that vectors k_d and k_r are separated by a small angle. It is shown in Section 4 that this angle is always less than 3 degrees for LAS altitudes less than 800 n. mi. Thus, if the DRS is the receiving satellite, $P_{rd} \approx P_{rr}$, and if it is the transmitter, $P_d \approx P_i$.

2.6.1 Received Power

Considering only specular reflection and depolarization, the ratio, R_o, of received reflected power to direct power is given by

$$R_o = \frac{\left|E_{hr}\, E_{hrr} + E_{vr}\, E_{vrr}\right|^2}{\left|E_{hd}\, E_{hrd} + E_{vd}\, E_{vrd}\right|^2} = \frac{\left|E_{hr}\right|^2 \left|E_{hrr}^2\right| \left|1 + P_r\, P_{rr}\right|^2}{\left|E_{hd}^2\right| \left|E_{hrd}\right|^2 \left|1 + P_d\, P_{rd}\right|^2} \qquad (53)$$

Now, by definition of the antenna power gains G_1, G_2, G_3, and G_4 in Equations 26 and 37,

$$G_1 = \left|E_{hd}\right|^2 + \left|E_{vd}\right|^2 = \left|E_{hd}\right|^2 \left(1 + \left|P_d\right|^2\right)$$

$$G_2 = \left|E_{hrd}\right|^2 + \left|E_{vrd}\right|^2 = \left|E_{hrd}\right|^2 \left(1 + \left|P_{rd}\right|^2\right)$$

$$G_3 = \left|E_{hi}\right|^2 + \left|E_{vi}\right|^2 = \left|E_{hi}\right|^2 \left(1 + \left|P_i\right|^2\right)$$

$$G_4 = \left|E_{hrr}\right|^2 + \left|E_{vrr}\right|^2 = \left|E_{hrr}\right|^2 \left(1 + \left|P_{rr}\right|^2\right) \tag{54}$$

Using Equations 39 and 46, Equation 53 becomes

$$R_o = \left(\frac{G_4 \left|E_{hr}\right|^2}{G_1 G_2}\right) \frac{\left|1 + P_r P_{rr}^*\right|^2 \left(1 + \left|P_d\right|^2\right) \left(1 + \left|P_{rd}\right|^2\right)}{\left|1 + P_d P_{rd}^*\right|^2 \left(1 + \left|P_{rr}\right|^2\right)} \tag{55}$$

From Equations 44 and 45,

$$E_{hr} = E_{hi} K_{hh} + E_{vi} K_{vh} = E_{hi} \left(K_{hh} + P_i K_{vh}\right) \tag{56}$$

Then from Equations 54 and 56,

$$R_o = \frac{G_3 G_4}{G_1 G_2} \left|K_{hh} + P_i K_{vh}\right|^2 PC \tag{57}$$

where PC is the polarization coefficient defined by

$$PC = \frac{\left|1 + P_r P_{rr}\right|^2 \left(1 + \left|P_d\right|^2\right) \left(1 + \left|P_{rd}\right|^2\right)}{\left|1 + P_d P_{rd}\right|^2 \left(1 + \left|P_i\right|^2\right) \left(1 + \left|P_{rr}\right|^2\right)} \tag{58}$$

For linearly polarized antennas, P_i, P_d, P_{rd}, and P_{rr} are positive real numbers. Horizontal polarization corresponds to $P = 0$, while vertical polarization corresponds to $P = \infty$, which presents computational problems in evaluating R_o as given by Equation 57. To overcome this difficulty, the inverse polarization factor, Q, may be defined by

$$Q = \frac{1}{P} = \frac{E_h}{E_v} \tag{59}$$

It can then be shown by a derivation identical to the one above that

$$R_o = \left(\frac{G_3\, G_4}{G_1\, G_2}\right) \left| K_{vv} + Q_i\, K_{hv} \right|^2 QC \tag{60}$$

where

$$QC = \frac{\left|1 + Q_r\, Q_{rr}\right|^2 \left(1 + \left|Q_d\right|^2\right) \left(1 + \left|Q_{rd}\right|^2\right)}{\left|1 + Q_d\, Q_{rd}\right|^2 \left(1 + \left|Q_i\right|^2\right) \left(1 + \left|Q_{rr}\right|^2\right)} \tag{61}$$

It may be noted from Equations 57 and 60 that

$$QC = PC \frac{K_{hh} + P_i\, K_{vh}}{K_{vv} + Q_i\, K_{hv}} \tag{62}$$

Then for horizontal polarization, $P = 0$, and for vertical polarization, $Q = 0$.

2.6.2 Relative Power

In Equations 57 and 60, the terms $\left|K_{hh} + P_i\, K_{vh}\right|^2$ and $\left|K_{vv} + Q_i\, K_{hv}\right|^2$ are equivalent to $\left|R_c\right|^2$ of Equations 26 and 37. The polarization coefficient PC or QC is an additional term that must be inserted. Thus, expressions for the relative power for both the smooth and rough earth cases can be made to include the antenna characteristics and the effects of depolarization.

2.6.3 Rough Earth Case

$$R_p = \frac{V_o^2}{4\pi G_1\, G_2} \int_S \frac{G_3\, G_4}{V_L^2\, V_D^2} \left| K_{hh} + P_i\, K_{vh} \right|^2 \frac{PC}{\eta^2 \cos^4 \gamma}\, S(\theta) \exp\left(\frac{-\tan^2 \gamma}{\eta 2}\right) dS \tag{63}$$

where dS is a small scattering patch on the earth's surface and each of the terms on the right side of the integral sign correspond to each dS.

2.6.4 Smooth Earth Case

Some simplifications can be made for the smooth earth case by noting, as was done in Subsection 2.5, that $K_{hh} = R_h$, $K_{vv} = R_v \sin^2\theta - R_h \cos^2\theta$, and $K_{hv} = K_{vh} = 0$. Then

$$R_p = \left(\frac{G_3\, G_4}{G_1\, G_2}\right)\left(\frac{V_o}{V_L + V_D}\right)^2 D\left|R_h\right|^2 PC = \left(\frac{G_3\, G_4}{G_1\, G_2}\right)\left(\frac{V_o}{V_L + V_D}\right)^2 D\left|R_v \sin^2\theta - R_h \cos^2\theta\right|^2 QC \qquad (64)$$

Equations 63 and 64 are the basis for some of the relative power calculations discussed in this report.

2.6.5 Antenna System Coordinates

The above development with the resulting expressions requires that the LAS and DRS antenna characteristics be known for every significant scattering point as well as for the direct path direction. For actual calculation, the gains and polarization factors can be expressed as functions of transmission direction with respect to a coordinate system fixed on each satellite. Such coordinate systems were defined in Subsection 2.1 and are shown in Figure 2-24.

The two angles ζ_L and φ_L relate the transmission direction V_L to the LAS coordinate system. Referring to Figure 2-24, it can be shown that

$$\cos\zeta_L = \frac{V_L \cdot L_1}{|V_L|} \qquad (65)$$

$$\left|\cos\varphi_L\right| = \frac{|V_{L3}|}{|V_L| \sin\zeta_L}$$

$$\varphi_L = \mathrm{sgn}(V_{L2}) \cos^{-1}\left(\frac{|V_{L3}|}{|V_L| \sin\zeta_L}\right) \qquad (66)$$

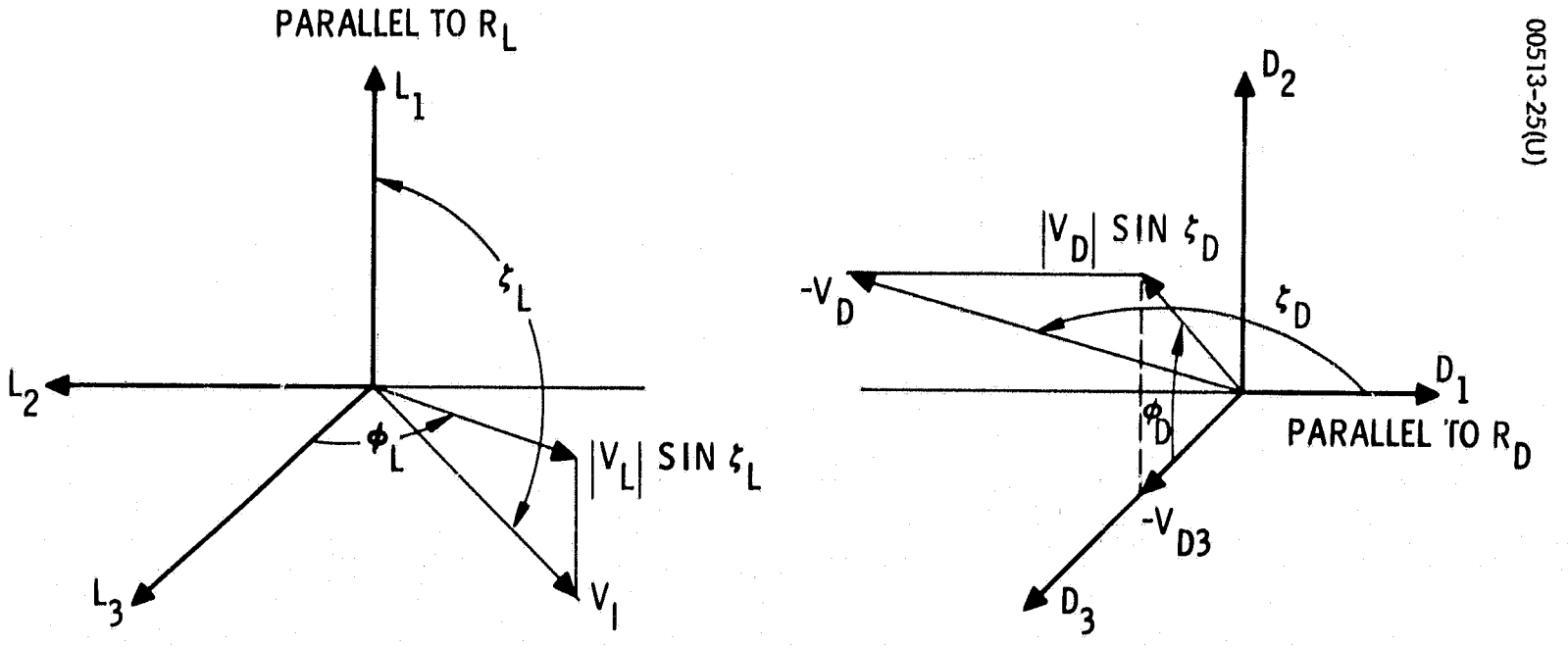

00513-25(U)

Figure 2-24. Antenna System Coordinates

where sgn( ) means "sign of" and the numeric subscript refers to the component in the L_1 L_2 L_3 coordinates of Figure 2-24. And, since reflection is symmetric about the transmission plane, $V_{L3} \geq 0$, and so

$$-90 \text{ degrees} \leq \varphi_L \leq 90 \text{ degrees}$$

$$0 \leq \zeta_L \leq 180 \text{ degrees}$$

Similarly, for the DRS antenna coordinates:

$$\cos \zeta_D = \frac{V_D \cdot D_1}{|V_D|} \tag{67}$$

$$|\cos \varphi_D| = \frac{|V_{D3}|}{|V_D| \sin \zeta_D}$$

$$\varphi_D = \text{sgn}(V_{D2}) \cos^{-1}\left(\frac{|V_{D3}|}{|V_D| \sin \zeta_D}\right) \tag{68}$$

The gains and polarization factors can be expressed as a function of ζ_L, ϕ_L, ζ_D, and φ_D after the antennas are related to the L_1 L_2 L_3 and D_1 D_2 D_3 coordinate systems.

2.6.6 Horizontal and Vertical Polarization

To provide numerical results useful for understanding the effects of the several parameters, two linear polarization orientations will be used. The horizontal polarization vector for both satellites will be taken as the normal to the transmission plane (the plane containing the LAS, DRS, and earth's center). The vertical polarization direction for each satellite will be parallel to the transmission plane, but an arbitrary choice of direction is required.

For the LAS, an omni capability for vertical polarization will be assumed. That is, the gains in the direction of the specular point and in the direct path direction will be taken as equal. This will allow the reflection process to be characterized nearly independent of the antenna characteristics. Thus, for any given value of the separation angle, there are two equal vertical

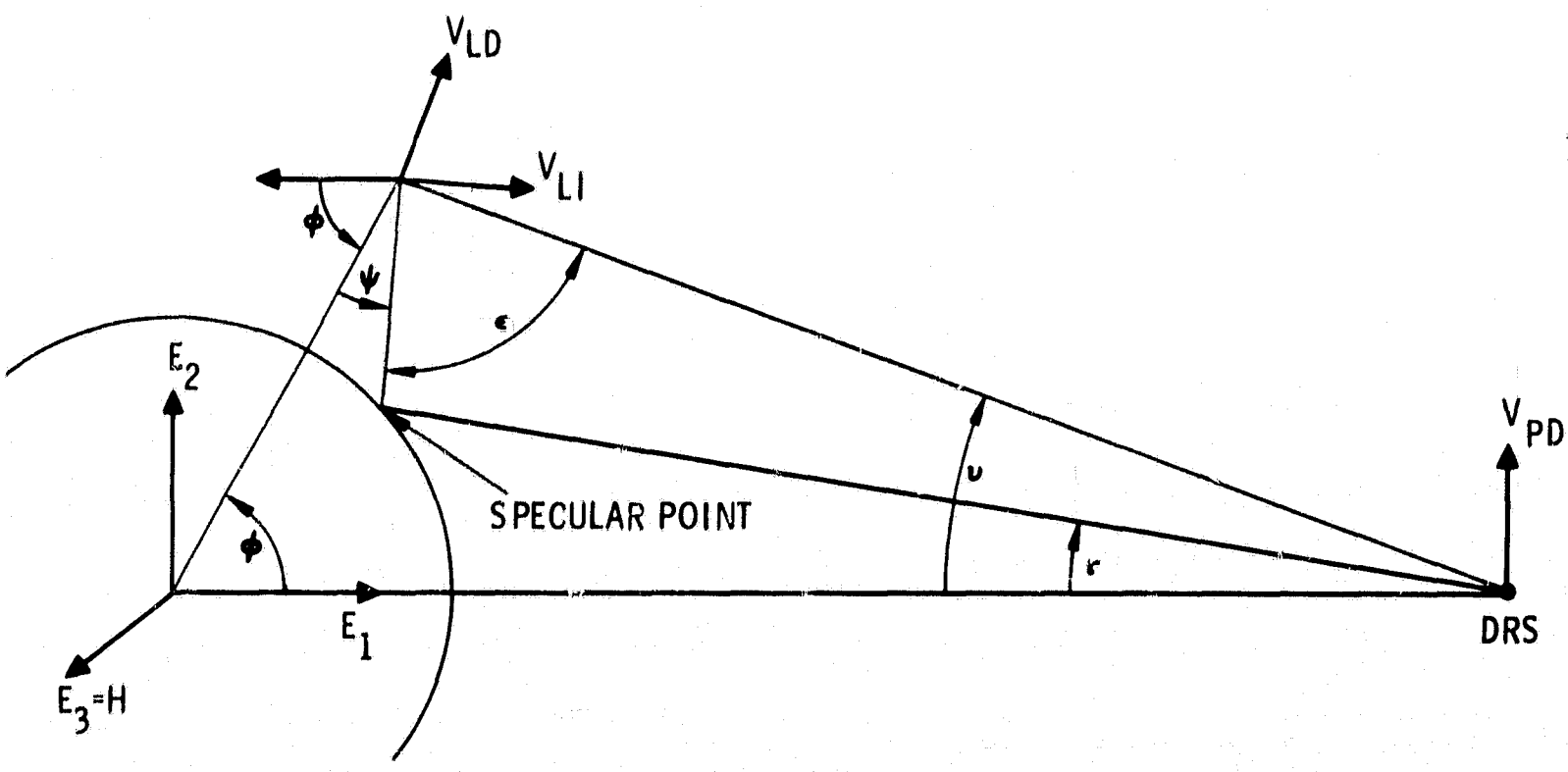

00513-26(U)

Figure 2-25. Definition of Horizontal and Vertical Polarization for LAS and DRS

polarization vectors, V_{LI} and V_{LD}, corresponding to specular point incidence and the direct path. These two vectors are illustrated in Figure 2-25 from which it can be shown that

$$V_{LI} = \begin{pmatrix} \cos a \\ -\sin a \\ 0 \end{pmatrix} \tag{69}$$

where

$$a = 90 - \psi - \varphi$$

and the E_1 E_2 E_3 coordinates of Subsection 2.1 are used.

For the DRS, the vertical polarization direction is chosen as the perpendicular to its earth radius vector, as shown in Figure 2-25. Thus,

$$V_{PD} = \begin{pmatrix} 0 \\ 1 \\ 0 \end{pmatrix} \tag{70}$$

This appears to be the most reasonable since the DRS antenna is most likely to be an earth coverage antenna pointed, nominally, at the center of the earth. Using these coordinates, the horizontal polarization vector, H, defined above can be expressed by

$$H = \begin{pmatrix} 0 \\ 0 \\ 1 \end{pmatrix} \tag{71}$$

With these definitions, and considering separately, horizontal and vertical transmitters with 1 watt of power, the gains and polarization factors could

be defined according to subsections 2.6.1 through 2.6.4. However, this case is of sufficient interest that additional relationships will be developed. First, define the following quantities:

$$
\begin{aligned}
G_{Hhi} &= H \cdot e_{hi} = e_{hi3} \\
G_{Hvi} &= H \cdot e_{vi} = e_{vi3} \\
G_{Vhi} &= V_{IL} \cdot e_{hi} = e_{hi1} \sin a + e_{hi2} \cos a \\
G_{Vvi} &= V_{PL} \cdot e_{vi} = e_{vi1} \sin a + e_{vi2} \cos a \\
G_{hHr} &= H \cdot e_{hr} = e_{hr3} \\
G_{vHr} &= H \cdot e_{vr} = e_{vr3} \\
G_{hVr} &= V_{PD} \cdot e_{hr} = e_{hr2} \\
G_{vVr} &= V_{PD} \cdot e_{vr} = e_{vr2}
\end{aligned}
\qquad (72)
$$

where the numerical subscripts corresponds to vector components in the $E_1\ E_2\ E_3$ coordinate system.

It can now be shown that, if horizontal polarization is transmitted, the reflected, horizontally polarized field is given by

$$E_{HRH} = G_{hHr}(G_{Hhi} K_{hh} + G_{Hvi} K_{vh}) + G_{vHr}(G_{Hhi} K_{hv} + G_{Hvi} K_{vv}) \qquad (73)$$

where K_{vv}, K_{vh}, K_{hv}, and K_{vv} are defined in Equation 44. The reflected vertical polarization is given by

$$E_{HRV} = G_{hVr}(G_{Hhi} K_{hh} + G_{Hvi} K_{vh}) + G_{vVr}(G_{Hhi} K_{hv} + G_{Hvi} K_{vv}) \qquad (74)$$

Similarly, if vertical polarization is transmitted, the received reflected vertical and horizontal polarization is given respectively by

$$E_{VRV} = G_{hVr}\left(G_{Vhi}\,K_{hh} + G_{Vvi}\,K_{vh}\right) + G_{vHr}\left(G_{Vhi}\,K_{hv} + G_{Vvi}\,K_{vv}\right) \quad (75)$$

$$E_{VRH} = G_{hHr}\left(G_{Vhi}\,K_{hh} + G_{Vvi}\,K_{vh}\right) + G_{vHr}\left(G_{Vhi}\,K_{hv} + G_{Vvi}\,K_{vv}\right) \quad (76)$$

For direct transmission, the received horizontal polarization is given by Equation 19 with $G_1 = G_2 = 1$. For vertical polarization with the convention chosen above, $G_1 = 1$ and $G_2 = \cos^2\nu$, where ν is defined in Figure 2-25.

Combining these results with the scattering cross section as was done above, the relative power for transmitting and receiving horizontal polarization (horizontal-horizontal) is given by

$$(R_P)_{HH} = \frac{V_o^{\,2}}{4\pi}\int_S \frac{\left|E_{HRH}\right|^2}{V_L^{\,2}\,V_D^{\,2}}\,\frac{S(\theta)}{\eta^2\cos^4\gamma}\,\exp\left(\frac{-\tan^2\gamma}{\eta^2}\right)dS \quad (77)$$

The horizontal-to-vertical relative power is given by this equation with E_{HRV} substituted for E_{HRH}.

The vertical-to-vertical relative power is given by

$$(R_P)_{VV} = \frac{V_o^{\,2}}{4\pi\cos^2\nu}\int_S \frac{\left|E^2_{VRV}\right|S^2(\theta)}{V_L^{\,2}\,V_D^{\,2}\,\eta^2\cos^4\gamma}\exp\left(\frac{-\tan^2\gamma}{\eta^2}\right)dS \quad (78)$$

and vertical-to-horizontal is given by substituting E_{VRH} for E_{VRV} in this equation.

2.6.7 Smooth Earth

For the smooth earth model where reflection comes from the specular point,

$$\left|E_{HRH}\right|^2 = \left|R_h\right|^2$$
$$\left|E_{VRV}\right|^2 = \left|R_v\right|^2 \cos^2\tau \qquad (79)$$

where τ is defined in Figure 2-25.

Thus,

$$(R_P)_{HH} = \left(\frac{V_o}{V_{LS} + V_{DS}}\right)^2 D\left|R_h\right|^2 \qquad (80)$$

$$(R_P)_{VV} = \left(\frac{V_o}{V_{LS} + V_{DS}}\right)^2 \left(\frac{\cos\tau}{\cos\nu}\right)^2 D\left|R_v\right|^2 \qquad (81)$$

3. MULTIPATH CHARACTERIZATION

The multipath phenomenon cannot easily be described by one quantity or function. However, it can be usefully characterized by its major effects upon a transmitted signal. The previous section developed expressions for the relative power (ratio of received reflected power to received direct power) for both the smooth and rough earth cases involving the major parameters of satellite-to-satellite communication and the reflection process. These expressions may be used to evaluate the following three distinct but interrelated aspects of the multipath phenomenon.

1) Power transmission - relative power reflected by the earth to the receiver

2) Time response - received reflected power as a function of time

3) Frequency effects - multipath effect on a fixed frequency signal

In providing quantitative estimates of the above multipath aspects, the effects of the following major parameters will be shown:

1) Geocentric LAS-DRS separation angle, φ

2) LAS altitude, h

3) Transmission frequency, f

4) Surface electrical properties (sea or land)

5) RMS surface slope (roughness factor), η

6) RMS surface variation, σ

7) Antenna polarizations

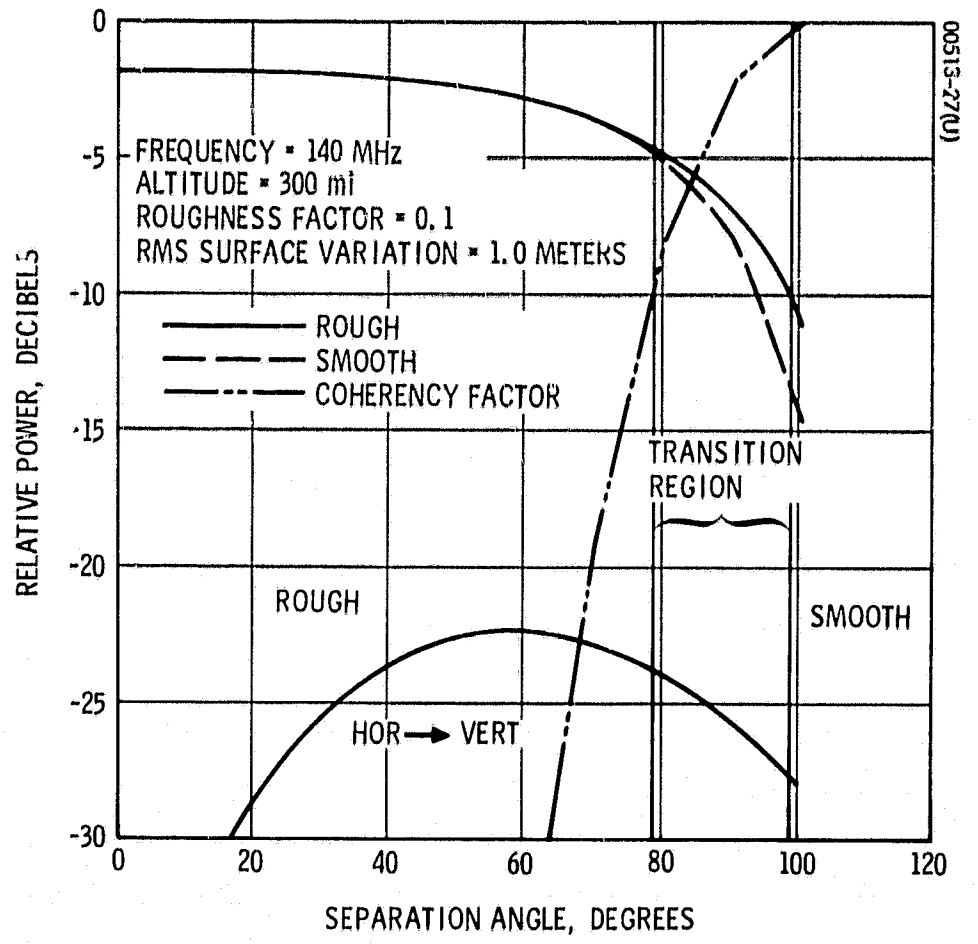

a) Horizontal Polarization

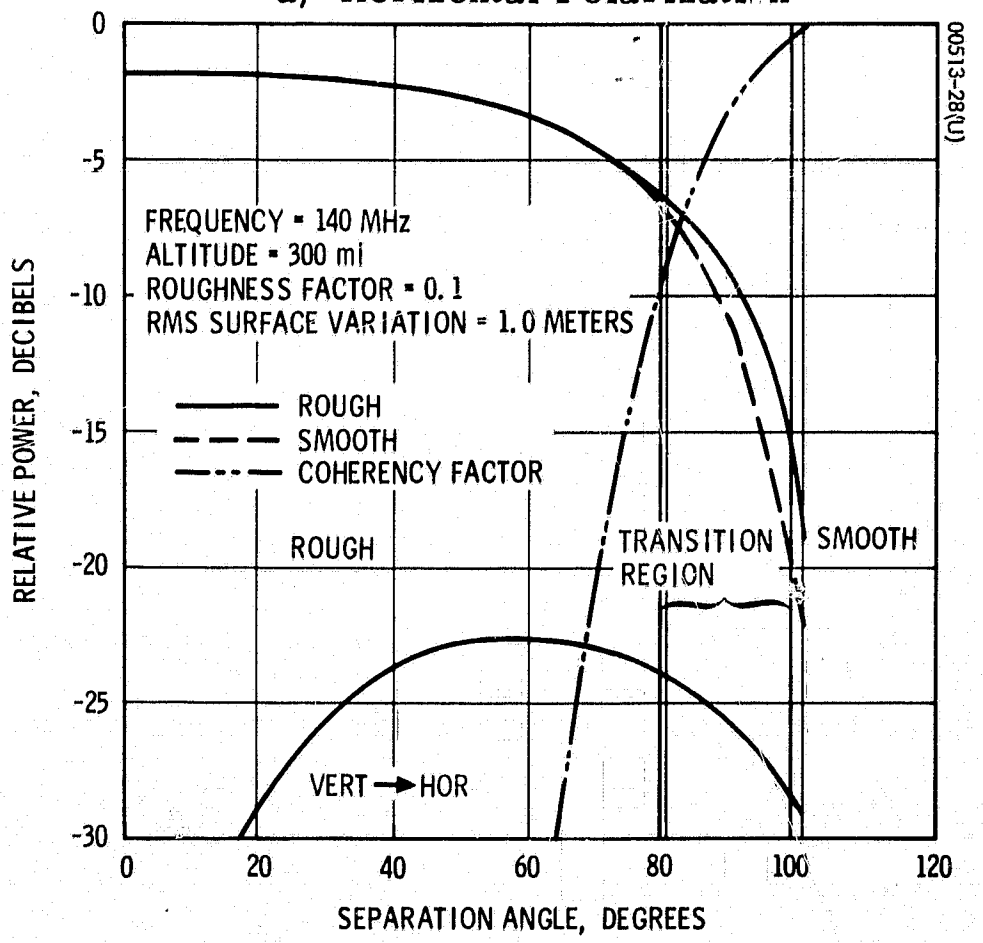

b) Vertical Polarization

Figure 3-1. Relative Power for Nominal Multipath Parameters

3.1 POWER TRANSMISSION

Power transmission has three aspects of interest: 1) magnitude of the received average reflected power with respect to the received direct power, 2) statistical variation about this average which results in a fading signal power, and 3) distribution of reflected power over the earth's surface. These three aspects are discussed in this subsection.

3.1.1 Reflected Power

A useful quantity for evaluating the received reflected power with respect to the received direct power is the relative power defined in Subsection 2.3. The relative power, R_p, is defined as the ratio of the average received reflected power to the received direct power. For the smooth earth model of Subsection 2.3, no statistical averaging is necessary, but for the rough earth model, such averaging is required as discussed in Subsection 2.4.

The final mathematical expressions are given by Equations 63 and 64. These equations require that the gains and polarizations of both LAS and DRS antennas be known for the direct path and over the scattering region. For purposes of characterizing the multipath phenomenon, two orthogonal linear polarizations were chosen and are described in Subsection 2.6.6 where the relative power expressions for these two polarizations are derived.

Using these equations, a digital computer program was written to compute the relative power for the smooth and rough earth models as a function of the above mentioned parameters. The program and details associated with the numerical computation are discussed in Appendix A. Since the separation angle, φ, is the major geometric parameter, the figures of this subsection will plot relative power as a function of φ with the effects of other parameters shown on these coordinates.

Surface Type

It can be seen from Figures 2-15 and 2-17 that reflection coefficients for the sea are greater than those for land. The difference between the reflection coefficients is due to the different electrical properties of the two surfaces, which are accounted for by the relative dielectric constant $\epsilon_r = \epsilon/\epsilon_0$ and conductivity, c, in Equation 21. For this study, the following two sets of parameters were chosen based on Reference 23 (Table 5.1, page 398) which are representative of each surface type:

Sea: $\epsilon_r = 80$ $\quad c = 6$ mho/meter

Land: $\epsilon_r = 10$ $\quad c = 10^{-3}$ mho/meter

For sea reflection, Figures 3-1a and b show the relative power as a function of separation angle, φ, for horizontal and vertical polarization,

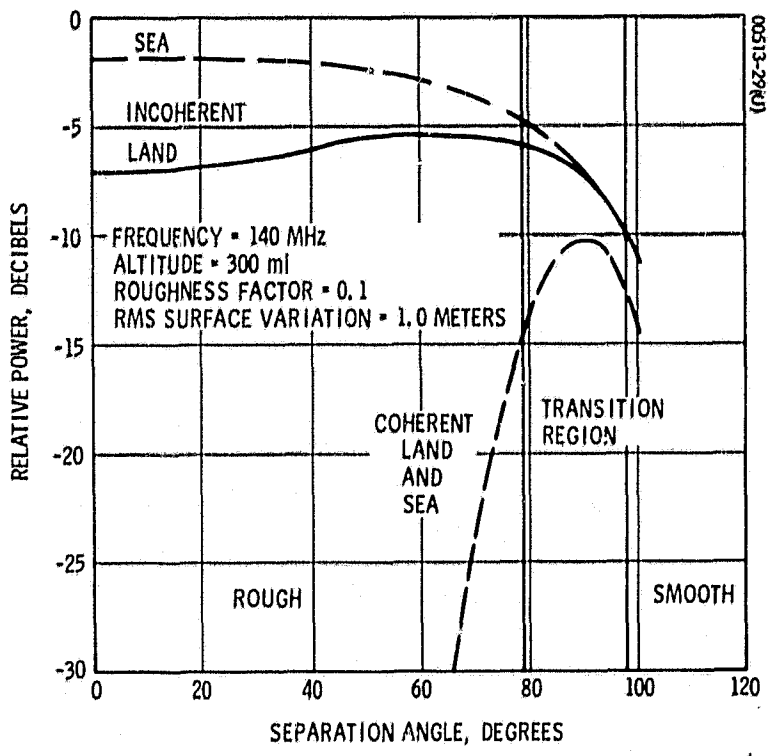

a) Horizontal Polarization

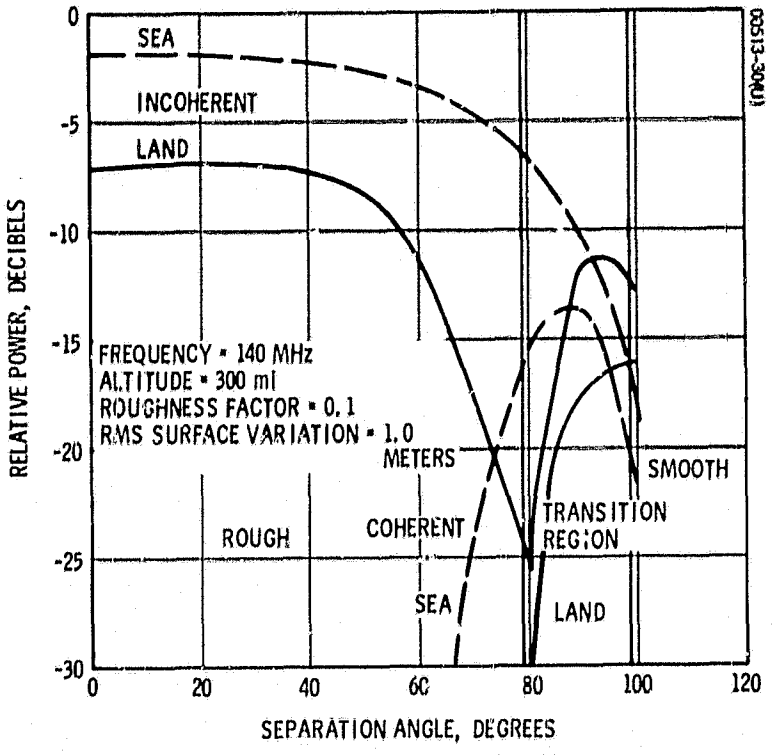

b) Vertical Polarization

Figure 3-2. Land and Sea Reflection

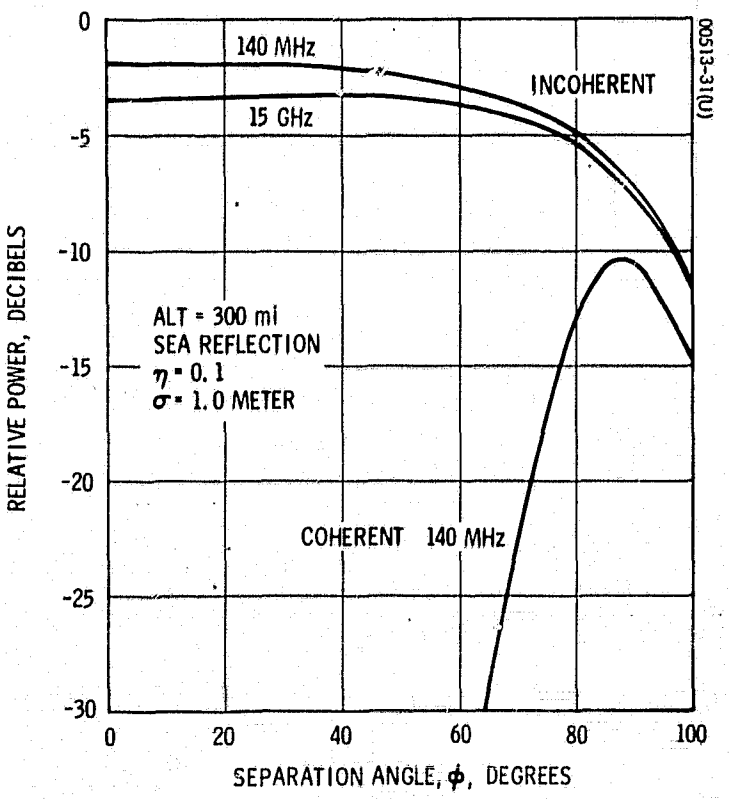

a) Horizontal Polarization

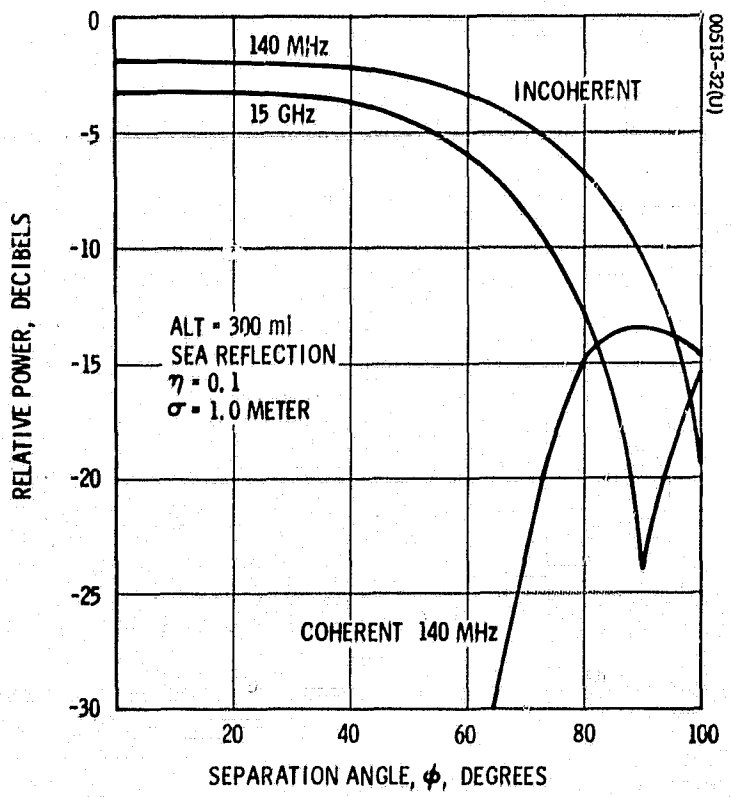

b) Vertical Polarization

Figure 3-3. Comparison of Relative Power at 140 MHz and 15 GHz

respectively, and a transmission frequency of 140 MHz. Both the perfectly smooth earth ($\sigma = 0$) and rough earth ($\eta = 0.1$) cases are shown along with the coherency factor, ρ, defined in Subsection 2.2. The coherency factor corresponds to $\sigma = 1.0$ meter. As mentioned in that subsection, the transition region can be considered to correspond to a range in the coherency factor, ρ, between 0.1 (-10 dB) and 0.9 (-0.457 dB). This region is shown in Figures 3-1a and b. Note that the results for the perfectly smooth and rough earth cases are nearly identical, even in the transition region; thus, it is not unreasonable to assume that the relative power will lie between these two values in the transition region or, at most, be equal to their sum.

Equally important is the nature of the reflected power. As discussed in Subsections 2.3 and 2.4, the power reflected from a smooth or slightly rough earth is phase coherent, while that reflected from a rough earth is incoherent. In the transition region, it is to be expected that the total reflected power will consist of both types. Using the coherency factor corresponding to the given value of σ, the relative incoherent and coherent power, respectively, are shown in Figures 3-2a and b. This method of representing the relative power appears to be the most appropriate and will be used subsequently in this section.

Figures 3-2a and b also show the relative incoherent and coherent power for nominal land reflection. Since the reflection coefficients for land are relatively independent for frequencies in the range of 140 MHz to 15 GHz, the incoherent curve remains the same over this range, but the coherent power is reduced to a negligible amount for nearly all separation angles with frequencies above 2 GHz. It can be seen that the relative power for sea reflection is greater than that for land reflection.

Inasmuch as the sea covers approximately 70 percent of the earth's surface and, at the same time, represents the worst-case reflection, this surface will be used for the remainder of this section to show the effects of other parameters. Typical roughness parameters for the sea correspond to $0.05 \leq \eta \leq 0.1$ and $\sigma = 1.0$ meter. When the effects of other parameters are being studied, $\eta = 0.1$ and $\sigma = 1.0$ will be used.

Transmission Frequency

The effect of transmission frequency can be seen in Figures 3-3a and b. As the frequency increases, the earth appears more and more rough, with the result that the reflected power is incoherent for almost all separation angles at frequencies above 2 GHz.

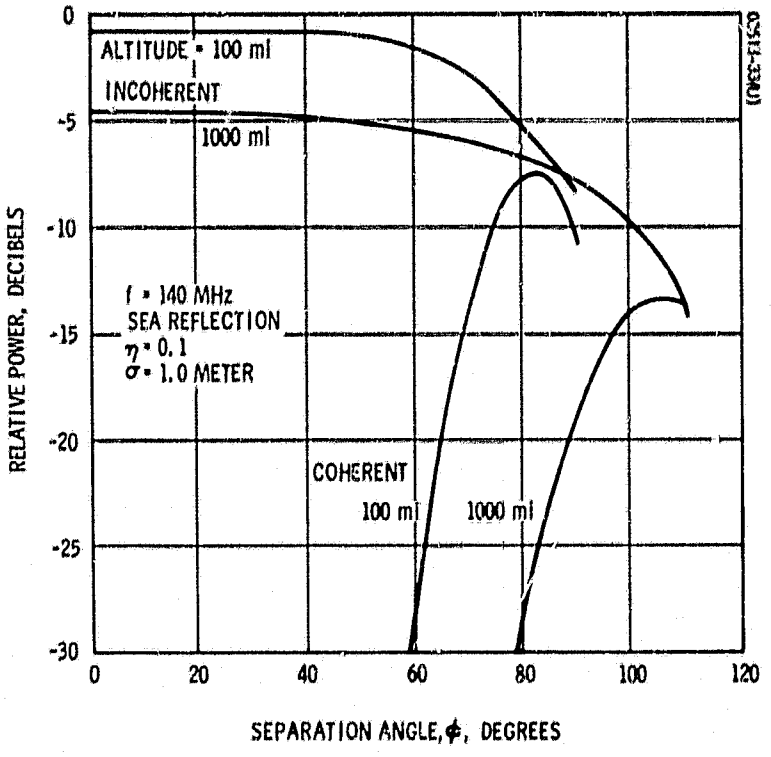

a) Horizontal Polarization

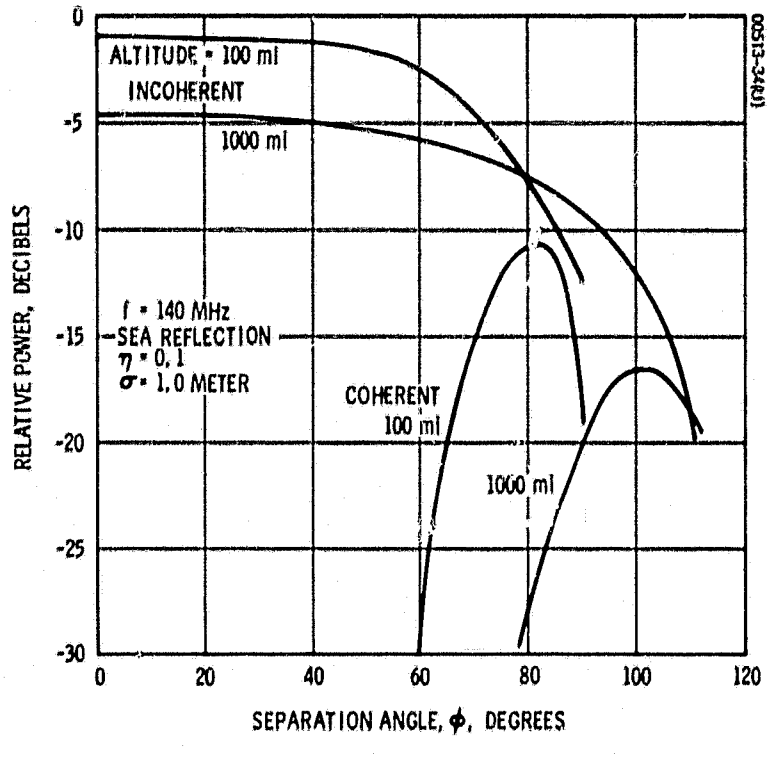

b) Vertical Polarization

Figure 3-4. Effects of Satellite Attitude

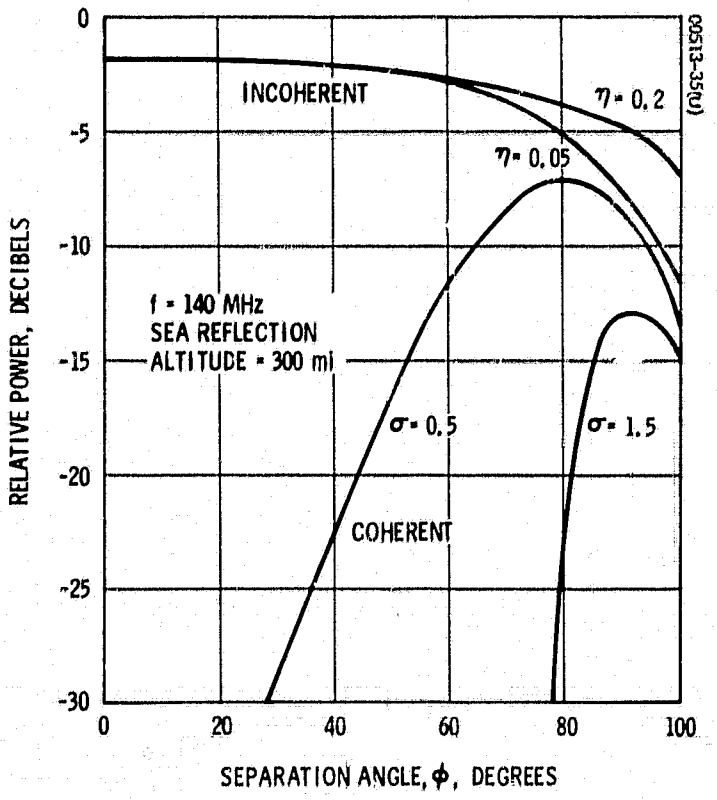

a) Horizontal Polarization

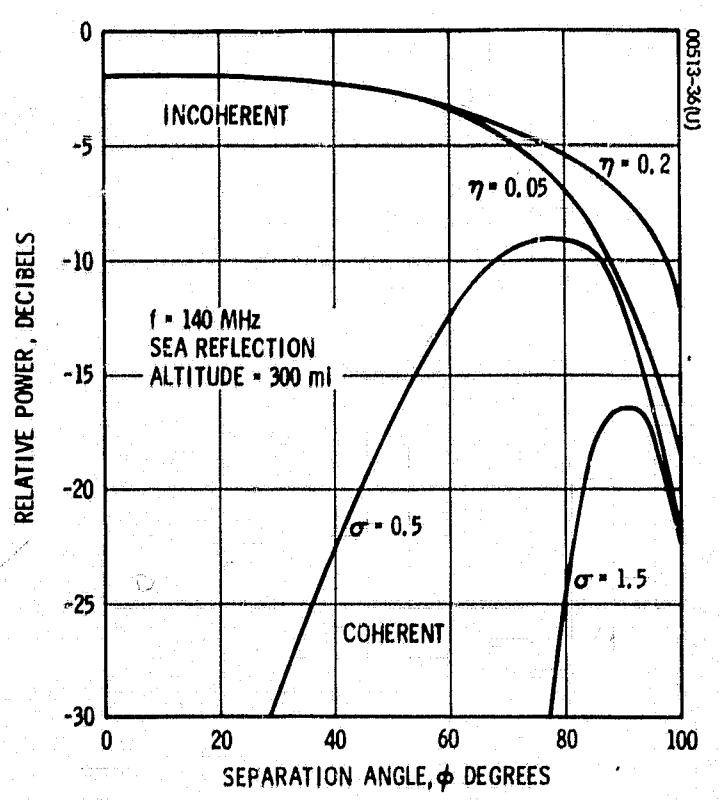

b) Vertical Polarization

Figure 3-5. Variation of Roughness Factor and RMS Surface Variation

LAS Altitude

The effect of LAS altitude on the relative power is shown in Figures 3-4a and b for a frequency of 140 MHz. The relative power decreases as the altitude increases.

Roughness Parameters

The roughness factor, η, representing the rms surface slope and the surface rms height variation, σ, are clearly not independent variables as can be seen from the definition

$$\eta = \frac{2\sigma}{T}$$

where T is the correlation length. However, as the surface becomes rougher, it is apparent that σ increases and T decreases. Thus, η will experience a greater variation than σ. Experimental studies discussed in Reference 2 show that the rms slope varies between 0 and 16 degrees, corresponding to a maximum variation in η from 0 to about 0.3. More common values correspond to $0.05 \leq \eta \leq 0.1$. The following data indicate the relationship between η and σ used to produce Figures 3-5a and b.

η	σ, meters
0.05	0.05
0.1	1.0
0.2	1.5
0.3	2.0

3.1.2 Fading

It is of interest to consider the fading of a single transmitted CW frequency. Modulation on this signal will change the fading characteristics, but the analysis of this situation is beyond the scope of this study. A coherently reflected signal will cause fading with a beat frequency equal to the difference in doppler shift between the direct and specular reflection paths. This difference depends on both the separation angle and satellite velocities with respect to the transmission plane. Doppler shift is discussed in Subsection 3.2. If the reflected and direct signal powers are nearly equal ($R_p \approx 0$), then the fade will be deep. The ratio of total power and direct power will have the maximum and minimum values given by

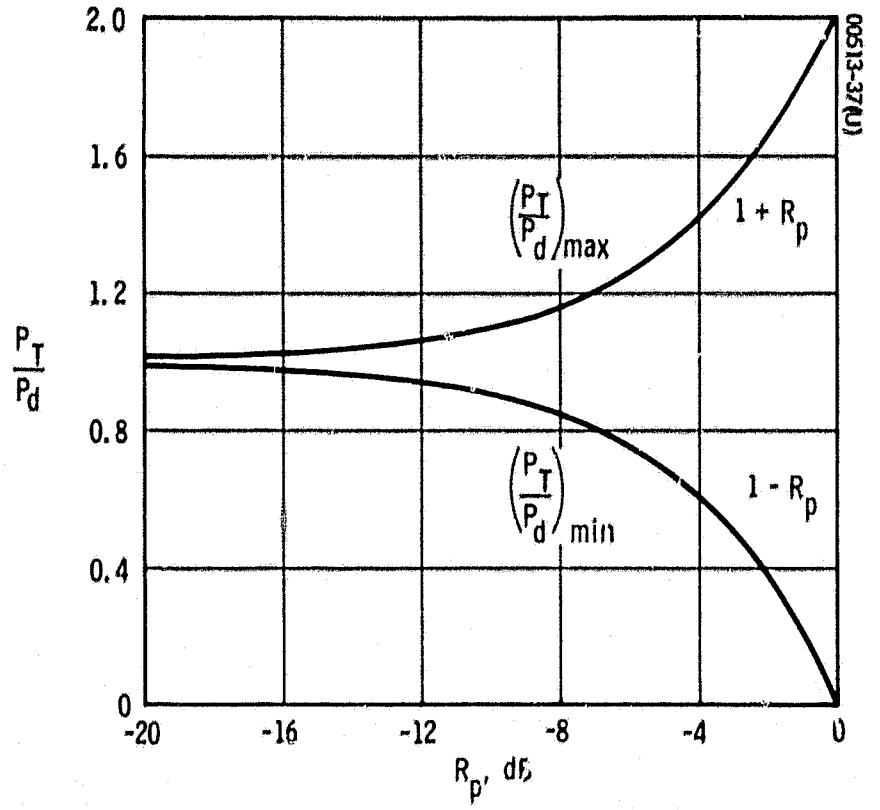

Figure 3-6. Maximum and Minimum Ratios of Total Received Power to Direct Power

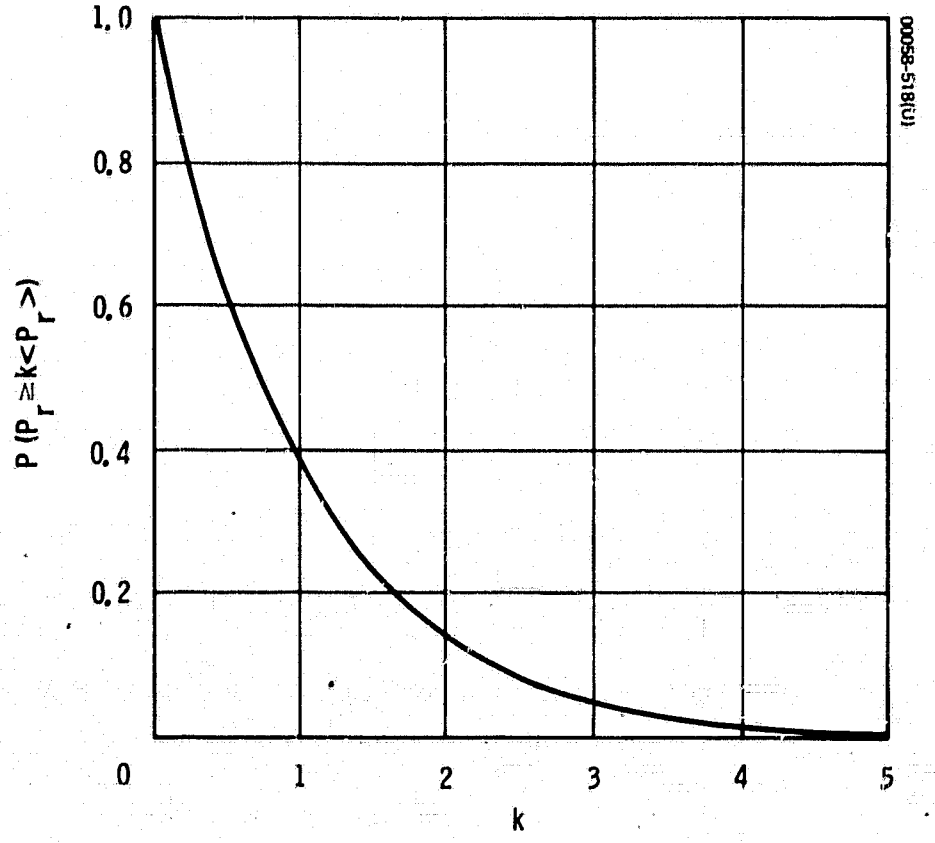

Figure 3-7. Probability That Received Reflected Power Is Greater Than k Times Average Power, $<P_r>$

$$\frac{P_t}{P_d} = \frac{P_d \pm P_r}{P_d} = 1 \pm R_p$$

This relationship is shown in Figure 3-6. The coherent case is deterministic and easily calculated for a particular geometry and a value for R_p. However, the incoherent case requires considerable analysis.

In Subsection 2.4, the relative power for incoherent reflection from a rough earth surface is defined as the ratio of the average reflected power and direct power. Variation from this average results in fading. Under the assumptions about the statistical nature of the surface given in Subsection 2.4, it can be shown that the envelope of the reflected electric field has what is known as the Rayleigh distribution (Reference 2). The voltage in the receiver is directly proportional to the electric field, and so the probability of the envelope of the voltage, v, lying between the values a and b is given by

$$P(a \le v \le b) = \int_a^b \frac{2x}{r^2} e^{-x^2/r^2} \, dx$$

where r is the rms value of the voltage. Since the received power is proportional to the square of the voltage, a change of variable yields the distribution for the received reflected power P_r.

$$P(P_r \ge A) = \int_A^\infty \frac{1}{\langle P_r \rangle} e^{-\frac{z}{\langle P_r \rangle}} \, dz = e^{-\frac{A}{\langle P_r \rangle}}$$

where $\langle P_r \rangle$ denotes the average reflected power (see Equation 29). Thus, the probability that the instantaneous reflected power is K times greater than the average is simply given by

$$P(P_r \ge k \langle P_r \rangle) = e^{-k}$$

and is plotted in Figure 3-7. Note that the probability of P_r being greater than $\langle P_r \rangle$ is only 0.37, not 0.5.

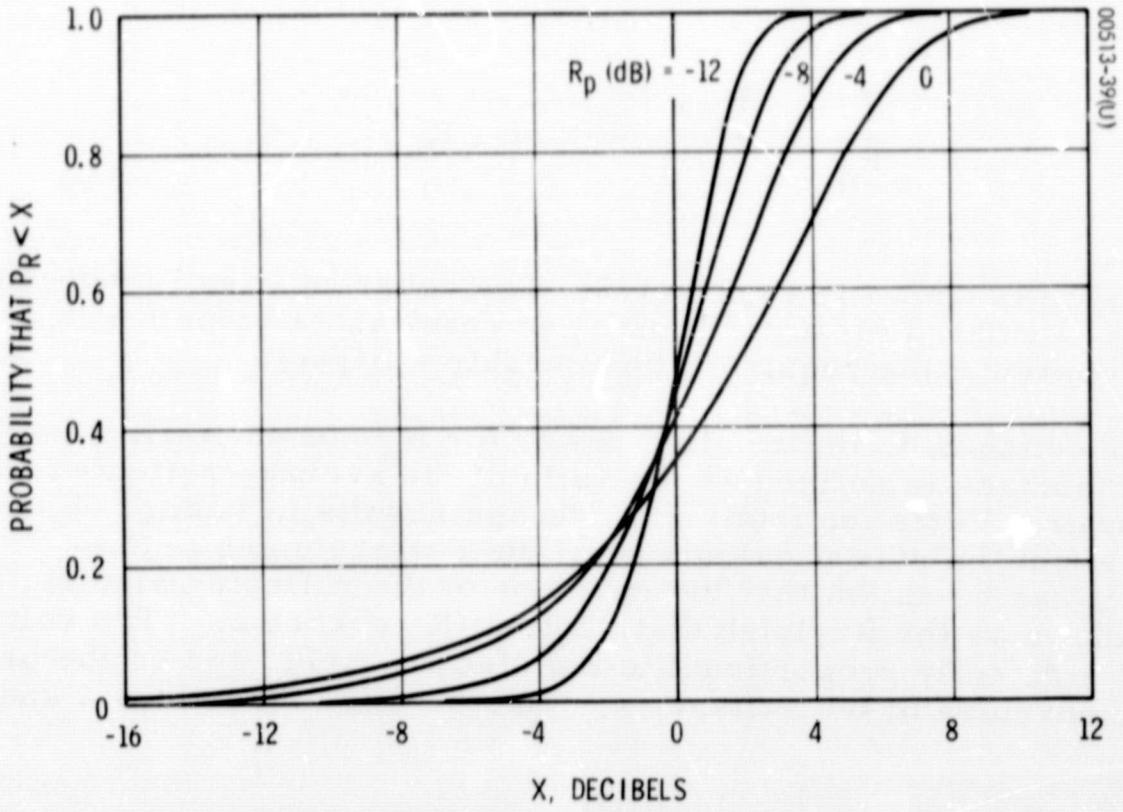

Figure 3-8. Probability Distribution of Ratio, P_R, of Total Instantaneous Power and Direct Power

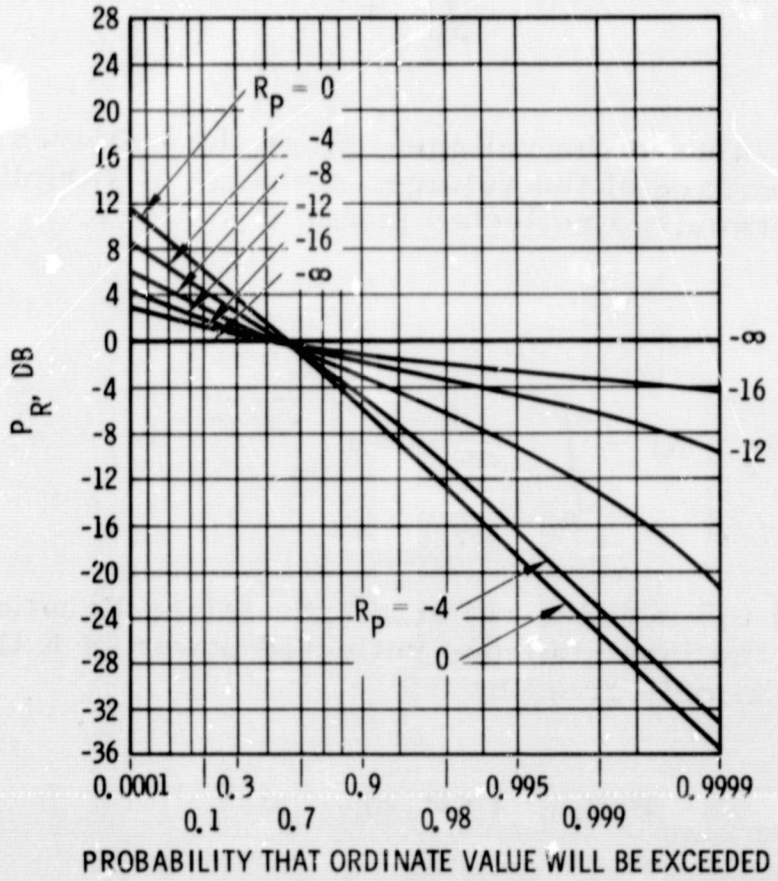

Figure 3-9. Inverse Probability Distribution of P_R

If the total — reflected plus direct signal — is considered, the instantaneous power, P_t, can be shown to have the Rician distribution given by

$$p(P_t) = \exp\left(\frac{-P_d}{\langle P_r \rangle}\right) \frac{2\sqrt{P_t}}{\langle P_r \rangle} \exp\left(\frac{-P_t}{\langle P_r \rangle}\right) I_o \left(\frac{2\sqrt{P_t P_d}}{\langle P_r \rangle}\right)$$

Defining the power ratio, P_R, by

$$P_R = \frac{P_t}{P_d}$$

where, again, P_t is the instantaneous total power. The probability distribution of P_R can be determined as was done in Reference 24. The results are repeated here as Figure 3-8.

This figure may be used to estimate the amount of time in which a given amount of fade will occur. For instance, if R_p = -4 dB, then from Figure 3-8, the amount of time that $P_t < P_d$, i.e., $P(P_R < 0$ dB), is about 40 percent. And the probability that $P_t < P_d/10$ is about 2 percent. The inverse probability distribution is shown in Figure 3-9. A special probability scale is used to show the probability that P_R will be greater than a given value. From this figure for R_p = -4 dB, it can be seen that 95 percent of the time $P_R > -7$ dB. Either one of these figures in combination with the relative power curves will allow a determination of the relative frequency of fading for the rough earth case.

3.1.3 Surface Reflectivity Distribution

For reflection of a plane wave by a smooth surface, most of the reflected signal comes from the first few Fresnel zones. In fact, the total reflected signal is approximately half the signal reflected by the first Fresnel zone. For small transmitter and/or receiver heights above the reflecting surface, other important contributions in the reflected field come from the area just in front of the transmitter and receiver. For the LAS/DRS geometry, the major reflecting area is the first few Fresnel zones.

As an illustration of the size of the active scattering region, Table 3-1 shows the size of the first Fresnel zone for various conditions.

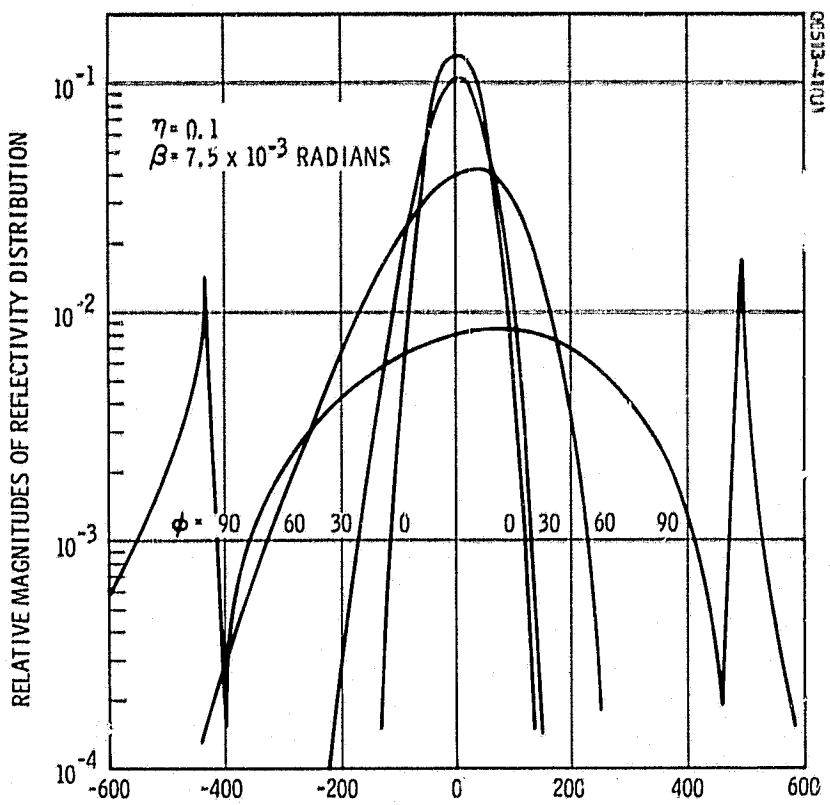

Figure 3-10. Reflectivity Distribution Near Transmission Plane

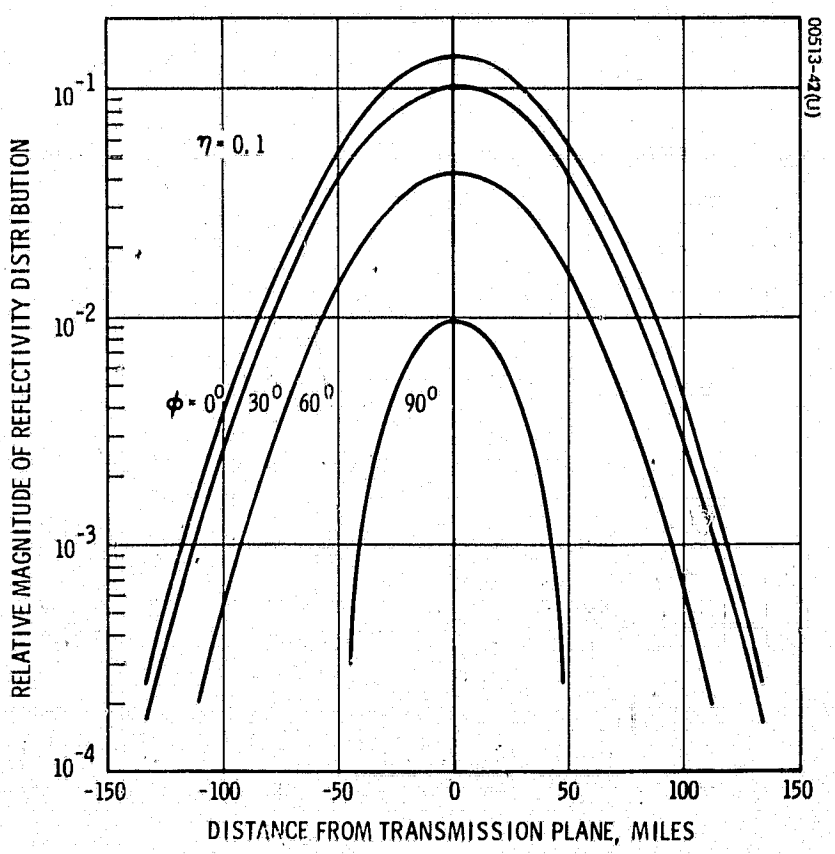

Figure 3-11. Reflectivity Distribution Normal to Transmission Plane From Specular Point

TABLE 3-1. SIZE OF FIRST FRESNEL ZONE
(LAS altitude = 300 n. mi.)

Frequency, MHz	135		400		8000	
Satellite separation angle, φ in degrees	0	90	0	90	0	90
First Fresnel zone area, square miles	0.4	2.0	0.13	0.66	0.0066	0.033

Table 3-1 emphasizes how extremely small the active scattering region really is for the perfectly smooth earth. These regions correspond to a subtending central angle less than 0.01 degree.

For a rough surface, most of the reflected energy comes from near the specular point, but the active scattering region is much larger than the Fresnel zones of the smooth earth model. The surface roughness determines the size of these regions, whereas, in the smooth earth case, optical considerations determine the Fresnel zones. In addition, the antenna gains in the direction of a scattering point and the corresponding reflection coefficient also affect the power reflected from the surface near that point. Thus, both the gains and polarizations for each antenna and for every scattering point must be known in order to calculate the relative power reflected from each point.

However, to provide some insight into the reflectivity distribution, both the antenna characteristics and the reflection coefficient will be disregarded by defining a geometrical reflection factor, F_R, given by

$$F_R = \frac{V_D^2}{4\pi V_L^2 V_D^2} \frac{S(\theta)}{\eta^2 \cos^4 \gamma} \exp\left(-\frac{\tan^2 \gamma}{\eta^2}\right) dS$$

This factor is a function of the separation angle, LAS altitude, and surface location. If the altitude is kept constant, variation with φ and distance from the specular point can be shown graphically. Figure 3-10 shows F_R as a function of the distance from the specular point along a line parallel to and very near the transmission plane, the distance from it being about 15 miles. Figure 3-11 shows F_R as a function of the distance from the specular point in a direction normal to the transmission plane.

Note in Figure 3-10 that the surface distribution is significantly different for φ = 90 degrees than for the smaller separation angles shown. This result is consistent with the analytical results of Spizzichino

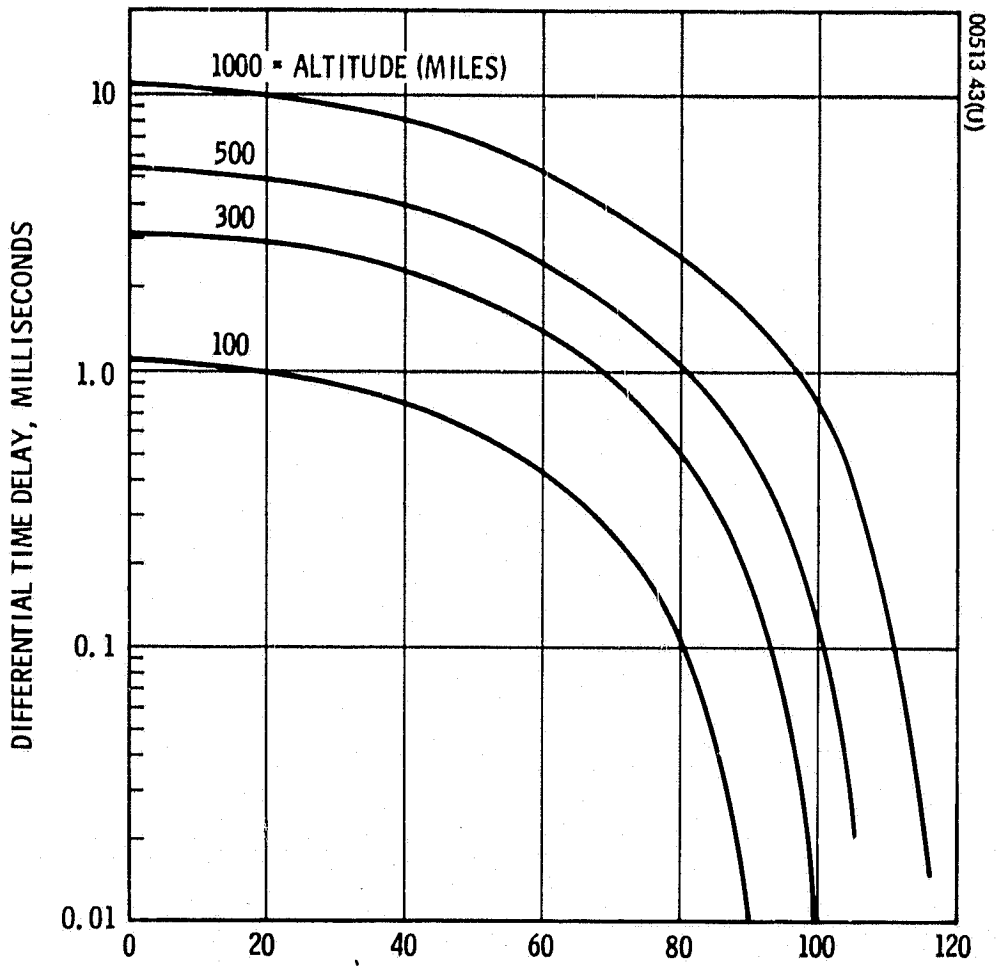

Figure 3-12. Specular Differential Time Delay

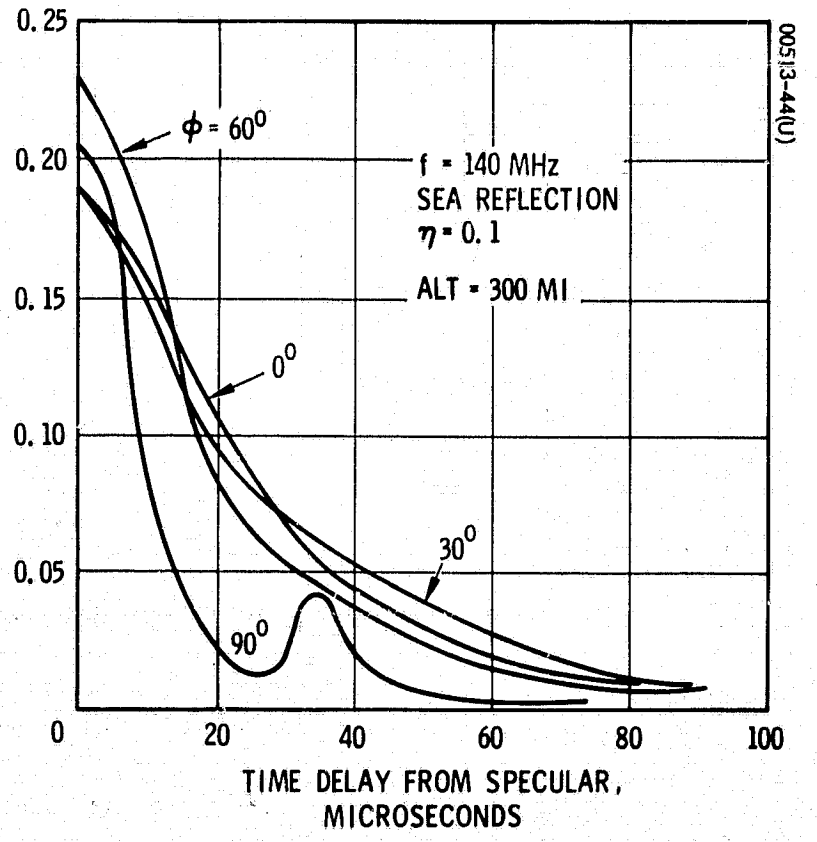

Figure 3-13. Time Response for Horizontal Polarization

(Reference 2, pp. 257-264) showing that, for small grazing angles, a significant portion of the reflected energy comes from points nearer to the receiver and transmitter than the specular point. Small grazing angles resulting in this phenomenon correspond to large separation angles.

3.2 TIME RESPONSE

Since, as seen in Subsection 3.1.3, the scattering region is a significant geometric area on the earth's surface, energy reflected toward the receiver from different parts of this region arrives at different times. Further, from the geometric considerations of Subsection 2.1, the length of the direct path and specular point reflection path are different for various values of separation angle.

A simple calculation involving path length shows that, for low-altitude orbits, i.e., altitudes between 100 and 1000 miles, the direct path time delay lies in the range of 115 to 155 milliseconds. Both the direct path time delay and time delay for specular point reflection as a function of separation angle can be computed and plotted. But a more meaningful quantity for this study is the difference of these two time delays. This difference, defined as the specular differential time delay, is shown in Figure 3-12 as a function of separation angle, ϕ. The reflection path is always longer than the direct path, and so the specular differential time delay is the amount of time the energy reflected from the specular point lags the corresponding direct path energy.

It can be shown that the specular reflection path, i.e., $V_{LS} + V_{DS}$ in Figure 2-4, is the shortest of all possible earth reflection paths. Thus, energy reflected to the receiver from other points in the scattering region will be delayed even longer than energy from the specular point. The numerical computation program of Appendix A calculates the power scattered from each surface patch and the associated time delay and then adds all the power delayed within specified time intervals. These summations are normalized so that the total reflected power is unity. The resulting time spreading distribution represents the impulse response of the reflection process.

The results are shown in Figure 3-13 for horizontal polarization, and the time response for vertical polarization is nearly identical. In Figures 3-14a and b, the curves have been normalized to the specular point power density, which emphasizes the relative shapes of the curves. In Figure 3-13, the roughness factor, η, is 0.1, whereas in Figures 3-14a and b, $\eta = 0.05$. Note that the roughness factor makes a considerable difference in the time spreading. Figure 3-14a shows one curve corresponding to $\phi = 0$ and $\eta = 0.02$, resulting in very small time spreading. For $\eta = 0.05$, time spreading is on the order of 30 microseconds, and for $\eta = 0.1$, the spreading is 80 to 100 microseconds.

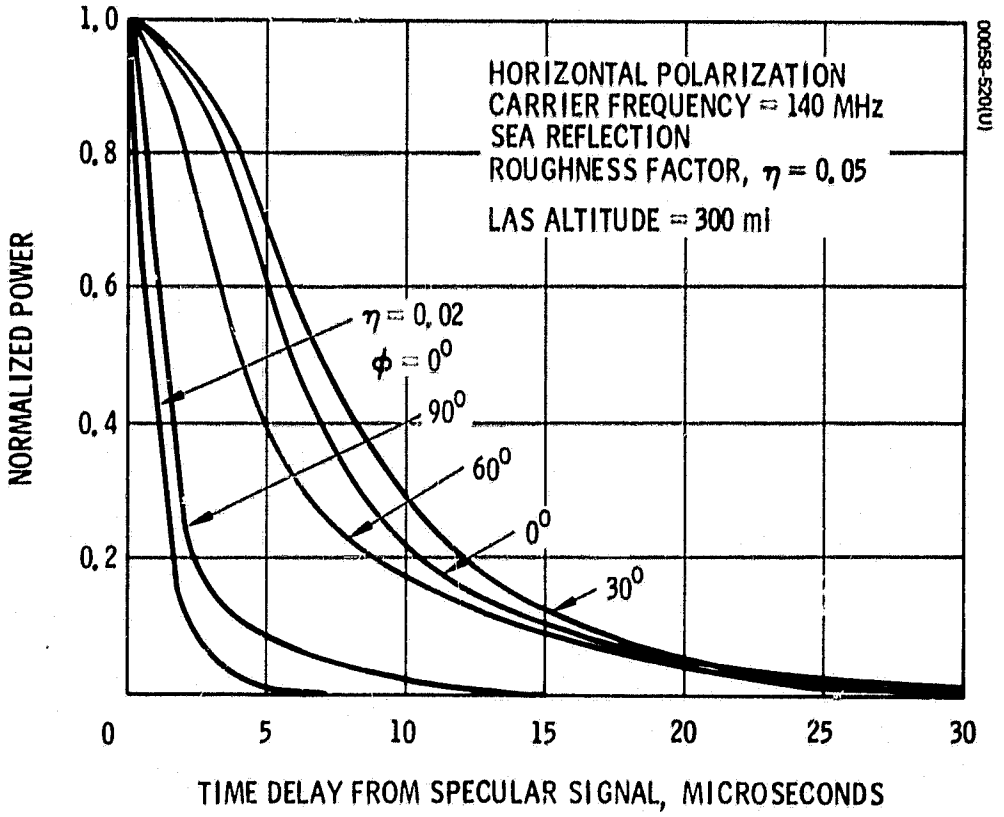

a) Horizontal Polarization

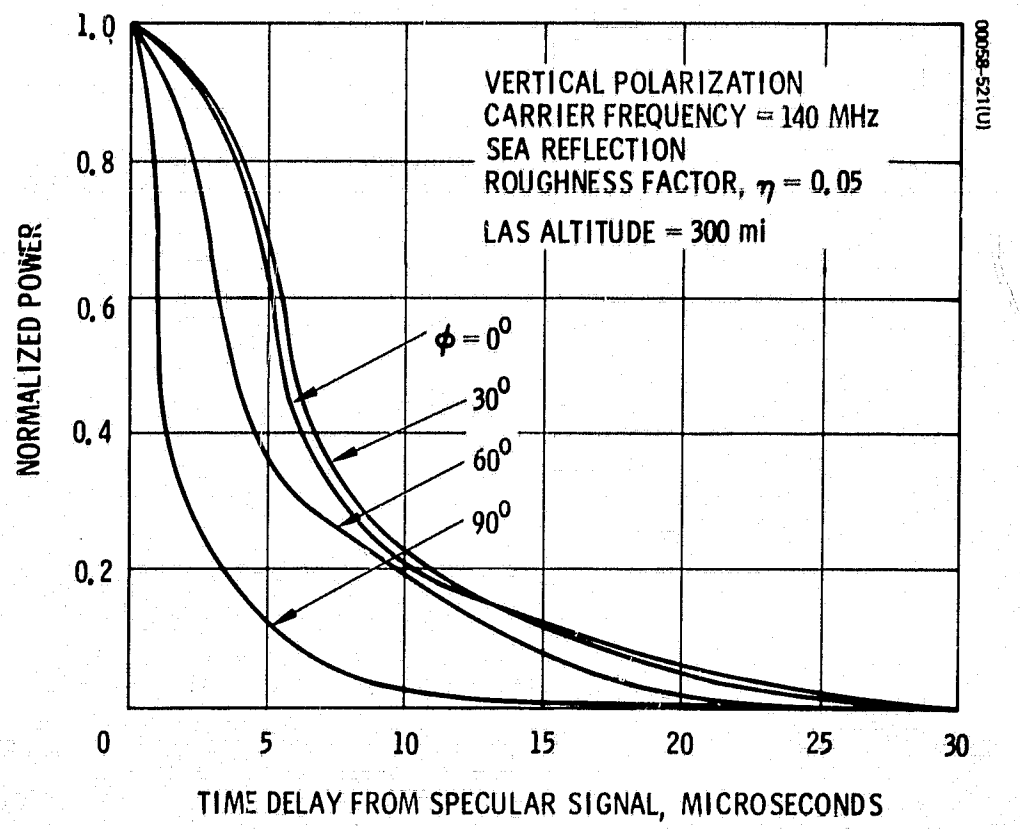

b) Vertical Polarization

Figure 3-14. Normalized Power Time Response

One of the more interesting observations concerning these figures is that time spreading is slightly larger for a separation angle of 30 degrees than for either 0 to 60 degrees. This occurs because there are two opposing mechanisms at work in the time spreading process:

1) As φ increases from zero, the scattering region increases (see Subsection 3.1.3), tending to cause a greater time spreading.

2) As φ increases from zero, the difference between individual path lengths decreases, tending to decrease the time spreading.

Near $\varphi = 0$ mechanism 1 dominates, while for large φ, mechanism 2 is dominant.

3.3 FREQUENCY EFFECTS

The frequency effects are due to the motion of the two satellites, which causes a doppler shift of both the direct and reflected signals. The frequency shifting effects may be separated into two components as was done for the time response: 1) doppler shifts of the direct and specular point paths, and 2) frequency spreading of the reflected signal.

The relative orientation of the two velocity vectors is the most significant variable. To illustrate the frequency effects and to provide bounds for these effects, three geometrical cases were chosen:

Case 1: The velocity vectors of both the LAS and DRS lie in the transmission plane and are pointed toward each other. This is the most extreme case and, assuming that the DRS is in an equatorial orbit, would require that the LAS also have an equatorial orbit with opposite orbital motion.

Case 2: The velocity vector of the LAS is in the transmission plane, while the DRS velocity is normal to it. This case corresponds to an LAS polar orbit and the DRS lying in the LAS orbit plane.

Case 3: The velocity vectors of both satellites are normal to the transmission plane and lie in opposite directions.

These three cases are illustrated in Figure 3-15.

The change in frequency of a received single frequency signal when there is relative motion between the transmitter and receiver is given by the simple formula

$$\Delta f = -\frac{f}{c}\frac{dV_o}{dt}$$

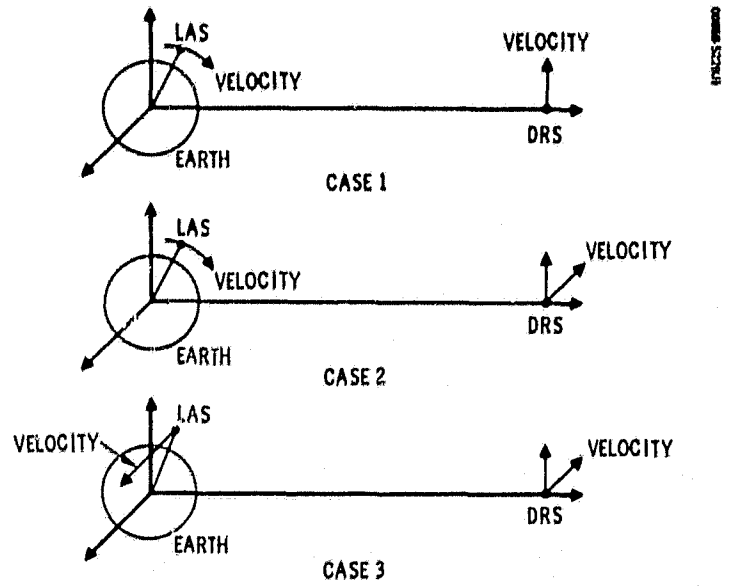

Figure 3-15. Three Cases of Relative Velocity Orientation

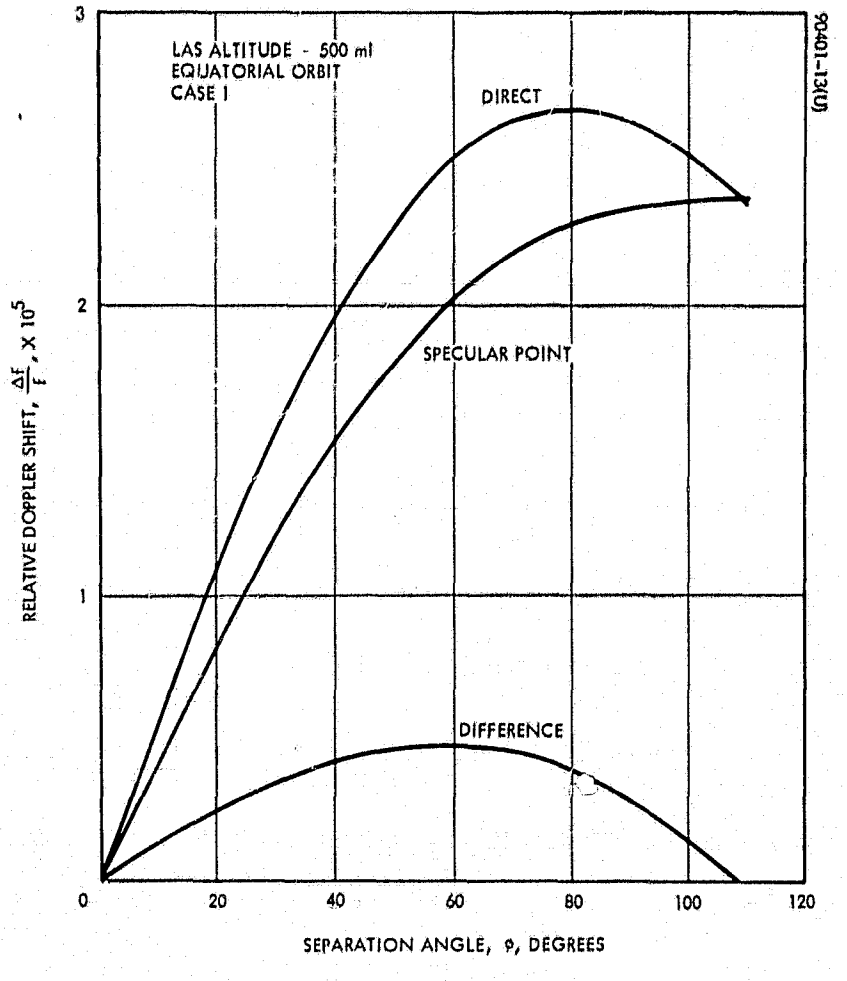

Figure 3-16. Relative Specular Doppler Shift

where f is the transmitted frequency, c is the speed of light, and V_o is the distance between the two satellites. Thus, if V_o is increasing, the received frequency is less than the transmitted frequency. For the reflection path, the rate of change of the path to the earth and from the earth must be added. The relative doppler shift is defined as the fractional change in frequency, $\Delta f/f$.

Figure 3-16 shows the relative doppler shift of both the direct and specular reflection paths for Case 1 and an LAS altitude of 500 miles. Of particular interest in analyzing the communication problem due to multipath interference is the difference between these two doppler shifts. This difference is shown in Figure 3-16 and again with an expanded scale in Figure 3-17. Figure 3-17 also shows the relative differential doppler for Case 2 and a modified Case 2 corresponding to the LAS velocity vector making a 45-degree angle with the transmission plane. Figure 3-18 shows the relationship between the relative specular differential doppler shift and altitude for Case 2. Figure 3-19 shows the actual doppler shift in Hertz for Case 2 at 140 MHz and also illustrates the effect of LAS altitude.

Since the scattering region can be visualized as many small contiguous scattering patches, the reflection path to a given patch will differ from other paths. Consequently, the doppler shift will be different for each patch, with a received reflected frequency spectrum being the composite effect upon a single transmitted frequency. Since for LAS/DRS geometry, the scattering region is nearly symmetrical about the specular point, it is expected that the received reflected spectrum will be nearly symmetric about the power density from the specular point.

Figure 3-20 presents the reflected spectra normalized so that the value of the specular point is unity. This figure illustrates the relative doppler shift of both the direct and reflected signals, as well as the spectrum spreading of the reflected signal. Increasing the altitude and/or increasing the roughness parameter, η, would result in greater spreading of the spectra.

Two points concerning Figure 3-20 are worth noting: 1) frequency spreading decreases as the separation angle, φ, increases, and 2) for the parameters indicated in the figure, the frequency of the direct signal does not fall within the spectrum of the reflected signal for separation angles greater than 30 degrees.

Figure 3-21 illustrates the received spectra for velocity orientations corresponding to Case 3. For this case, the specular differential doppler shift is zero, i.e., there is no doppler shift between the direct signal and the signal reflected from the specular point. Thus, the only effect is the frequency spreading shown in Figure 3-21. So the direct signal frequency lies at the center of these spectra.

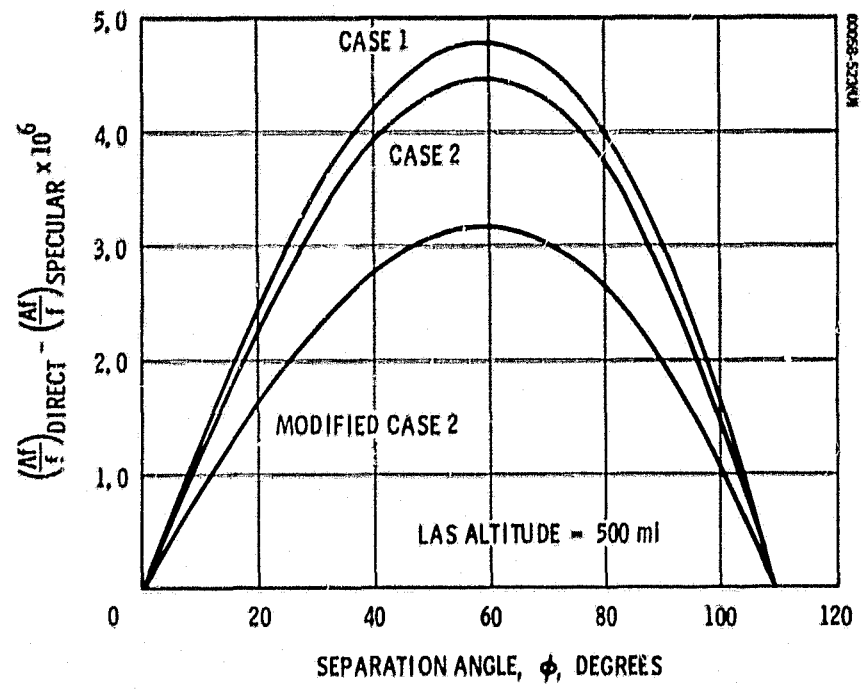

Figure 3-17. Relative Specular Differential Doppler Shift Versus Separation Angle, ϕ

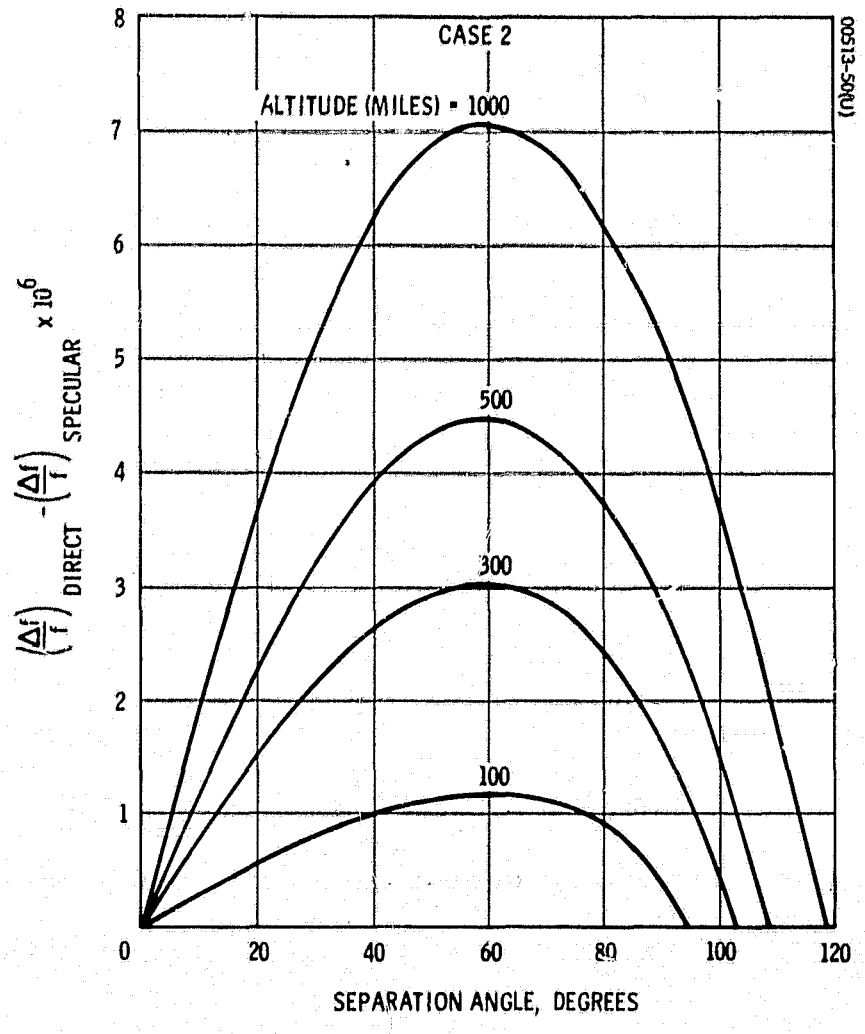

Figure 3-18. Relative Specular Doppler Shift, Case 2

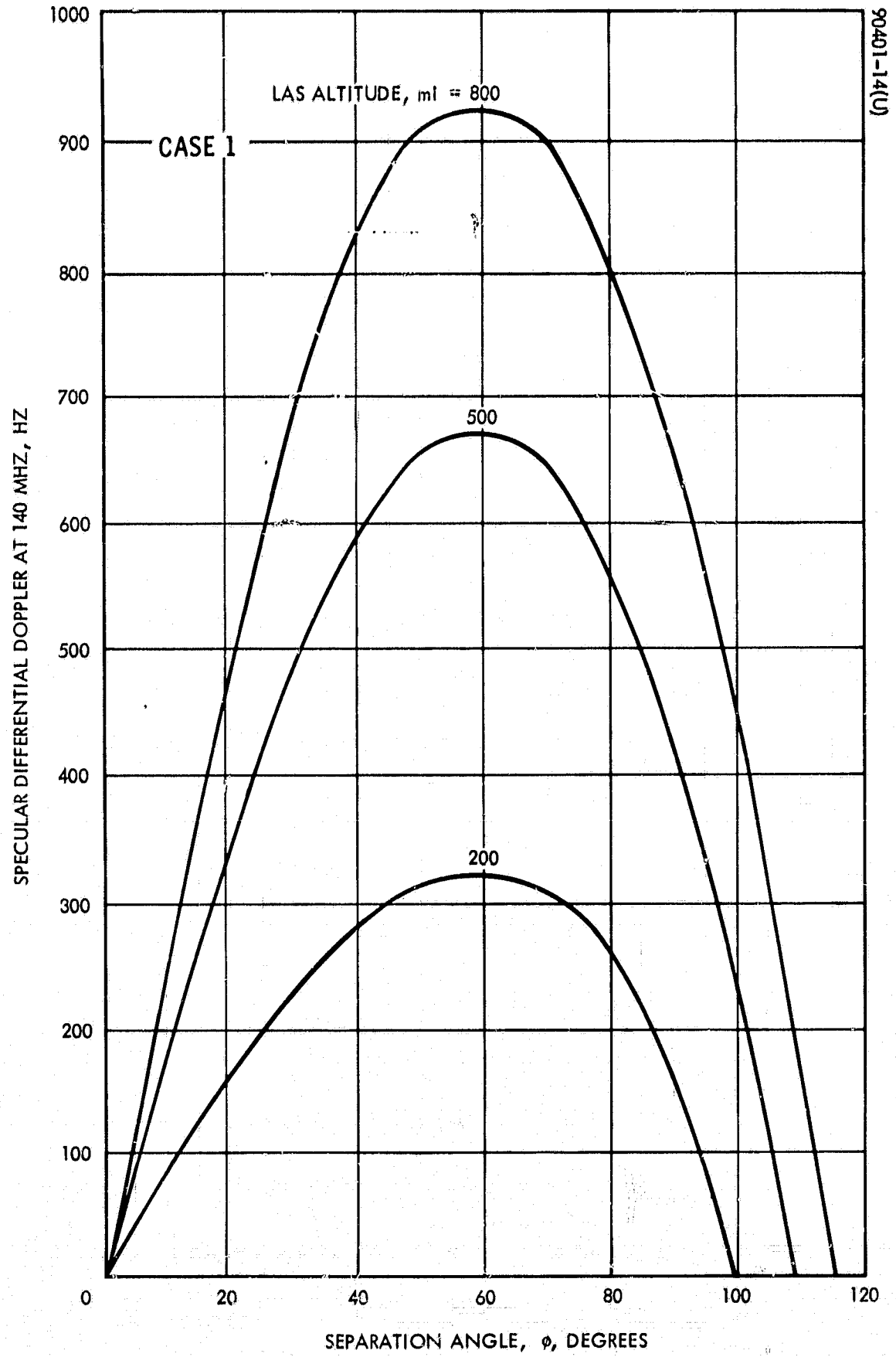

Figure 3-19. Specular Differential Doppler Shift at 140 MHz

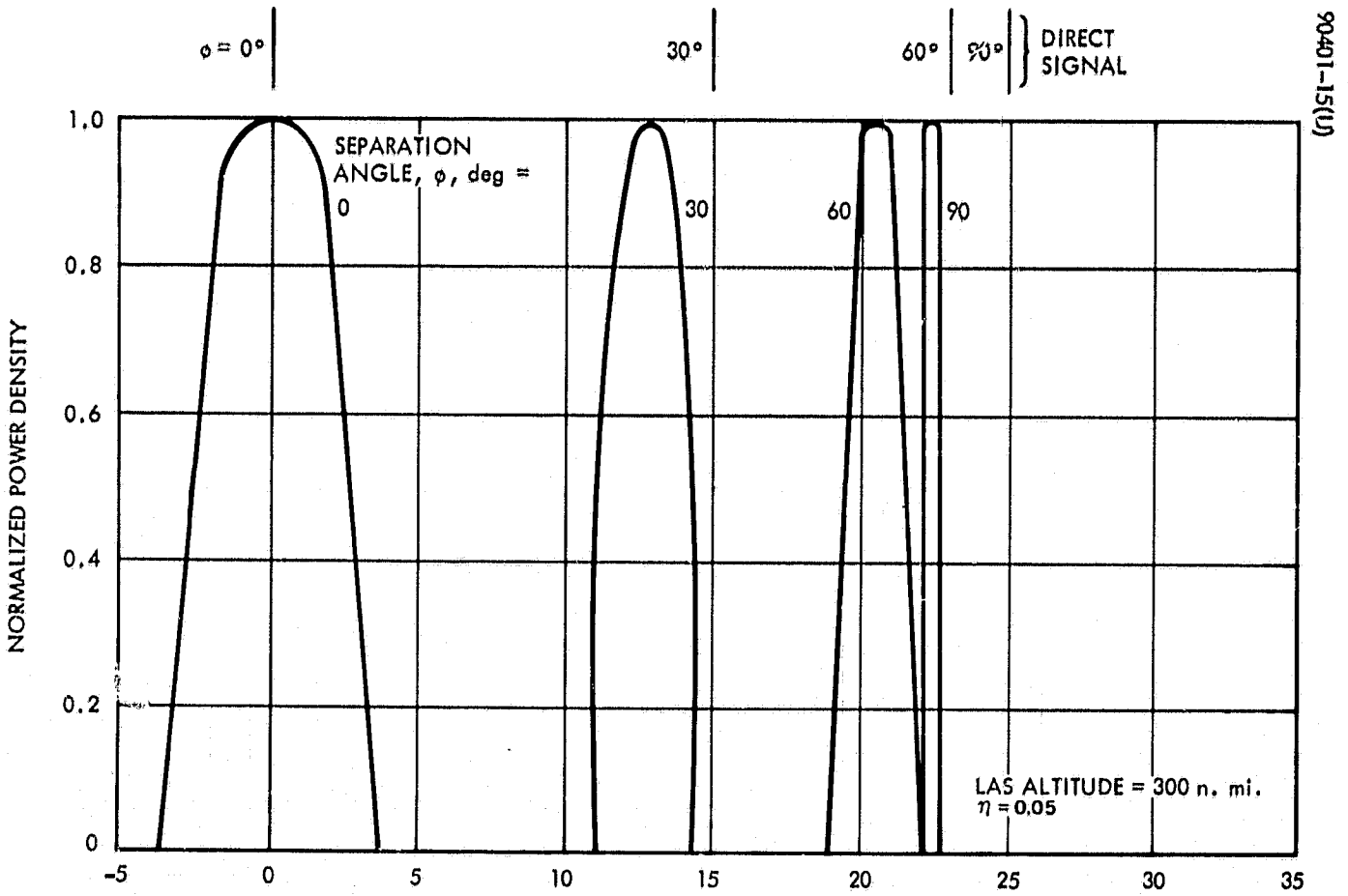

Figure 3-20. Reflected Signal Spectra

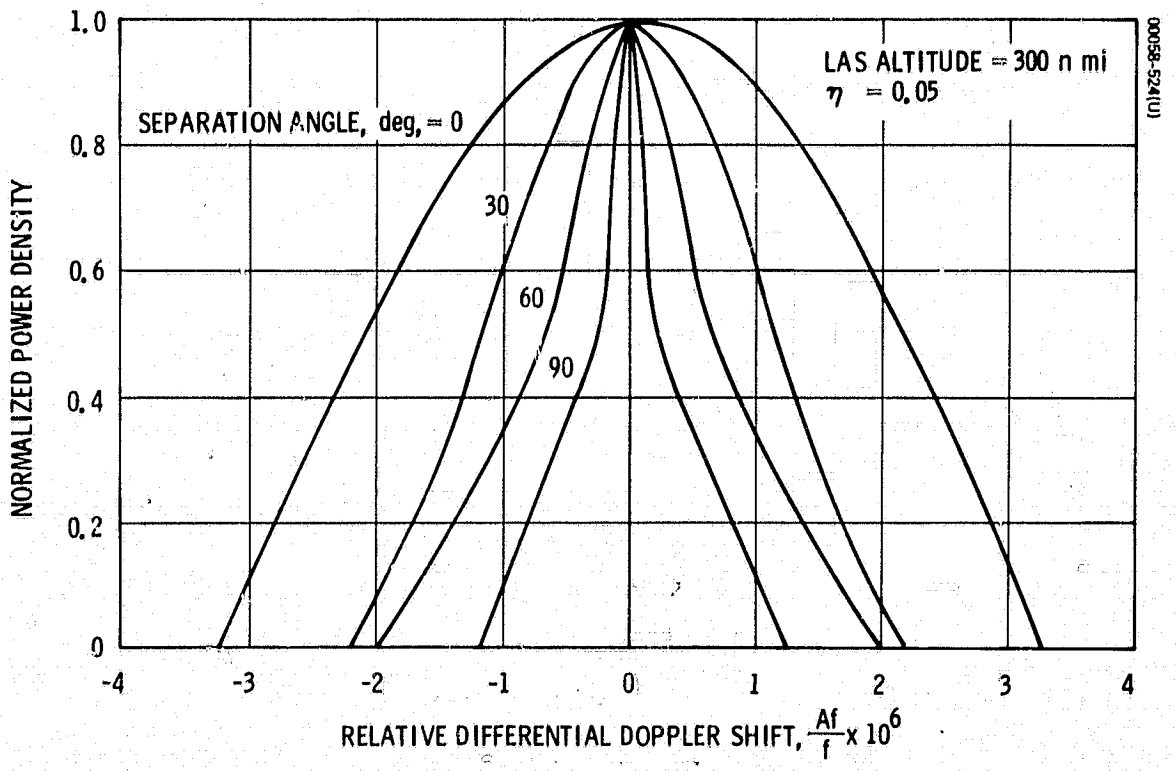

Figure 3-21. Reflected Signal Spectra, Case 3

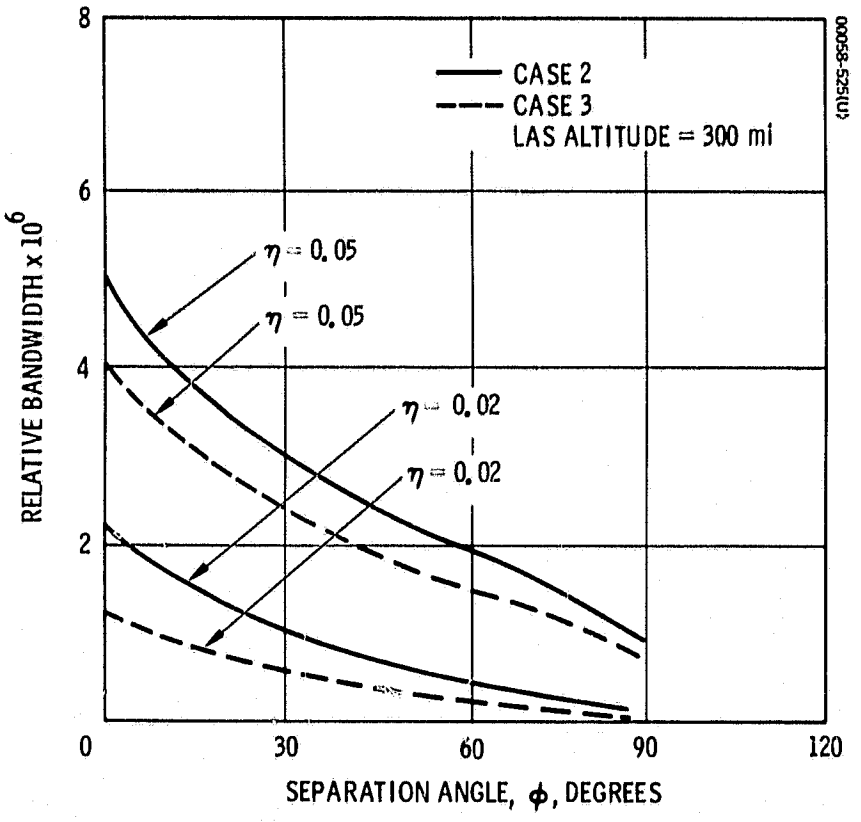

Figure 3-22. Relative Bandwidth of Received Reflected Spectra

Figure 3-22 shows the 3-dB relative bandwidth of the received reflected spectra as a function of the separation angle. The bandwidths for two roughness factors are shown, and, as expected, the bandwidth from the smoother surface is less than that from the rougher surface. This figure may be combined with a plot of the relative specular differential doppler to estimate the range of separation angle for which the relative specular differential doppler shift is greater than one-half the reflected spectrum bandwidth, i.e., where the direct signal frequency lies outside the major portion of the spectrum of the reflected signal. Figure 3-23 is such a combination of these two curves for Case 2 and an LAS altitude of 300 n. mi. It can be seen that, for a roughness factor of $\eta = 0.05$, the direct signal lies outside the bandwidth of the reflected spectrum for $20 \leq \varphi \leq 103$ degrees. If $\eta = 0.02$, this occurs for $\varphi \geq 10$ degrees.

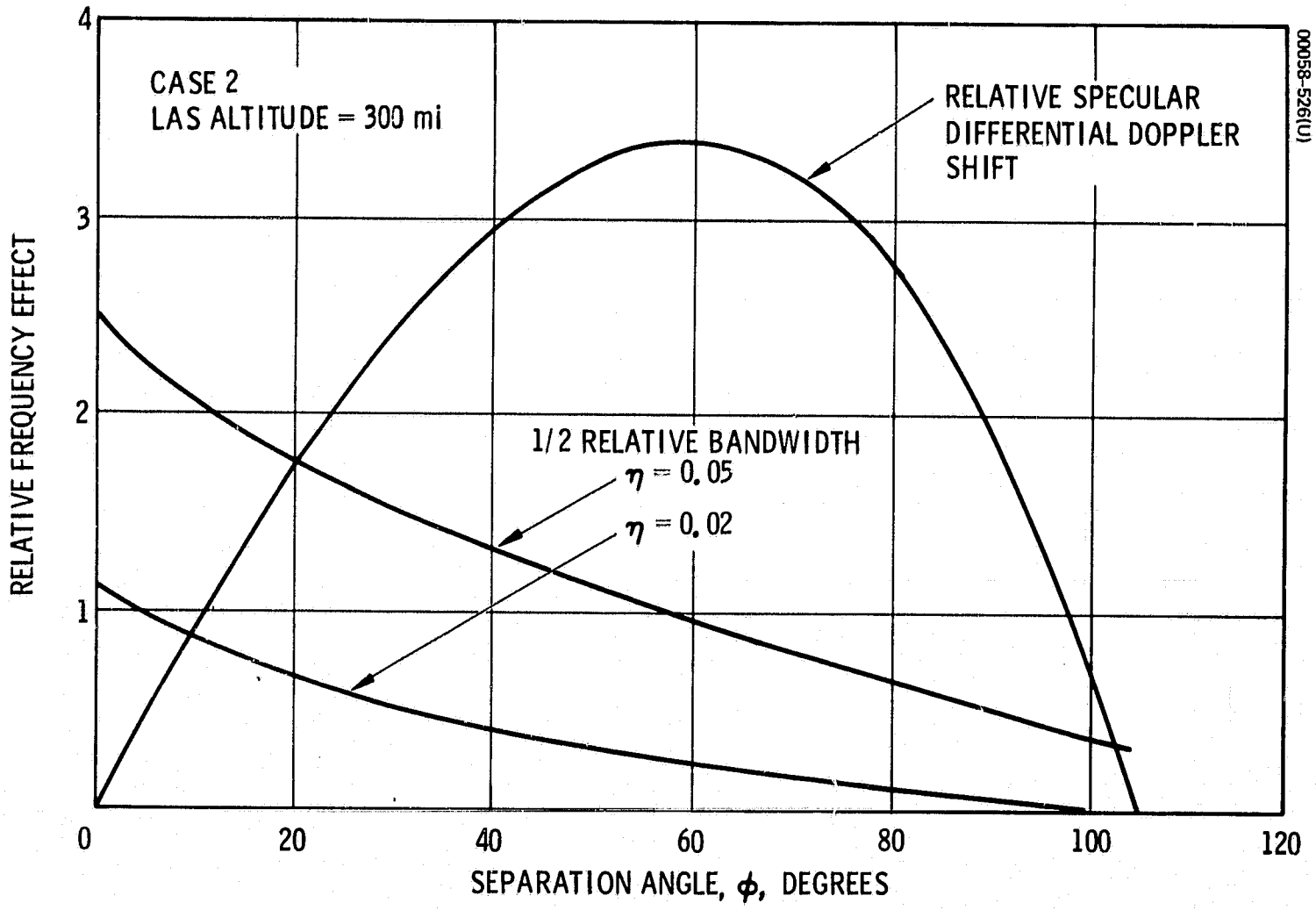

Figure 3-23. Direct Signal Frequency Relationship to Reflected Spectrum

4. COMMUNICATION IMPROVEMENT TECHNIQUES

In Section 3, the various aspects of the multipath phenomenon have been quantitatively displayed and discussed. The next logical consideration is the manner in which communication in the multipath environment can be improved. The link between the LAS and DRS consists of the transmitter and receiver and the environment between them called the "channel." For the sake of this discussion, the channel includes the antennas and feeds, while receiver and transmitter refer, respectively, to the initial and final electronic stages.

From a general viewpoint, assuming that the best possible receiver is used, there are three basic approaches to communication improvement:

1) Increased transmitter power

2) Improved channel characteristics

3) Signal processing

The first approach has limitations which are somewhat intuitive; if more power is transmitted, then the interferring, reflected power will increase with the direct power. Increasing power does provide some improvement, but because the reflected power is also increased, this method is inefficient.

The second approach refers to antenna and feed designs. The physical medium between two antennas is determined by the orbits of the two satellites, but the antennas themselves, as part of the channel, may be designed to discriminate against the reflected signal. Both the directivity and polarization of the antenna may be used to improve communication. These techniques are discussed below, but since the emphasis in this study is on a low data rate omnidirectional (LAS) link, the emphasis is on polarization discrimination.

The third approach concerns the manipulation of the signal itself so that the direct signal may be discriminated from the reflected signal at the receiver. Almost all methods in this category result in an increased transmission bandwidth. Feasible techniques include pseudo-noise coding,

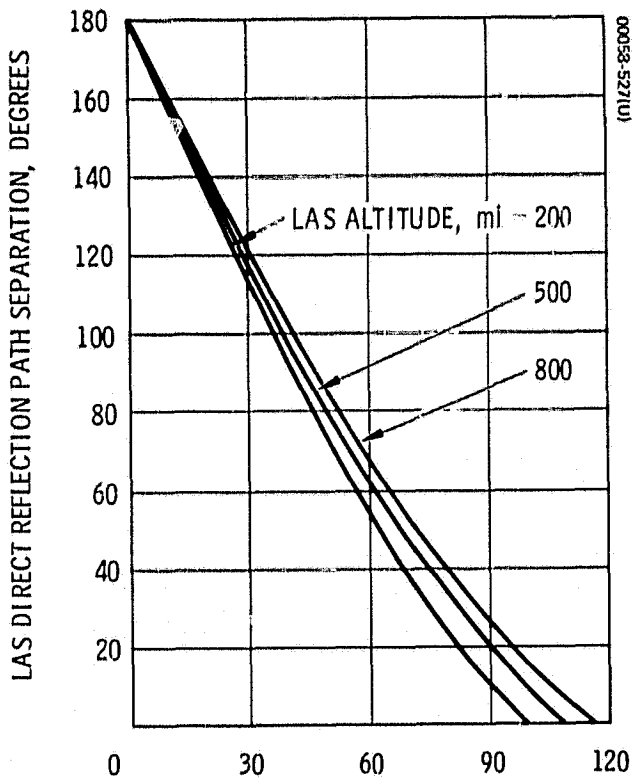

a) LAS

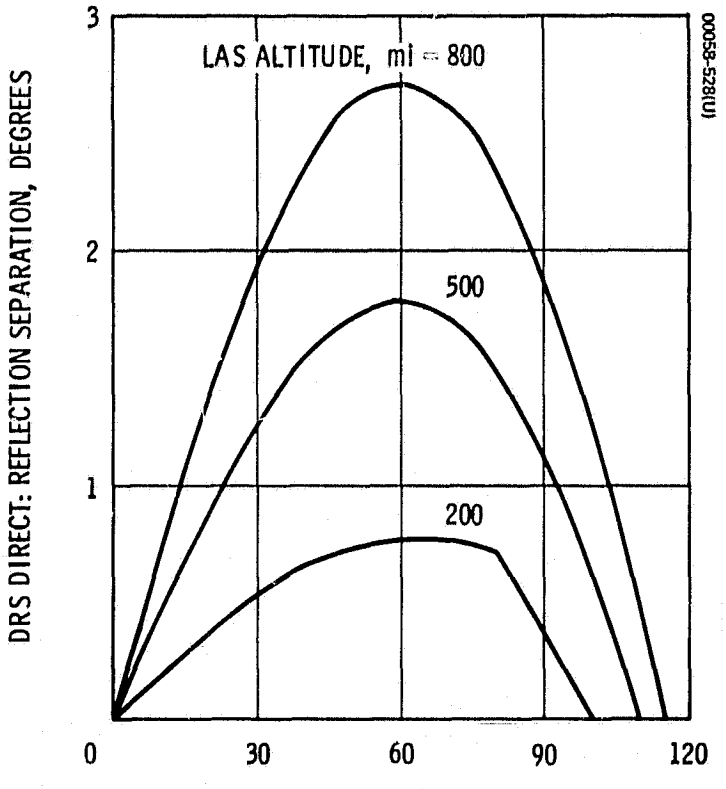

b) DRS

Figure 4-1. Angle Between Direct Path and Specular Point

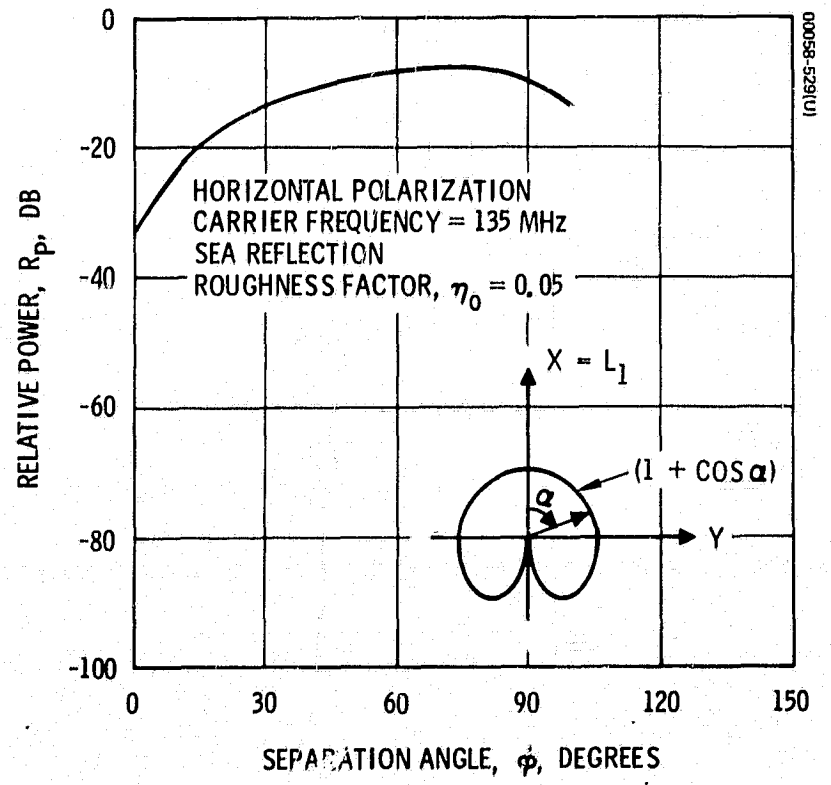

Figure 4-2. Broad Coverage Antenna

diversity techniques, frequency hopping, burst transmission, and data rate limiting. These topics are discussed very briefly later in this section.

4.1 DIRECTIVE ANTENNAS

The interference due to the reflected signal can be essentially eliminated by using directive antennas. The purpose of this discussion is merely to indicate the effectiveness of this approach. Figures 4-1a and b show the angular separation between the direct transmission path and the reflection path to the specular point as a function of the separation angle, φ, for the LAS and DRS, respectively. From Figure 4-1b, it can be seen that the DRS antenna must be highly directional in order to discriminate between the direct and reflection paths. Combining Figures 4-1b and 2-9, it can be seen that, for a 500-mile polar orbit (i = 90 degrees), the direct reflection path separation is greater than 1.0 degree about 70 percent of the time, but is less than 1.0 degree 30 percent of the time and is always less than 1.8 degrees.

A DRS antenna with a 2.0-degree beamwidth would result in a 3-dB reduction of multipath interference 70 percent of the time. Although this is helpful, it does not yield the significant advantage that a less directive antenna on the LAS will give.

Consider a planar array with a gain of 20 dB which corresponds to a beamwidth of about 17 degrees. Then for a 500-mile polar orbit, a 3-dB improvement is possible 90 percent of the time. The gain of the antenna drops below -15 dB for angular deviations from the boresight greater than 14.5 degrees. From Figures 4-1a and 2-9, such an antenna will result in a 15-dB improvement 80 percent of the time. If the LAS antenna has a gain of 30 dB with a 5.0-degree beamwidth, a 15-dB improvement over the omnidirectional case is possible 93 percent of the time for a 500-mile orbit.

The above discussion indicates the effectiveness of directive antennas, particularly on the LAS, in reducing the interfering multipath signal. For any given antenna whose radiation characteristics are known, Figure 4-1a, and 2-9 can be used to evaluate the improvement in multipath reduction.

4.1.1 Broad Coverage Antenna

The use of a broad coverage, but not omnidirectional, antenna may meet mission requirements while reducing multipath interference. An idealized broad coverage antenna pattern is shown in Figure 4-2 along with the resultant received relative power, R_p, for horizontal polarization and sea reflection at 135 MHz. The antenna is mounted on the LAS so that the maximum gain axis, X, coincides with L_1 in Figure 2-3 (the local vertical). The gain pattern is a figure of revolution about the X-axis. Note that because of the null in the pattern in the $-X = -L_1$ direction, the pattern

reduces the multipath signal the most where it would otherwise be the worst — at $\varphi = 0$.

4.2 POLARIZATION DISCRIMINATION

In general, the LAS spacecraft transmits an elliptically polarized wave which is received by the DRS with an elliptically polarized antenna. As special cases, either or both spacecraft may have linearly polarized antennas. Should both spacecraft have linear antennas, these antennas must be aligned for maximum signal reception. Should they become crossed or perpendicular to each other, no direct signal would be received, and, hence, no communication would be possible. For this reason, linearly polarized antennas are not usually employed on both satellites. Should one spacecraft have a linear antenna and the other a circularly polarized antenna, communication would be possible whatever the orientations of the antennas, and the relative power would be essentially that shown in Figures 3-2a and b. However, elliptically polarized antennas may be employed on both spacecraft so as to favor the direct signal over the reflected signal.

Polarization discrimination is based on the fact that, during reflection, the sense of rotation of a circularly polarized wave is reversed if the angle of incidence is smaller than the pseudo-Brewster angle. Referring to Figures 2-16 and 2-18, it can be seen that the horizontally polarized radiation is reflected with a phase shift of approximately 180 degrees with respect to the vertically polarized radiation. Thus, a circularly polarized wave, one with equal horizontal and vertical components has its sense of rotation reversed upon reflection. Most circularly polarized antennas have at least a 20-dB rejection of circularly polarized waves of the opposite sense; therefore, an antenna adjusted to receive the direct signal will reject the reflected signal.

To more clearly illustrate the effect of antenna polarization, consider the polarization coefficient, PC, given by Equation 58 in Subsection 2.6.

$$PC = \frac{\left|1 + P_r P_{rr}\right|^2 \left(1 + \left|P_d\right|^2\right)\left(1 + \left|P_{rd}\right|^2\right)}{\left|1 + P_d P_{rd}\right|^2 \left(1 + \left|P_i\right|^2\right) \left(1 + \left|P_{rr}\right|^2\right)} \qquad (1)$$

where the polarization factors are defined at the beginning of Subsection 2.6. If the DRS antenna is circularly polarized, then from Equation 47 in Subsection 2.5,

$$P_{rr} \approx P_{rd} = j = \sqrt{-1}$$

Similarly, if the LAS transmits circular polarization in both the direct path and scattering region directions, then

$$P_i = P_d = -j$$

For angles less than the pseudo-Brewster angle, the phase of the vertical polarization is reversed, resulting in $P_r = j$. Then, clearly,

$$1 + P_r P_{rr} = 1 + j^2 = 0$$

and so PC = 0.

Of course, a real LAS antenna will not transmit exact circular polarization in two different directions, and the polarization is not completely reversed during reflection. This can be accounted for by antenna ellipticity.

The relative power expressions given by Equations 63 and 64 in Subsection 2.6 contain the polarization coefficient as a factor and may be used to evaluate the effects of elliptical polarization. It was shown in Subsection 3.1 that the smooth earth model gives results very close to those of the rough earth model. Thus, most of the numerical computation associated with this section used this model because of the reduced machine computation expense. Several rough earth computations were made to justify this approach. Figures 4-3 through 4-6 present the computation results.

Figure 4-3 shows the effect of polarization discrimination on the relative power as a function of separation angle for a 140-MHz transmission frequency and sea water reflection. Since the direction of the scattering region and the direct path is nearly the same for the DRS because of its relatively large distance from the earth, the polarization can be considered constant for both the direct and reflection paths. Thus, Figure 4-3a corresponds to a circularly polarized DRS antenna with respect to both the reflection and direct paths (polarization ellipticity = 0). Figure 4-3b corresponds to a DRS polarization ellipticity of -4 dB, which represents a greater amount of vertical polarization. The nine curves in each of these figures correspond to polarization ellipticities of the LAS antenna. Positive ellipticities represent more horizontal polarization than vertical and negative ellipticities imply the converse.

Note that in Figure 4-3a the curve corresponding to a circularly polarized LAS antenna results in excellent reduction of R_p. In Figure 4-3b, the most significant reduction occurs when the LAS has the opposite type of polarization. That is, in Figure 4-3b, the DRS is mostly vertically polarized; thus, if the LAS antenna is mostly horizontally polarized, the relative power will be greatly reduced.

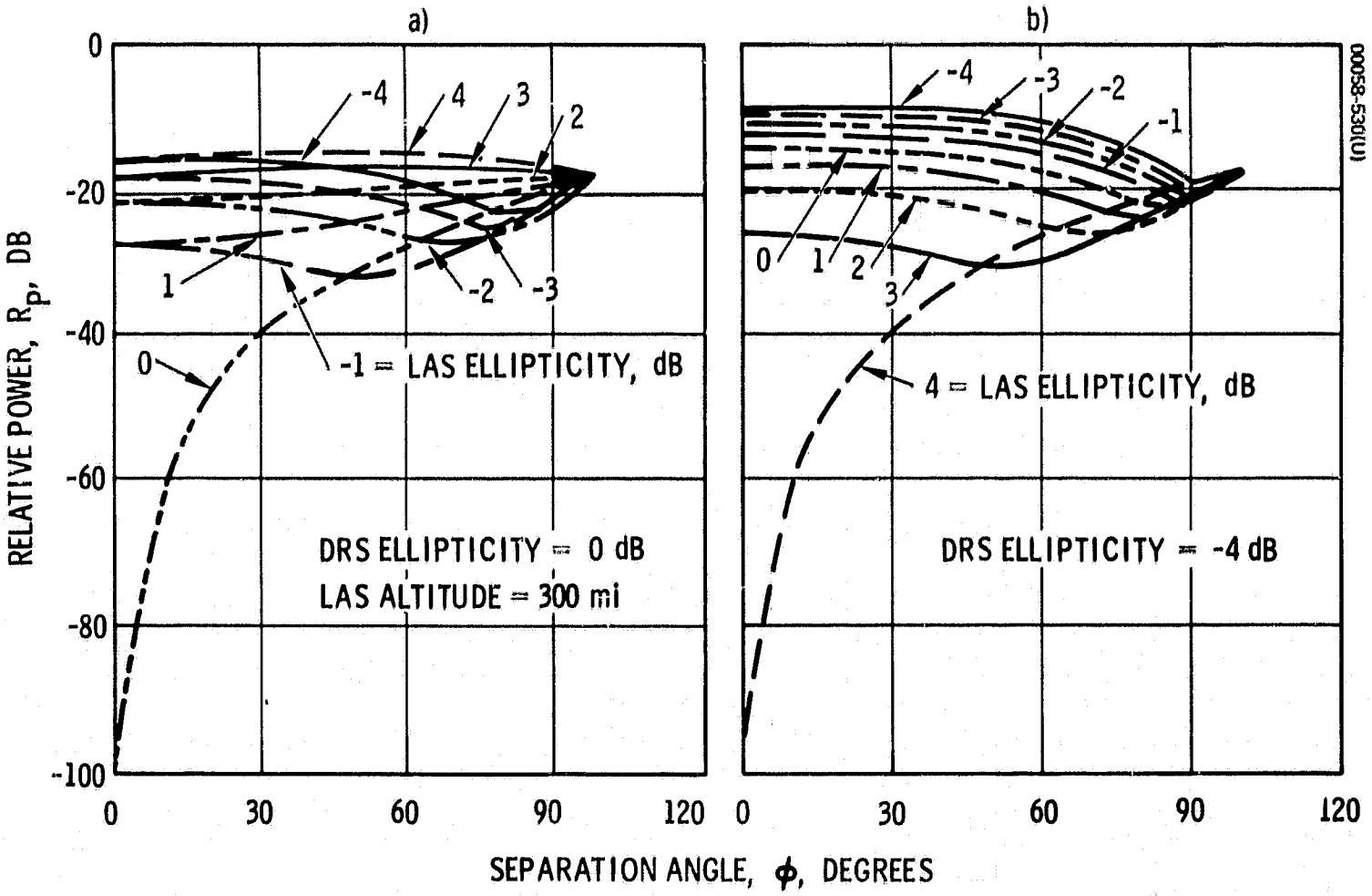

Figure 4-3. Polarization Discrimination for Smooth Earth Model
Sea water reflection for 140 MHz

Figure 4-4 corresponds to sea water reflection for a 2-GHz transmission frequency, and Figure 4-5 corresponds to land reflection for frequencies in the range of 140 MHz to 2 GHz. Comments similar to those above pertaining to Figure 4-3 apply to these also.

Figure 4-6 is the result of rough earth computations for both LAS and DRS antennas circularly polarized with respect to the two transmission paths. For separation angles greater than 10 degrees, there is very close agreement between these results and the circular polarization curves of Figures 4-3a, 4-4a, and 4-5a. For smaller separation angles, the rough earth calculations are deemed to be the more correct.

4.2.1 Conclusion

From examination of Figure 4-3 and 4-5, it appears that, at a transmission frequency of 140 MHz, circularly/elliptically polarized antennas on the LAS and DRS will reduce the relative power to -9 dB or less.

4.3 SIGNAL PROCESSING

Signal processing here refers to all methods whereby the data or information signal is manipulated, modulated, or modified prior to the transmitter output stage and to any such signal manipulation following the receiver input stage. A variety of feasible techniques are presented below with a brief qualitative discussion. These techniques are discussed in greater detail in other literature and are presented here mainly for completeness of this study.

4.3.1 Pseudo-Noise Coding

Pseudo-noise (PN) coding is part of the general class of spread spectrum techniques and is one of the most attractive for combating the effects of LAS/DRSS multipath propagation. Basically, the data signal is modulated prior to transmission by a signal corresponding to a PN sequence. This combined signal is demodulated at the receiver in a correlation process which improves the signal-to-noise ratio and discriminates against the reflected signal.

The three defining properties of an important class of PN sequences called maximum length linear sequences are as follows:

1) In each period of the sequence, the number of ONE's differs from the number of ZERO's by, at most, one.

2) Among the runs of ONE's and of ZERO's in each period, one-half of each kind are of length one, one-fourth of each

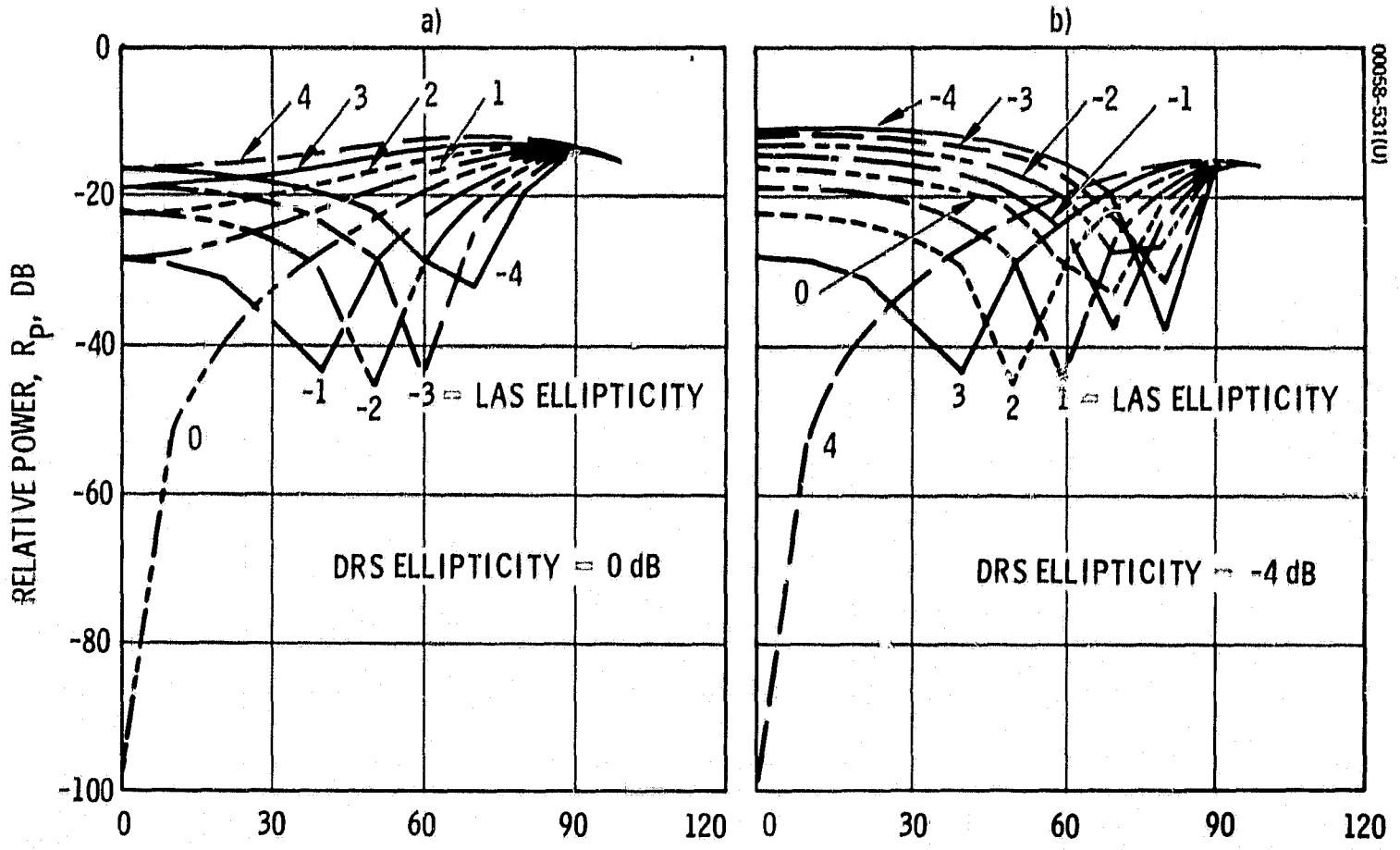

Figure 4-4. Polarization Discrimination for Smooth Earth Model
Sea water reflection for 2 GHz

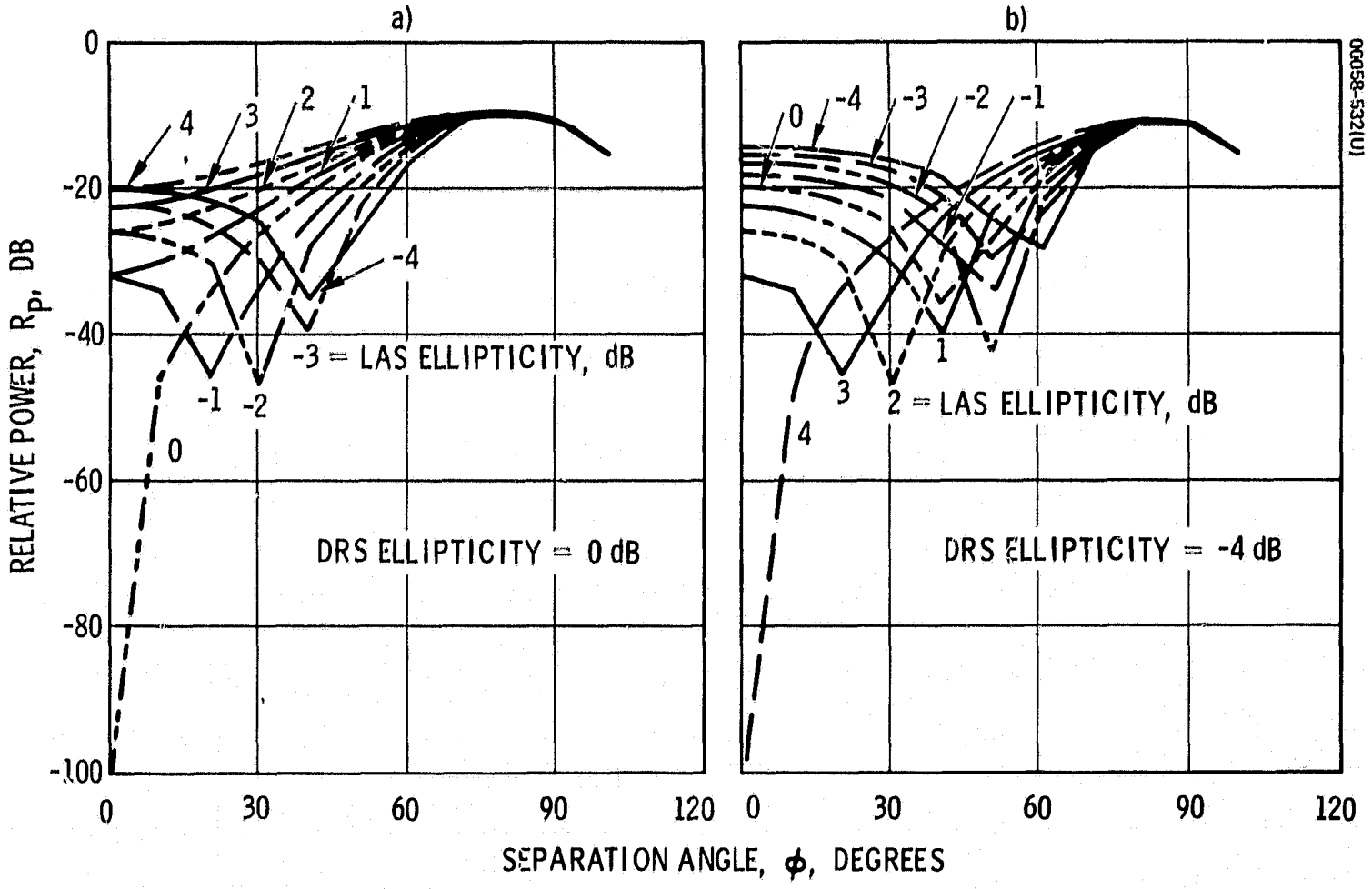

Figure 4-5. Polarization Discrimination for Smooth Earth Model
Land reflection for 140 to 2 GHz

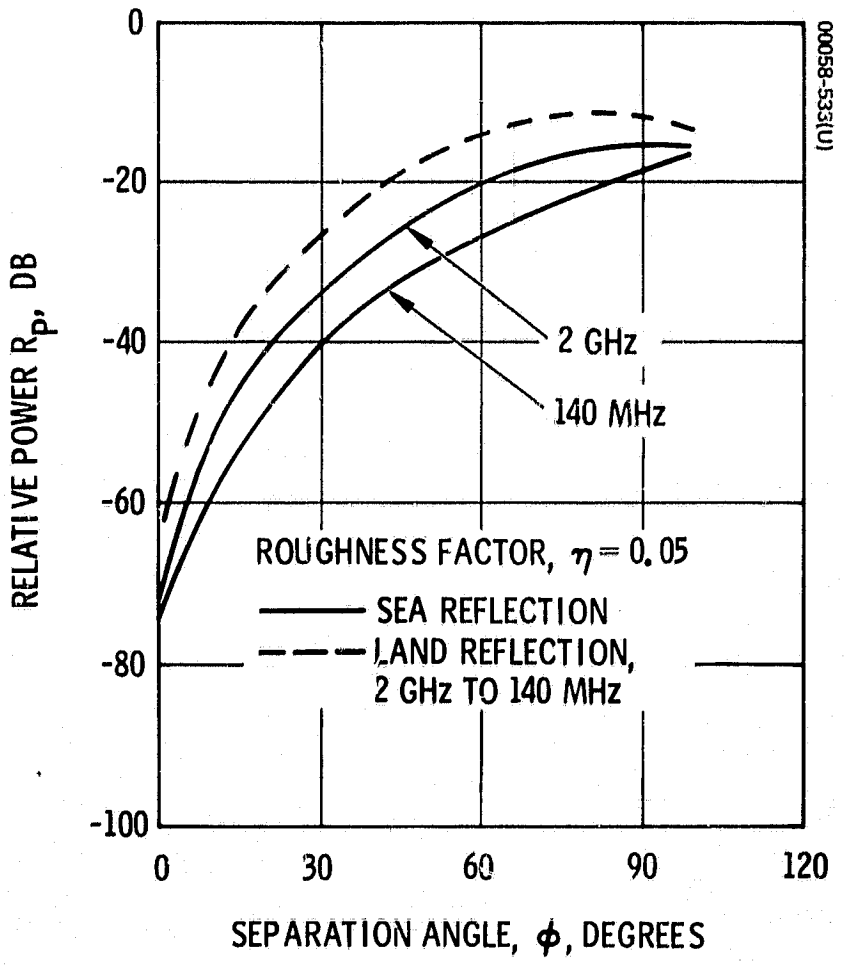

Figure 4-6. Polarization Discrimination for Rough Earth Model LAS and DRS antennas circularly polarized

kind are of length two, one-eighth are of length three, and so on as long as these fractions give meaningful numbers of runs.

3) If a period of the sequence is added modulo 2 with any cyclic shift itself, the number of agreements differs from the number of disagreements by one at most.

This last property can be restated as follows: For integral phase displacements, the autocorrelation function of a PN sequence is two valued. Specifically, it looks as is shown in Figure 4-7, where, if s(t) represents a normalized PN code signal

$$R_s(\tau) = \frac{1}{T} \int_o^T s^*(t)\ s(t + T)\ dt$$

It is the nature of the autocorrelation function which makes a PN sequence useful for signal detection.

By performing the correlation process on the received signal and detecting the peak of the autocorrelation function, interfering noise and signals such as the multipath signal can be rejected. One requirement for a PN system to operate properly in the LAS/DRS multipath environment is that a code pulse length be shorter than the delay between the direct and reflected signals. Referring to Figure 3-12, if the code pulse width is 0.1 millisecond, then this system will operate correctly in a 300-mile altitude satellite for separation angles less than 93 degrees. When the separation angle is larger, the time delay between the direct and reflected signals is less than the pulse width which corresponds to an RF bandwidth of approximately 20 kHz. Decreasing the pulse width, which requires an increase in bandwidth, will allow greater communication time. Thus, mission requirements and frequency allocations will have a major influence in determining the code pulse width.

4.3.2 Diversity Techniques

Diversity techniques involve the establishment of N distinguishable, dissimilarly fading signal transmission channels. The diversity receiving system chooses at each instant a desirable combination of these signals. The techniques include space diversity, angle of arrival diversity, polarization diversity, frequency diversity, time diversity, and multipath diversity. The first three are not purely signal processing techniques as defined above. Space diversity and angle of arrival diversity require two or more antennas and receivers, which is somewhat impractical on a spacecraft. Polarization diversity requires crossed linearly polarized feeds with separate receivers. Frequency diversity requires transmission of the signal

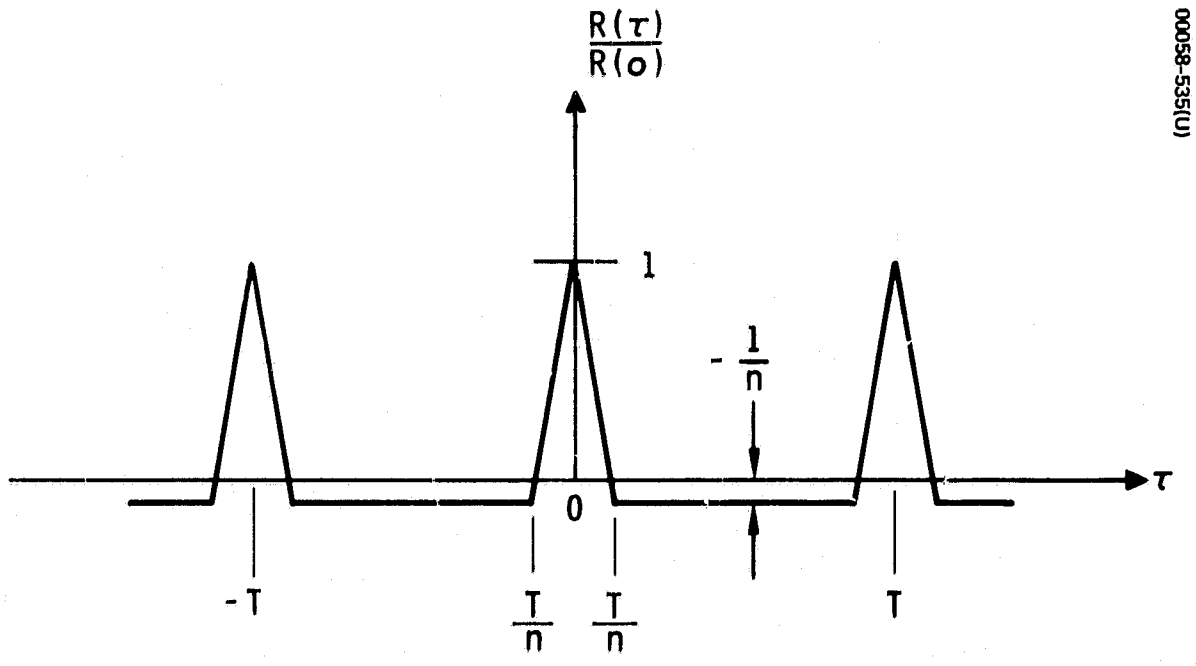

Figure 4 7. Autocorrelation Function of PN Sequence

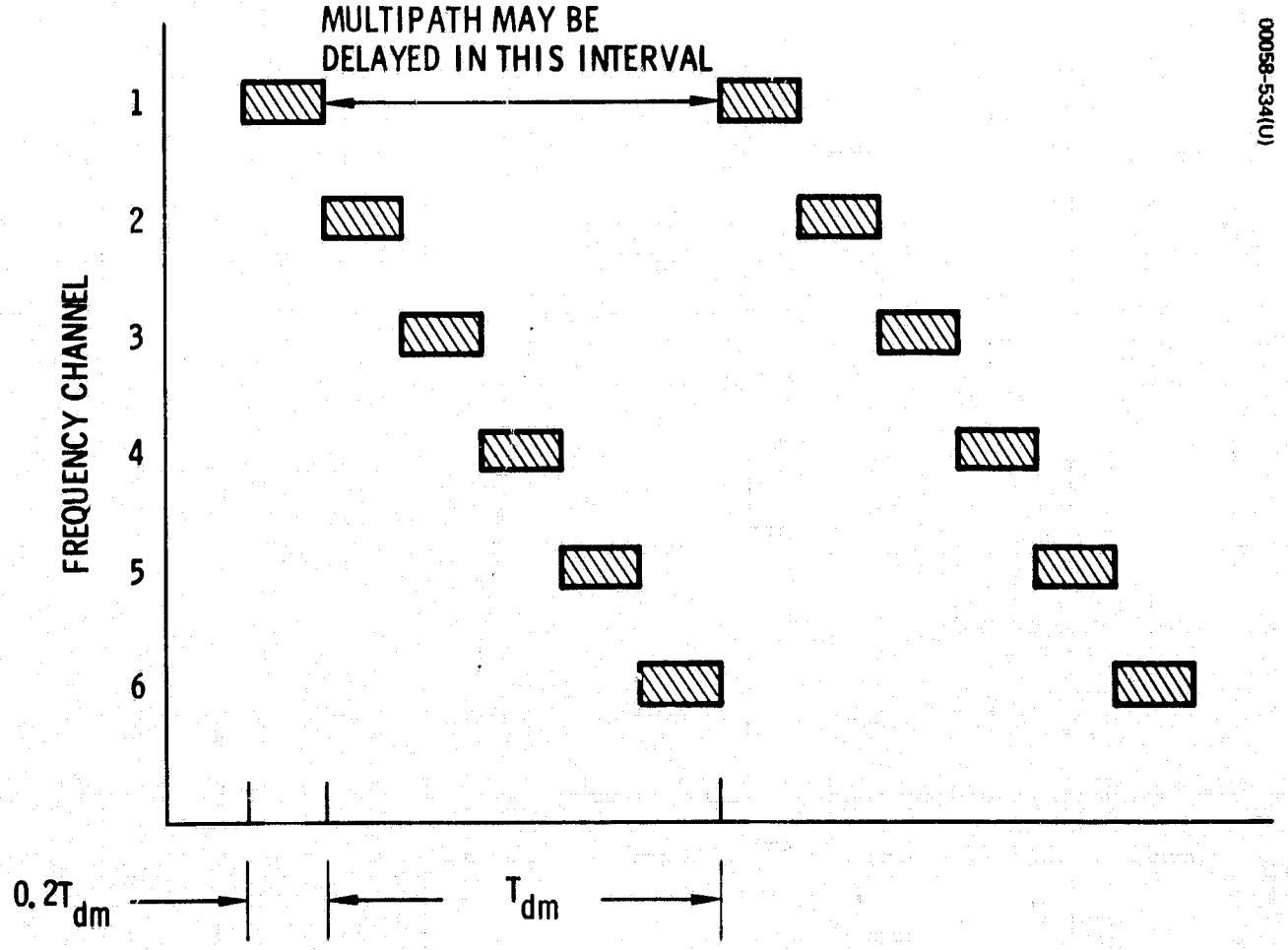

Figure 4-8. Frequency Hopping

on two or more different carrier or subcarrier frequencies. Time diversity and multipath diversity are closely related and have been applied only to digital transmission. In time diversity, the same information bit is repeated at time intervals greater than the reciprocal of the fading rate. This technique requires storage at both the transmitter and receiver. If the multipath consists of many channels with various delay times, with a multipath diversity system the received signal can be processed to separate the signals corresponding to different paths and then be recombined. These techniques, along with combination analysis are treated at length in Reference 24.

Diversity techniques are usually employed in a multipath environment similar to the reflection path alone, and they are used to combat the Rayleigh fading that occurs in this phenomenon. But, for the geometry and physics of this problem, there are only two basic paths rather than many, even though the reflection path consists of a collection of many subpaths. Thus, a diversity technique would establish a number of channels to provide a signal combination which would ameliorate the fading caused by interference of the two basic transmission paths.

4.3.3 Frequency Hopping

In the frequency hopping scheme, the carrier frequency of the transmitter is switched in a cyclic progression through several values. The receiver must be synchronized to the transmitter and thus rejects the delayed multipath signal whose frequency differs from that being instantaneously accepted by the receiver. To clarify this technique, consider an example where each frequency is to be transmitted for a period equal to one-fifth the maximum specular differential time delay, T_{dm} (see Subsection 3.2). After completion of transmission at one frequency, the corresponding multipath signal may arrive at the receiver until T_{dm} seconds after completion of the transmission. Thus, 1.2 T_{dm} seconds are required between the beginnings of transmissions at each frequency, and, since each transmission lasts 0.2 T_{dm} seconds, six frequencies will be required. Figure 4-8 illustrates these concepts.

Power requirements are the same as for continuous transmission at a single frequency, but the bandwidth must be increased to something larger than six times the original bandwidth. The relationship between the original bandwidth and the frequency hopping bandwidth depends on the size of the original bandwidth and the doppler shift effects (see Subsection 3.3).

It should be noted that, in the above example, multipath interference can be eliminated when the multipath delay is greater than 0.2 T_{dm}, but, when it is less, interference will occur. If the LAS altitude is 500 miles, then according to Figure 3-12, the system in the above example would not eliminate interference for separation angles larger than about 80 degrees. Thus, from Figure 2-9, this system would eliminate interference about 54 percent of the mission lifetime for an LAS polar orbit, and about 74 percent of the time for an equatorial orbit.

4.3.4 Burst Transmission

Related to the frequency hopping method is the technique of burst transmission. Only one transmission frequency is used, but data is transmitted in periodic bursts where a burst transmission period is a fraction α of the maximum specular differential time delay, T_{dm}. The time between bursts is $(1 + \alpha)T_{dm}$, and so the data compression factor is given by $C_d = (1 + \alpha)/\alpha$. If α is again chosen to be 0.2, then $C_d = 6$, and the RF bandwidth must be increased by this factor. For this system, the peak power increases also by the factor C_d, but the average power is the same as for continuous transmission.

4.3.5 Data Rate Limiting

With data rate limiting, a simple technique, data bits are transmitted with pulse lengths which are large compared to the maximum specular differential time delay, T_{dm}. Thus, if the pulses have lengths of βT_{dm}, where β is a factor based on system concideration ($\beta > 2$), then the bit rate, R_b is given by

$$R_b = \frac{1}{\beta T_{dm}}$$

If $\beta = 4$ and the LAS altitude is 500 miles, then from Figure 3-12, $R_b = 46.5$ bits/sec. This rate may be adequate for housekeeping telemetry and command data. For a given value of β, the data rate will decrease with increasing LAS altitude.

5. EXPERIMENTS

Experimental data is needed to validate the statistical and mathematical assumptions employed in developing the mathematical model of Subsection 2.4. Sections 3 and 4 present the results of computation based on this model, but this quantitative data is no more valid than the assumptions used to produce it. If experimental data differs significantly from the results based on the model, then this data may be used to modify the model, i.e., to correct and calibrate it. Whether or not the experimental data agrees with mathematical results, it is required for confidence in the characteristics of the multipath phenomenon.

5.1 EXPERIMENT DEFINITION

The characteristics to be measured experimentally are those discussed in Section 3, namely the relative power, time response, and frequency effects. Of these three, the relative power, i.e., the ratio of average reflected power to direct path power, is most important. The time spreading of the reflected signal is much smaller than the differential delay, which can be computed from purely geometric considerations, and, hence, is of least importance. Measurement of frequency spreading will allow evaluation of the statistical assumptions used in developing the rough earth mathematical model (see Subsection 2.4).

A number of propagation aspects influence the multipath phenomenon; they are quantitatively included in the mathematical model in the parameters of the basic formulas (see Section 2). These aspects include:

Surface state: Determines the roughness factor, η, of Equations 63, 77, and 78

Surface type: The electrical properties of the surface influence the reflection coefficient, R_c, in Equations 20 and 37

Polarization: The polarization of the electromagnetic wave with respect to the surface and the receiving antenna influences the reflection coefficient and the polarization efficiency, respectively (see Subsections 2.4 and 2.5)

Transmission frequency: Influences both the reflection coefficient and the smoothness factor

Geometry: This is probably the most important aspect since the separation angle is the single most important parameter. The altitudes of the satellites also influence the reflection and direct path characteristics. In particular, the distances V_O, V_L, and V_D; the reflection coefficient; and the incidence angle, θ, are a function of the geometry. For known antenna characteristics, both the gain and polarization for the two paths will be determined by the geometry.

A complete experimental program will provide a sufficient variation of each parameter associated with these aspects to evaluate the validity of the mathematical model over the range of interest. For the roughness factor, η, a range of variation should be established.

5.1.1 Signal Reception

The evaluation of data is facilitated if signals from the reflection path and direct path can be received separately. This can be accomplished by either two antenna and receiving systems or a single receiving system which separates reception from the two paths by time. That is, first the reflected signal is passed through the receiver and then processed, and then the direct signal is passed through the same receiver and processor. The scheme employing two receivers eliminates any possibility of error due to the time separation of the two measurements, while the latter method, employing only one receiver, eliminates the need for calibration.

This separation of signals requires directive antennas. From Figure 4-1, it can be seen that, for a satellite-to-satellite link, beamwidths as large as 20 degrees will allow signal separation over a wide range of separation angles. However, at aircraft altitudes, the angular separation of the two paths is much smaller, and, consequently, a highly directive antenna will be required to separate the two signals. Directive antennas imply the use of higher frequencies, yet some of the multipath characteristics are particularly of interest at VHF where directive antennas are not feasible. Thus, while many aspects of the mathematical model may be checked with the use of high-frequency transmission (1 GHz and above), a complete evaluation of the model will require measurements at VHF with broad coverage antennas.

By proper shielding, VHF antennas can be made somewhat directive, thus effecting a separation of the reflected and direct signals over a range of geometric variation. But when separation of the two signals with directive antennas is not feasible or practical, modulation and signal processing may be employed to aid in evaluating the multipath characteristics. Further, even with separated signals, the modulation technique affects the ease of processing and evaluating the data.

5.1.2 Modulation

An attempt was made to evaluate the efficiency of various types of modulation in determining various characteristics of the reflected signal when the signals can be separated. These qualitative results are shown in Table 5-1. Thus, when reflected and direct signals can be separated, transmission of a single frequency carrier will allow determination of the major characteristics, i.e., the frequency spreading, polarization effects, reflection coefficients, and hence, the relative power. The time delay and time spreading may be measured by short pulses.

When the two signals cannot be separated, short pulses again will allow evaluation of all characteristics, but the processing complexity is much greater than for the separate signal case.

5.2 LABORATORY MEASUREMENTS

A relatively simple and inexpensive series of experiments could be performed using simulated sea surfaces in a laboratory environment. Based upon existing knowledge of sea state and sea statistics, a computer-generated sea surface may be constructed of clay or plaster of paris and then given the appropriate electrical properties by spray-coating this surface. This type of surface model would allow variation of the geometry, polarization, and transmission frequency, and frequency spreading and relative power could be evaluated. These two reflection characteristics may be used to evaluate the validity of many of the assumptions and approximations used in the development of the mathematical model. Further, several surfaces could be simulated in order to allow variation of the roughness and electrical properties.

TABLE 5-1. TYPE OF MODULATION*

Type of Modulation	Data That Can Be Extracted From Multipath Signal			
	Differential Time Delay	Frequency Spread	Polarization	Reflection Characteristics
CW	No	Yes 1	Yes 1	Yes 1
Narrow pulses	Yes 2	Yes 2	Yes 2	Yes 2
FM	Yes 4	Yes 3	Yes 3	Yes 3
Frequency sweep	Yes 1	Yes 3	Yes 3	Yes 3
PCM-FM	Yes 3	Yes 3	Yes 3	Yes 3

*The numbers 1 through 4 indicate the range of implementation difficulty, i.e., 1 = easy, 4 = difficult.

5.3 REAL ENVIRONMENT EXPERIMENTS

Although laboratory measurements can provide an intermediate and useful step in evaluating the characteristics of the multipath phenomenon and in evaluating the mathematical model developed in this study, confidence will be lacking in the conclusions drawn from these results because the measurements are based upon a simulation of the natural phenomenon rather than the actual phenomenon itself. It is, therefore, most natural to turn to the real earth reflection process in order to gain confidence in the data and the mathematical model it may validate. Feasible experiments, in order of sophistication and usefulness, are described below.

5.3.1 Aircraft/Aircraft Propagation

Transmission between two aircraft with highly directive antennas will allow reflection coefficients and polarization effects to be evaluated. Relative power and frequency spreading will provide data points for verifying the mathematical model. The geometry, frequency, and polarization may be varied, and it is relatively easy to make measurements of wave height in the scattering region.

5.3.2 ATS-V/Aircraft

A directional antenna on an aircraft, which may be pointed upward to receive the pulse-like transmission direct from the ATS-V spinning spacecraft and then toward the earth for receiving the reflected signal, would allow determination of relative power for verifying the mathematical model. Because of the short pulse nature of the received transmission, frequency spreading data will require more processing than the aircraft/aircraft experiment. The advantages of this experiment over that described in Subsection 5.3.1 are: 1) only one aircraft need be equipped and flown, and 2) the geometry is closer to that of the LAS/DRSS geometry, resulting in scattering from a larger region than the aircraft/aircraft experiment. The disadvantages are: 1) the frequency is fixed in the L-band, and 2) polarization measurements are limited. This experiment is particularly attractive because of the relative ease of implementation and the near LAS/DRS geometry.

5.3.3 ATS-F/Nimbus E

At present, an experiment is planned for data transmission between the Nimbus E, low-altitude spacecraft, and the ATS-F synchronous satellite. Thus, the geometry is exactly that of interest in this study. An S-band directive antenna is used for this link. The feasibility of using these two satellites for multipath measurements depends on the ability of the Nimbus E to point the directive antenna toward the earth. At the time of this writing, the antenna's location and pointing capabilities allow the antenna to point at the earth only for large separation angles when Nimbus E is operating in its normal earth pointing mode. If the attitude could be changed and monitored, the antenna could point toward the specular point for earth reflection to ATS-F. This experiment would provide excellent data and allow an evaluation of the actual effects experienced in the LAS/DRSS environment.

5.3.4 ATS-G/LAS

An e. periment specifically for measuring multipath characteristics could be designed to employ a low-altitude satellite transmitting to the ATS-G spacecraft. This experiment should be designed to supplement data acquired by any previous experiments and, further, should allow variation of as many parameters as possible while providing data for evaluating the three effects mentioned in Subsection 5.1.

APPENDIX A. COMPUTER PROGRAM FOR MULTIPATH COMPUTATIONS

A computer program was written in the FORTRAN IV language for computing the quantities of interest in Section 3, i.e., total relative power, time spreading, and frequency spreading. The basis for computations is given in Section 2, and the final equations which are employed in the program are given by Equations 63, 64, 77, 78, 80, and 81 of Subsection 2.6. There are many quantities in the expressions of these equations which must be determined in intermediate steps.

The only geometric input quantity is the LAS altitude. From this, the maximum value of the separation angle, ϕ, is determined, and then the program progresses in increments of ϕ from an initial value, both of which are input quantities, to a final value of ϕ, which differs from ϕ_{max} by less than the increment. For each value of ϕ, a complete computation of all the characteristics is performed.

The specular point is determined first by an iterative procedure, and then many quantities related to the specular point are calculated. These include:

1) Reflection coefficients – horizontal and vertical

2) Geometric angles shown in Figure A-1

3) The magnitudes of V_o, V_L, and V_D shown in Figure A-1

4) Specular time delay

5) Differential time delay

6) Specular relative doppler

7) Differential relative doppler

8) The differential doppler for the input frequency of interest

9) Coherency factor

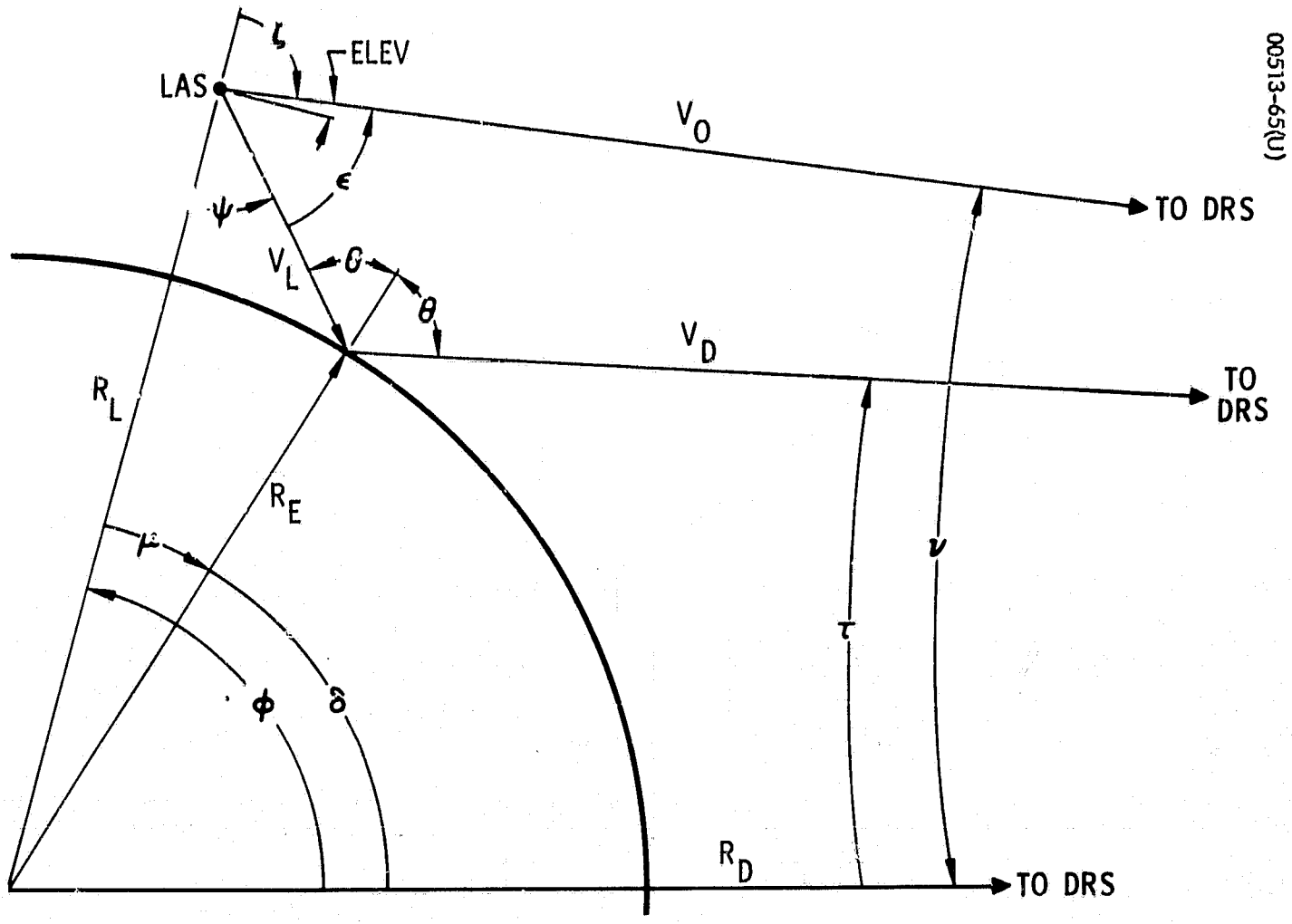

Figure A-1. Specular Point Quantities

10) Divergence factor

11) Shadowing coefficient

The input quantities which are used in the above computations are:

1) Surface relative dielectric constant

2) Surface conductivity

3) Transmission frequency

4) Roughness factor, η

5) RMS surface variation, σ

Characteristics for antennas different from the two linear orientations defined in Subsection 2.6 can be specified via subroutines. The output of the subroutines are gains and polarization factors in the direct and scattering point directions for both the DRS and LAS antennas. Using these, the program also computes a value for the polarization coefficient at the specular point.

With the above computed quantities, the relative power is computed for a perfectly smooth earth for the two linear polarizations and for the subroutine antenna characteristics. Using the coherency factor corresponding to the input frequency and rms surface variation, the smooth earth relative power multiplied by the coherency factor yields an estimate of the coherent relative power. The program then begins its rough earth calculations.

The rough earth relative power estimates are a result of numerical integration over the earth's surface. However, since the significant reflected power is scattered from a limited region surrounding the specular point, it is necessary to determine some bounds on this region. Referring to Figure 2-7, the integration is performed for surface increments dS by varying the two geocentric angles α and β in small increments. The size of a patch is $R_E^2 \cos\beta \, d\alpha \, d\beta$. The size of the scattering region varies with the separation angle as shown in Subsection 3.1.3. But, limits on the angles α and β can be established for a given value of φ. It can be shown that for $\varphi = 0$

$$\gamma \approx \frac{R_E \, d\alpha}{2h}$$

where h represents the LAS attitude.

Using the above equation, define α_o by

$$\alpha_o = \frac{2h\eta}{R_E}$$

which is the value of α where $\gamma \approx \eta$. Since the scattering cross section is a function of $\exp(-\tan^2\gamma/\eta^2) \approx \exp(-\gamma^2/\eta^2)$, the limit on both α and β for $\varphi = 0$ was chosen to be $4\,\alpha_o$. But, for $40 \leq \varphi < 80$ degrees, the limit on α was increased to $8\,\alpha_o$, and for $80 \leq \varphi < 120$ degrees, $\alpha_{lim} = 12\,\alpha_o$. The limit on β remained the same for all values of φ.

To determine the integration increments $d\alpha$ and $d\beta$, several values were tried, and reliable results with reasonable computation time were achieved with

$$d\alpha = d\beta = 0.4\,\alpha_o$$

The program then performed the summation of incremental relative power for

$$-\alpha_{lim} \leq \alpha \leq \alpha_{lim}$$

$$-\beta_{lim} \leq \beta \leq \beta_{lim} = 4\,\alpha_o$$

with α and β varied in increments of $0.4\,\alpha_o$. For $\varphi = 0$, this amounts to dividing the scattering region into 400 scattering patches, and for $\varphi \geq 80$ degrees, 1200 patches comprise the scattering region.

The formulas used are given by Equations 63, 77, and 78 of Subsection 2.6 where the following common factor is first computed.

$$C_s(\alpha, \beta) = \left(\frac{V_o^2}{V_L^2 V_D^2}\right) \frac{S(\theta)}{4\pi \eta^2 \cos^4\eta} \exp\left(-\frac{\tan^2\gamma}{\eta^2}\right)$$

Then the factors accounting for the antenna characteristics are employed. For instance, from Equation 77 of Subsection 2.6 for horizontal polarization

$$(dR_p)_{HH} = \left|E_{HRH}(\alpha, \beta)\right|^2 C_s(\alpha, \beta)$$

and so

$$(R_p)_{HH} = \sum_S \left|E_{HRH}(\alpha, \beta)\right|^2 C_s(\alpha, \beta)$$

where E_{HRH} is given by Equation 73 of that same subsection. Similarly, for vertical polarization, as defined in Subsection 2.6

$$(dR_p)_{VV} = \frac{\left|E_{VRV}\right|^2}{\cos^2 \nu} C_s$$

For a general set of antenna characteristics, from Equation 63 of Subsection 2.6

$$dR_p = \frac{G_3 G_4}{G_1 G_2} \left| K_{hh} + P_i K_{vh} \right|^2 (PC) C_s$$

where the quantities in the above expression are defined in Section 2.

For each value of α and β, the differential time delay between the reflection paths corresponding to specular point and the scattering patch center is calculated. The incremental relative power is then accumulated in time slots, resulting in an impulse response for the reflection process.

Similarly, for relative velocities of the two satellites, corresponding to Case 2 of Subsection 3.3, the relative differential doppler shift between the specular point and scattering patch center is calculated. Then the incremental relative power is accumulated in relative frequency slots, resulting in a relative power spectrum corresponding to a single, constant, transmitted frequency. However, since relative frequency is merely the fractional change in frequency, the results can be used to estimate the effect of reflection on a transmitted frequency spectrum.

The results of total relative power, time response, and frequency response, as calculated by this program, are discussed in Section 3.

REFERENCES

1. V. Twersky, "On Multiple Scattering of Waves by Rough Surfaces," IRE Transactions on Antennas and Propagation, Vol. 5, 1957, p. 81.

2. P. Beckman and A. Spizzichino, The Scattering of Electromagnetic Waves From Rough Surfaces, MacMillan, 1963.

3. W. H. Peake, "The Interaction of Electromagnetic Waves With Some Natural Surfaces," PhD Dissertation, Ohio State University, 1959. Appears as Report 898-2, Antenna Laboratory, Ohio State University Research Foundation, 30 May 1959, prepared under Contract AF33(616)-6158, Wright Air Development Center, Wright-Patterson Air Force Base, Ohio. Also appears as "Theory of Radar Return From Terrain," IRE Convention Record, Vol. 7, p. 27.

4. Donald E. Barrick and William H. Peake, "Scattering From Surfaces With Different Roughness Scales: Analysis and Interpretation," Technical Report, Battelle Memorial Institute, No. BAT-187A-10-3, November 1967.

5. G. Valenzuela, "Depolarization of EM Waves by Slightly Rough Surfaces," IEEE Transaction on Antennas and Propagation, AP-15, No. 4, 1967, p. 552.

6. H. Davies, "The Reflection of Electromagnetic Waves From a Rough Surface," Proceedings of the IEE (Great Britain), Vol. 101, Pt. IV, 1954, p. 209.

7. M. Isakovich, "The Scattering of Waves From a Statistically Rough Surface," Zhurnal Eksperimental 'noi Teoreticheskoi Fiziki (Morris Friedman, trans.), Vol. 23, 1952.

8. B. Semenov, "Reflection of Electromagnetic Waves From Restricted Portions of Rough Surfaces With Finite Conductivity," Radiotekhnika i Elecktronika, Vol. 10, No. 1, 1952.

9. A. Stogryn, "Electromagnetic Scattering From Rough, Finitely Conducting Surfaces," Radio Science, Vol. 2, No. 4, 1967, p. 415.

10. D. Muhleman, "Radar Scattering From Venus and the Moon," Astronomical Journal, Vol. 69, No. 1, 1964, p. 34.

11. T. Hagfors, "Relationship of Geometric Optics and Auto-correlation Approaches to the Analysis of Lunar and Planetary Radar," Journal of Geophysical Research, Vol. 71, No. 2, 1966, p. 379.

12. R. Kodis, "A Note on the Theory of Scattering From an Irregular Surface," IEEE Transactions on Antennas and Propagation, AP-14, No. 1, 1966, p. 77.

13. D. Barrick, "Rough Surface Scattering Based on the Specular Point Theory," IEEE Transactions on Antennas and Propagation, AP-16, No. 4, July 1968.

14. S.H. Durrani and H. Staras, "Multipath Problems in Communications Between Low Altitude Spacecraft and Stationary Satellites," RCA Review, March 1969, pp. 77-105.

15. J.L. Massey and John J. Uhran, Jr., "Final Report for Multipath Study," Department of Electrical Engineering, University of Notre Dame, for NASA, GSFC, Contract No. NAS5-10786, August 1969.

16. J.N. Birch, "Multipath/Modulation Study for the Tracking and Data Relay Satellite System," Magnavox Company Report for NASA, Contract No. NAS5-10744, January 1970.

17. H. Bremmer, "Propagation of Electromagnetic Waves," Handbuch der Physik, Vol. 16, Springer-Verlag, Berlin, 1958, pp 423-639.

18. A.K. Fung and R.K. Moore, "The Correlation Function in Kirchoff's Method of Solution of Scattering of Waves From Statistically Rough Surfaces," Journal of Geophysical Research, Vol. 71, No. 12, June 15, 1966, p. 2939.

19. P. Beckman, "Shadowing of Random Rough Surfaces," IEEE Transactions on Antennas and Propagation, Vol. AP-13, May 1965, pp. 384-388.

20. R.A. Brockelman and T. Hagfors, "Note on the Effect of Shadowing on the Backscattering of Waves From a Random Rough Surface," IEEE Transactions on Antennas and Propagation, AP-14, No. 5, September 1966, pp. 621-629.

21. Bruce G. Smith, "Geometrical Shadowing of a Random Rough Surface," IEEE Transactions on Antennas and Propagation, AP-15, No. 5, September 1967, pp. 668-671.

22. R. Wagner, "Shadowing of Randomly Rough Surfaces," Journal of the Acoustical Society of America, Vol. 41, No. 1, 1967, p. 138.

23. Donald E. Kerr (ed.), Propagation of Short Radio Waves, Dover, 1951.

24. K.A. Norton, et al, "The Probability Distribution of the Amplitude of a Constant Vector Plus a Rayleigh Distributed Vector," Proceedings of the IRE, Vol. 43, October 1955, p. 1354.

25. Mischa Schwartz, W.R. Bennet, and Seymour Stein, Communication Systems and Techniques, McGraw-Hill, 1966.